February 28, 1997

The following lists the change page instructions for Revision 1 of the non-proprietary version of *NOTRUMP Final Validation Report for AP600.*

Remove:	**Replace with:**
Revison 0 Cover and Spine	Revision 1 Cover and Spine
Revision 0 Title Page	Revision 1 Title Page
Revision 0 pages vii to xvi	Revision 1 pages vii to xviii
Revision 0 Section 8 Blank Page	Revision 1 Section 8 (pages 8.1-1 to 8.5-1)
Revision 0 Section 9 (pages 9-1 to 9-2)	Revision 1 Section 9 (pages 9-1 to 9-3)

WESTINGHOUSE NON-PROPRIETARY CLASS 3

WCAP-14808
Revision 1

NOTRUMP Final Validation Report for AP600

February 1997

R. L. Fittante
A. F. Gagon
K. E. Halac
L. E. Hochreiter
J. Iyengar
R. M. Kemper
D. A. Kester
K. F. McNamee
P. E. Meyer
R. A. Osterrieder
R. F. Wright

Westinghouse Electric Corporation
Energy Systems Business Unit
P.O. Box 355
Pittsburgh, PA 15230-0355

TABLE OF CONTENTS (Cont.)

TABLE OF CONTENTS (Cont.)

LIST OF TABLES

LIST OF TABLES (Cont.)

LIST OF TABLES (Cont.)

LIST OF FIGURES[1]

Note:

(1) Most of the figures for Sections 4 through 8 are listed in tables preceding each set of figures in each subsection.

LIST OF ACRONYMS

ADS	Automatic depressurization system
AICC	adiabatic isochoric complete combustion
AOV	air-operated valve
ASME	American Society of Mechanical Engineers
CCFL	countercurrent flow limit
CHF	critical heat flux
CL	cold leg
CMT	core makeup tank
CNS	containment system
COL	combined operating license
CRDM	control rod drive mechanism
CRT	core reflood tank
CVCS	chemical and volume control system
DAS	data acquisition system
DCP	design change proposal
DEG	double-ended guillotine
DECLG	double-ended cold leg guillotine
DF	decontamination factor
DG	diesel generator
DNB	departure from nucleate boiling
DOE	United States Department of Energy
DSER	draft safety evaluation report
DVI	direct vessel injection
ECCS	emergency core cooling system
EPRI	Electric Power Research Institute
ESF	engineered safety feature
HL	hot leg
HT	heat transfer
HVAC	heating, ventilation and air conditioning
HX	heat exchanger
IASCC	irradiation-assisted stress corrosion cracking
I&C	instrumentation and control
ICAP	International Code Assessment and Application Program
IIS	incore instrumentation system
IRWST	in-containment refueling water storage tank
ITAAC	inspection, tests, analysis and acceptance criteria
L/D	length over diameter
LBLOCA	large-break LOCA
LOCA	loss-of-coolant accident
LTC	long-term cooling
MFWIV	main feedwater isolation valve
MSLB	main steam line break
MSLIV	main steam line isolation valve
MSS	main steam system
NRC	Nuclear Regulatory Commission
NRHR	normal residual heat removal system

NSSS	nuclear steam supply system
PAMS	post-accident monitoring system
P&ID	piping and instrumentation diagram
PBL	pressure break line
PCS	passive containment cooling system
PCT	peak clad temperature
PIRT	phenomena identification and ranking table
PLS	plant control system
PMS	protection and safety monitoring system
PORV	power-operated relief valve
PRA	probabilistic risk assessment
PRHR	passive residual heat removal
PWR	pressurized water reactor
PXS	passive core cooling system
QDPS	qualified data processing system
RAI	request for additional information
RAM	reliability, availability, and maintainability
RCDT	reactor coolant drain tank
RCP	reactor coolant pump
RCS	reactor coolant system
RHR	residual heat removal
RTD	resistance temperature detector
SBLOCA	small-break LOCA
SCC	stress corrosion cracking
SER	safety evaluation report
SFS	spent fuel cooling system
SFWS	startup feedwater system
SG	steam generator
SGS	steam generator system
SGTR	steam generator tube rupture
SI	safety injection
SIMARC	simulator advanced real-time code
SMS	special monitoring system
SPS	passive containment spray system
SSAR	standard safety analysis report
STD	standard
UET	unfavorable exposure time
UPTF	upper plenum test facility
URD	utility requirements document
USC	utility steering committee
VBS	non-radioactive ventilation system
VES	passive control room ventilation system
VFS	containment air filtration system

Nomenclature

A	=	flow area, ft.^{2}
A_k	=	flowlink area (ft.^{2})
[		
		]^{a,c}
BDFL	=	flowlink downstream end mixture fraction, $b_{d(l),l}$
BUFL	=	flowlink upstream end mixture fraction, $b_{u(l),l}$
c	=	user-supplied constant default valve = 0.13
$(C_D)_k$	=	discharge coefficient
CFDFL	=	flowlink downstream liquid flow fraction, $C^f_{D(l),l}$
CFUFL	=	flowlink upstream liquid flow fraction, $C^f_{U(l),l}$
CGDFL	=	flowlink downstream gas flow fraction, $C^g_{D(l),l}$
CGUFL	=	flowlink upstream gas flow fraction, $C^g_{U(l),l}$
[		
		]^{a,c}
C_o	=	drift flux distribution parameter
CONV	=	10^{-6}
$C^f_{i,k}, C^g_{i,k}$	=	contact coefficients for liquid and vapor flow between fluid node i and flowlink k
D	=	diameter, ft.
DCONTFL	=	continuous contact flowlink diameter, ft.
DELWFL	=	flowlink change in either W or Q state variable, lbm/sec. or ft.^{3}/sec.
D_H	=	hydraulic diameter, ft.
DWFFL	=	flowlink partial derivative of liquid mass flow rate with respect to either W or Q state variable, lbm/ft.^{3}
D_{Taylor}	=	Taylor instability diameter, ft.
E	=	elevation, ft.
EBOTFN	=	fluid node bottom elevation, E_{bot}, ft.
EDFL	=	flowlink downstream elevation, E_D, ft.
EMIXFN	=	mixture elevation, E_{mix}, ft.
ETOPFN	=	fluid node top elevation, E_{top}, ft.
EUFL	=	flowlink upstream elevation, E_U, (ft.)
FULRFL(I,L)	=	Fraction of liquid flow through link IULRFL(I,L) that is contributed to the flow in internally calculated liquid-reflux flowlink L
g	=	gravitational acceleration, ft./sec.^{2}
g_c	=	conversion factor, 32.174, lbm-ft./lbf/sec.^{2}
G	=	total mass flux, lbm/sec./ft.^{2}
h	=	specific enthalpy, Btu/lbm
h	=	film heat-transfer coefficient, Btu/sec./ft.^{2}/°F
H	=	pump head, ft.

h_{fg}	=	latent heat of vaporization, Btu/lbm
h_f	=	heat-transfer coefficient assuming all the mass flowing is liquid, Btu/sec./ft.^{2}/°F
IDRNFN	=	fluid node mixture level overshoot drain flag
IFILLFN	=	fluid node mixture level overshoot fill flag
IREDOFL	=	flag for redoing certain flowlink calculations
ISMFN	=	fluid node mixture region state flag
ISTAKFN	=	node stack and mixture level backing flag
ITYPEFL	=	flowlink type flag
ITYPEFN	=	fluid node type flag
IULRFL(I,L)	=	Identification number of the Ith link that can potentially contribute to the flow of internally calculated liquid-reflux flowlink L
j	=	total volumetric flux, ft.^{3}-sec.$^{-1}$/ft.^{2} = ft./sec.
J	=	Joule's constant, 778.156, ft.-lbf/Btu
JFLUXON	=	local logical flag (if true, drift flux is done on a volumetric flow bases; otherwise on a mass flow basis)
JREDOIT	=	local flag to cause drift flux to be done twice, first on a mass flow basis and second on a volumetric flow basis
j_f^*, j_g^*	=	dimensionless form of the liquid and vapor component volumetric flux
$J_{f/g}$	=	denominator of the liquid and vapor component dimensionless volumetric flux expression, ft./sec.
K	=	drift flux/flooding parameter, ft./sec.
k_f	=	conductivity of saturated liquid, Btu/sec./ft./°F
L	=	length, ft.
[		]^{a,c}
M	=	mass, lbm
NULRFL(L)	=	Number of flowlinks that potentially contribute to the flow of internally calculated liquid-reflux flowlink L
P	=	pressure, psia
Pr_L	=	Prandtl number of liquid
Q	=	volumetric flow rate, ft.^{3}/sec.
$\dot{Q}$	=	time rate of change of Q, ft.^{3}/sec.^{2}
Q^M	=	mass heat rate
Q^V	=	volumetric heat rate
R	=	radius of continuous flowlink
Re	=	Reynolds number
s	=	entropy, Btu/lbm/°F
t	=	time at beginning of time step, sec.
Δt	=	time step size, sec.
T	=	temperature, °F
TMMFN	=	fluid node mixture region mass, M_M, lbm
TMMOFN	=	fluid node mixture region mass from previous time step, M_M^{old}, lbm

TMVFN	=	fluid node vapor region mass, M_V, lbm
TMVOFN	=	fluid mode vapor region mass from previous time step, M_V^{old}, lbm
U	=	internal energy, Btu
V	=	volume, ft.^{3}
V_{gj}	=	drift velocity of vapor relative to the total volumetric flux, ft./sec.
W	=	net mass flow rate, lbm/sec.
$\dot{W}$	=	time rate of change of W, lbm/sec.^{2}
$\|W_f\|$, $\|W_g\|$	=	absolute value of liquid and vapor flow, lbm/sec.
WFFL	=	flowlink liquid mass flow rate, W_f, lbm/sec.
$(Wh)^M_{i,k}$, $(Wh)^V_{i,k}$	=	net energy flow rate to or from the mixture and vapor regions of fluid node i for flowlink k, Btu/sec.
X	=	quality
ΔZ	=	characteristic liquid level difference term, ft.
Z_{tot}	=	overall height of flowlink, ft.
α	=	void fraction
σ	=	surface tension, lbf/ft.
μ_g, μ_f	=	saturated vapor and liquid viscosities, lbm/ft.-sec.
ρ	=	density, lbm/ft.^{3}
υ	=	specific volume, ft.^{3}/lbm

Subscripts:

bcr	=	critical bubble rise
bot	=	bottom end of flowlink or bottom node
BR	=	bubble rise
[		]^{a,c}
D	=	downstream
donor	=	donor
f	=	liquid phase
g	=	vapor (gas) phase
k	=	flowlink k
M	=	mixture region
mix	=	mixture elevation
recipient	=	recipient
top	=	top end of flowlink or top node
U	=	upstream
[		]^{a,c}
V	=	vapor region

Superscripts:

crit	=	critical
donor	=	donor
recipient	=	recipient
stag	=	stagnation
Q	=	volumetric flow-based
t	=	throat
W	=	mass flow-based

8 NOTRUMP COMPARISONS TO THE OREGON STATE UNIVERSITY INTEGRAL SYSTEMS TESTS

8.1 Introduction

This section contains the comparisons of the NOTRUMP code to the Oregon State University (OSU) integral systems tests. A full description of the OSU test results and analysis of the test data are given in References 8-1 and 8-2. The OSU facility description is given in Reference 8-3. The OSU tests simulate AP600 small-break loss-of-coolant accidents (LOCAs), steam generator tube ruptures (SGTRs), and main steam line breaks (MSLBs). Selected small-break LOCAs are simulated using the NOTRUMP code.

The OSU tests capture all the highly ranked phenomena as identified from the small-break LOCA phenomena identification and ranking table (PIRT) as given in Table 1.3-1. Since the OSU tests are integral systems tests, the important PIRT phenomena are not only captured but they interact during the transient. The interactions of the phenomena are important since they determine the timing of the transient events such as the reactor coolant system (RCS) draindown, end of core makeup tank (CMT) circulation, CMT balance line draining, initiation of CMT draining, and activation of the automatic depressurization system (ADS) blowdown. Once the ADS is activated, the nature of the transient changes and a more rapid, staged blowdown occurs that leads to in-containment refueling water storage tank (IRWST) injection. As the RCS depressurizes, the CMT injection flow increases when CMT draining begins. Also, as the RCS continues to depressurize, the accumulators inject. These sources of injection into the simulated vessel maintain sufficient core inventory so that core uncovery does not occur.

Since the OSU tests capture the important PIRT phenomena, validation of the NOTRUMP code with the OSU data provides confidence that NOTRUMP is appropriate for assessing the accident mitigation capability of the AP600 passive core cooling system.

8.2 NOTRUMP Modeling of the Oregon State University Small-Break Loss-of-Coolant Accident Tests

8.2.1 Oregon State University Test Facility Description

8.2.1.1 Facility Layout

The OSU test facility is a scaled model of the AP600 RCS, steam generator (SG) system, passive core cooling system (PXS), ADS, lower containment sump (LCS), chemical and volume control system (CVS), and normal residual heat removal system (RNS). In addition, the facility simulates the AP600 passive containment cooling system (PCS) condensate return process. Figure 8.2-1 is an isometric drawing of the test facility. The facility reflects the scaled AP600 geometry, including the piping routings. All components and piping are fabricated from austenitic stainless steel. The relative locations of all tanks and vessels—such as the IRWST, CMTs, and accumulators were maintained as determined by the scaling approach. The facility uses a unique break and ADS measurement system (BAMS) to measure two-phase break and ADS flow.

The RCS is composed of a reactor vessel, which has electrically heated rods to simulate the decay heat in the reactor core, and two primary loops. Each primary loop consists of two cold-leg pipes and one hot-leg pipe connecting an SG to the reactor vessel. A reactor coolant pump (RCP) on each cold leg takes suction from the SG channel head (downstream of the SG U-tubes) and discharges it into the downcomer region of the reactor vessel. A pressurizer with an electric heater is connected to one of the two hot legs through surge-line piping. The top of the pressurizer is connected to the ADS 1-3 line. An ADS-4 line is connected to each hot leg.

The reactor vessel contains two direct vessel injection (DVI) nozzles that connect to the DVI lines of the PXS. A flow venturi is incorporated in each DVI nozzle to limit the loss of inventory from the reactor vessel in the event of a double-ended DVI line break.

This test facility models the primary and secondary side of the SGs with one generator per primary loop. A simulated feedwater line is used for each loop to maintain proper secondary water level. The steam produced in each SG is measured and exhausted to the atmosphere through a common diffuser and stack.

The test control logic simulates the response of the AP600 by providing a safety (S) signal at a fixed time following a break.

The passive safety-related injection systems consist of two CMTs, two accumulators, one IRWST, and one passive residual heat removal heat exchanger (PRHR HX). The test facility simulates the AP600 IRWST with a cylindrical tank with scaled water volume and height. The IRWST is located above the reactor core; two injection lines connect to the two DVI lines. Each IRWST injection line also connects to the sump tank with interconnecting piping and isolation valves. The PRHR HX is located

inside the IRWST, using IRWST water as the heat sink. The inlet of the PRHR HX is connected to the pressurizer-side hot leg via a tee at the ADS-4 line, and the outlet is connected to the SG channel head at the cold-leg side. Since the inlet is hot and the outlet is cold, water is circulated through this system by natural convection. The water volume and elevation of each CMT are scaled and modeled. They are elevated above the reactor vessel and the DVI lines. A line connecting the top of each CMT to its cold leg provides pressure balance between the RCS and the CMT. Therefore, the CMT injects cooling water by its own elevation head. The accumulators are also modeled with scaled volume and height. However, they are pressurized with nitrogen and, therefore, inject when RCS pressure is below the preselected scaled accumulator pressure.

The AP600 uses four stages of valves to depressurize the RCS. The first three stages of the ADS are provided through connections to the pressurizer. These three stages are arranged in parallel, with each stage containing two lines with each line containing an isolation and control valve. The fourth stage of the ADS contains four separate lines.

The OSU test facility uses only one set of valves to model the ADS 1-3 stages for AP600. This is done using removable flow nozzles to match the scaled flow characteristics of either one or two lines of valves. The lines of ADS 1-3 split into parallel lines from one connection off the pressurizer in the AP600.

The discharge lines from the ADS 1-3 valves are joined into one line connected to the ADS 1-3 separator. This two-phase flow is separated using a swirl-vane separator. The liquid and vapor flows are measured to obtain the ADS total flow for mass and energy balance analysis. The separated flow streams are then recombined and discharged into the IRWST through a sparger.

The OSU test facility uses one ADS-4 line connected to the top of each hot leg. Each line contains a pneumatically operated, full-port ball valve acting as the ADS-4 isolation valve and a flow nozzle simulating the flow area in the AP600. Two sets of flow nozzles are used in the test: one simulates 100-percent flow area and the other simulates 50-percent flow area. In the test facility, ADS-4 discharge flows to the ADS-4 separators, where the steam and liquid flows are separated and measured. Steam flow is measured and exhausted to the atmosphere.

The LCS in the AP600 consists of two volumes: normally flooded and normally nonflooded. The normally flooded volume consists of those compartments that collect liquid break flow and ADS flow. The normally flooded volume is modeled in OSU with a cylindrical tank, identified as the primary sump tank. The normally nonflooded volume includes those compartments that do not collect any liquid flow. The normally nonflooded volume is modeled in OSU with a cylindrical tank, identified as the secondary sump tank. These two tanks are connected with a line at a level simulating the curb level in the AP600.

In the AP600, the RNS is used to provide nonsafety-related cooling water injection to the reactor core. The RNS pump takes suction from the IRWST and discharges it into the DVI lines. The test facility

RNS pump takes suction from the IRWST at the scaled location and elevation and discharges equal flow to both DVI lines at scaled locations.

BAMS is uniquely designed for the test facility to indirectly measure two-phase flow and energy leaving the break and ADS location. This system separates two-phase flow into single-phase liquid and single-phase steam flows for direct flow rate and temperature measurements. The BAMS consists of steam-liquid separators and the interconnecting pipes and valves to the various break sources, the primary sump tank, the ADS 1-3 lines, and the main steam header.

Two-phase flow (steam and water) from the ADS 1-3 lines enters the ADS 1-3 separator, where the steam is separated from the mixture. Steam flows out of one outlet while liquid drains down the other. These two lines recombine the separated flows downstream and discharge into the IRWST via the sparger located inside the IRWST. Therefore, the mass and energy from ADS 1-3 are transferred to the IRWST as in the AP600.

Two ADS-4 separators are used, one for each ADS-4 line. Each ADS-4 separator separates two-phase flow into single-phase steam and single-phase liquid for flow rate, pressure, and temperature measurements. The steam line connects to a common steam header, and the liquid line connects to the primary sump tank. These connections simulate the ADS-4 operation process in the AP600, where the steam flow rises to the containment wall and liquid drains to the sump.

8.2.1.2 OSU Test Matrix

The OSU tests examine the passive safety-related system response for the small-break loss-of-coolant accident (LOCA) transition into long-term cooling. A range of small-break LOCAs is simulated at different locations on the primary system, such as the cold leg, hot leg, cold leg to CMT balance line, and DVI line. The break orientation (top or bottom of the cold leg) is also studied. Different single failure cases are examined to confirm that the worst situation is used in the AP600 SSAR analysis. Selected tests continue into the long-term cooling, post-accident mode in which passive safety injection (SI) is from the reactor sump as well as the IRWST. A larger-break, post-accident, long-term cooling situation is also simulated. A summary of the test matrix is provided in Table 8.2-1.

These tests provide a wide range of data on the performance of the passive core cooling systems used in the AP600. The tests were intended to provide overlap with the full-height, full-pressure SPES-2 tests as well as the AP600 plant SSAR calculations. The test parameters investigated are:

- Cold-leg break sizes of 1/2, 1, 2, 4 (bottom of cold leg), and 4 in. (top and bottom of cold leg)
- Break locations of cold leg with CMTs, cold leg without CMTs, top of pipe, bottom of pipe, balance line breaks, DVI line breaks, and no breaks with inadvertent ADS actuation
- Different single failures, one of four ADS-4 valves, ADS-1 valves, and ADS-3 valves

- Beyond-design-basis tests with multiple failures

- Spurious S signal (no break)

The break size range and location, as well as the different assumed single failure disruptions, provide a thorough and comprehensive set of integral systems data for code validation.

8.2.1.3 Facility Operation

A general sequence of events applies to the facility operation for most of the tests. At the beginning of each test, the rod bundle heaters are shifted to power control mode, and the power increases to the maximum level (600 kW) for 140 seconds followed by a decaying power function simulating the total decay energy input of AP600 nuclear fuel. A specific break valve (or valves if required) is opened to begin break flow. A reactor trip signal occurs coincident with the break, and a safety signal occurs 0.5 seconds later. The reactor trip and safety signals initiate the following actions:

- The main steam line isolation valves (MSLIVs) close
- The main feedwater isolation valves (MFWIVs) shut off
- The CMT injection valves open
- The PRHR return flow valve opens
- The RCPs trip

The circulation flow through the CMTs and flow through the PRHR begin immediately after the CMT injection valves and the PRHR return flow valve are opened. ADS-1 is actuated on CMT volume of 75 percent with the other ADS stages following the delay time specified in the test procedure. The accumulators begin injecting when the primary pressure falls to ~245 psia. The IRWST begins injecting water when the primary system pressure is approximately 18 psia.

8.2.1.4 General Scaling Criteria

The OSU test facility is designed to develop a database to validate the safety analysis codes that are used to predict the performance of the AP600 passive safety-related systems.

To ensure that the OSU tests provide valid thermal-hydraulic data and capture the key phenomena over the range of conditions for which the passive safety-related systems require validation, a detailed state-of-the-art scaling analysis was performed to establish the facility design and test conditions. The following sections present a summary of the scaling process applied to the OSU APEX tests.

Existing data on standard pressurized water reactors (PWRs), coupled with engineering judgement and calculations for the AP600, are used to determine which thermal-hydraulic phenomena might impact core liquid inventory or fuel peak clad temperature. These phenomena are ranked and included in the AP600 small-break LOCA PIRT.

The important phenomena identified through the use of the small-break LOCA PIRT are used to divide the scaling analysis into four parts. Each part corresponds to a different phase of a small-break LOCA:

- Natural circulation scaling analysis
- System depressurization scaling analysis
- Venting, draining, and injection scaling analysis
- Recirculation scaling analysis

The hierarchial, two-tiered scaling analysis (H2TS) method is used to analyze each phase of the small-break LOCA transient. The H2TS method is an essential part of the U.S. NRC's severe accident scaling methodology (SASM).

There are four basic elements of the H2TS analysis method:

- System decomposition
- Scale identification
- Top-down/system scaling analysis
- Bottom-up/process scaling analysis

The height scaling ratio is set at 1:4, and the diameter scaling ratio at 1:6.93. These ratios are based on the objective of minimizing power requirements while maximizing height and maintaining sufficient system volume to properly model loop pressure drop and three-dimensional flow in the downcomer, core, and plenum regions.

Once the length and diameter scaling ratios were determined, the dimensions of the test facility could be geometrically scaled. The scaling ratios for the test facility are:

Geometry

Length scaling ratio	1:4
System diameter scaling ratio	1:6.93
Area scaling ratio	1 48
Volume scaling ratio	1:192

Flow

Velocity scaling ratio	1:2
Mass flow rate scaling ratio	1:96

Residence Time

Time scaling ratio	1:2

Power

Power scaling ratio	1:96
Power density scaling ratio	2:1

8.2.1.5 Results and Observations

The key results and observations for the OSU tests are:

- The core remains covered for all design basis transients.

- All passive systems function as expected, with no adverse consequences, including CMT recirculation and draindown, PRHR HX heat removal, ADS depressurization, accumulator injection, IRWST gravity draining, and stable long-term sump injection.

Additional observations include:

- The CMTs refill due to condensation effects during long-term recirculation.
- Steam condensation events occur in the upper downcomer region.
- Thermal stratification occurs in both the hot and cold legs.
- For most tests, regular oscillations occur during long-term recirculation.

8.2.2 Description of NOTRUMP Oregon State University Model

The NOTRUMP OSU input deck is characterized by the following:

- Fluid nodes
  - 62 internal fluid nodes
  - 5 boundary fluid nodes
  - 2 accumulators

- Flowlinks
  - 93 noncritical flowlinks
  - 12 critical flowlinks

- Metal nodes
  - 32 metal nodes

- Heatlinks
  - 51 normal heatlinks
  - 1 critical heatlink

- Core nodes
  - 4 core nodes

- Pumps
  - 4 pumps

8.2.2.1 Fluid Nodes

Figure 8.2-2 presents the noding diagram for the NOTRUMP model of the OSU test facility. All fluid nodes are stratified unless stated otherwise. Those nodes representing the RCS, including the SG secondaries, are noded consistent with the methodology used in standard PWR modeling wherever possible. In all cases, node top and bottom elevations, as well as connecting flowlink elevations, are preserved to correctly account for gravitational head calculation. The noding of the safety components, such as the CMTs, PRHR, and so on, is done according to the general principles used in the RCS. In addition, all noncritical flowlinks use the new volumetric flow model.

Node 1 represents the vessel downcomer volume.

Node 2 represents the lower plenum and takes into account the volume contained between the bottom of the power channel and the bottom of the active fuel length.

Nodes 3 through 6 each represent one-fourth of the volume inside the core barrel adjacent to the heated length of the core.

Node 7 represents the upper plenum volume from the top of the core heated length to the bottom of the upper support plate and inside the core barrel.

Node 8 is a "T" variable area node, representing the upper head volume above the upper support plate.

Node 9 is a "T" variable area node, representing the pressurizer tank and surge line volume.

Nodes 10 and 20 are horizontal cylinder area nodes representing hot legs 2 and 1, respectively. The vertical portion of the hot legs going to the steam generators are modeled via nodes 11 and 21, respectively.

Nodes 12 through 15 each represent one-fourth of the volume inside SG-2 tubes.

Nodes 16 and 26 represent the pump suction for loops A and B, respectively.

Nodes 18 and 38 represent RCP-2 and RCP-4, which are attached to cold legs 2 and 4, respectively.

Nodes 19 and 39 represent cold legs 2 and 4 from loop A and are modeled as horizontal-cylinder, variable-area nodes.

Nodes 22 through 25 each represent one-fourth of the volume inside SG-1 tubes.

Nodes 28 and 48 represent RCP-1 and RCP-3, which are attached to cold legs 1 and 3, respectively.

Nodes 29 and 49 represent cold legs 1 and 3 from loop B and are modeled as horizontal-cylinder, variable-area nodes.

Nodes 30 and 40 are "T" variable area nodes that represent the secondary side of SG-2 and SG-1, respectively.

Nodes 50 and 54 through 56 are a group of fluid nodes used to model CMT-1. The size of these nodes is staggered from the largest (node 50) at the bottom to the smallest (node 56) at the top.

Nodes 51 and 61 are the accumulator-type fluid nodes, representing the accumulators attached to the CMT-1 and CMT-2 DVI piping, respectively.

Node 52 represents the volume of the CMT-1 side DVI line piping from the vessel to the CMT-1 outlet.

Nodes 53 and 153 represent the pipe connecting cold leg 3 to CMT-1.

Node 58 is a homogeneous fluid node representing the piping leading from the pressurizer to the ADS stage 1 through 3 valves.

Node 59 is an inverted "T" variable area node used to represent the volume from the top of the PRHR inlet line piping to the tube sheet in the PRHR tube inlet.

Nodes 60 and 64 through 66 are a group of fluid nodes used to model CMT-2. The size of these nodes is staggered from the largest (node 60) at the bottom to the smallest (node 66) at the top.

Node 62 represents the volume of the CMT-2 side DVI line piping from the vessel to the CMT-2 outlet.

Nodes 63 and 163 represent the pipe connecting cold leg 1 to CMT-2.

Nodes 67 and 77 represent the IRWST volume minus the volume of the PRHR tube bundle. Node 77 is a "T" variable area node that includes the piping volume from the IRWST to the DVI piping.

Node 70 is a boundary fluid node, representing the total mass contained in the facility except for SG secondaries and accumulators.

Node 74 is a "T" variable area node representing the PRHR inlet line from the top of hot leg 2 to the end of the horizontal section at the top of the piping leading to the PRHR.

Node 76 is a homogeneous node, representing the volume of the PRHR outlet line from the outlet side tube sheet to the SG-2 outlet plenum.

Node 78 is the boundary fluid node connected to pressurizer node 9. It maintains a defined pressure in the steady state.

Node 79 is the boundary fluid node used to set donor conditions for the main feedwater.

Node 80 is a boundary fluid node used as an ultimate sink for break flow and so on. It nominally represents containment, but time-dependent pressure or temperature calculations are not performed for this node.

Node 82 is a boundary fluid node for SG nodes 30 and 40. This node keeps a defined pressure in the steady state.

Nodes 94 and 95 are homogeneous fluid nodes representing the piping upstream of the ADS fourth-stage valves.

Nodes 111 through 114 are homogeneous fluid nodes, representing the volume inside the PRHR tubes along the top run, while node 75 represents the volume along the bottom.

Nodes 116 and 117 are homogeneous fluid nodes representing the vertical section of the PRHR tubes.

8.2.2.2 Flowlinks

Link 1 represents the flow from the downcomer into the lower plenum.

Links 2 through 6 represent the flow through the core region from the lower plenum to the upper plenum.

Link 7 represents flow from the upper head to the upper plenum though the open holes in the upper support plate.

Link 8 represents flow from the downcomer to the upper head.

Link 9 represents flow from the inclined portion of hot leg 2 (modeled as part of node 11) to the pressurizer.

Link 10 represents the flow from the upper plenum to hot leg 2. It uses the levelizing model for drift flux.

Link 11 is a continuous-contact flowlink that represents the flow from the horizontal part of hot leg 2 to the vertical part of hot leg 2.

Link 12 represents the flow from the SG-2 inlet plenum into the first tube node.

Link 13 represents the flow from the first to the second tube node in SG-2.

Link 14 is a continuous-contact flowlink from the top of the uphill side to the top of the downhill side of the SG-2 tubes. This link does not use the carryover model that is used in the standard PWR noding. Instead, it uses the levelizing model for drift flux.

Link 15 represents the flow from the third to the fourth tube node in SG-2.

Link 16 represents flow from SG-2 tubes into the pump suction.

Links 17 and 37 are continuous-contact flowlinks that model the flow from the SG-2 pump suction node into RCP-2 and RCP-4 nodes, respectively.

Link 18 represents flow from the RCP-2 node to cold leg 2. It uses the levelizing model for drift flux.

Link 19 represents flow from cold leg 2 to the downcomer. It uses the levelizing model for drift flux.

Link 20 represents the flow from the upper plenum to hot leg 1. It uses the levelizing model for drift flux.

Link 21 is a continuous-contact flowlink that represents the flow from the horizontal part of hot leg 1 to the vertical part of hot leg 1.

Link 22 represents the flow from the SG-1 inlet plenum into the first tube node.

Link 23 represents the flow from the first to the second tube node in SG-1.

Link 24 is a continuous-contact flowlink from the top of the uphill side to the top of the downhill side of the SG-1 tubes. This link does not use the carryover model that is used in the standard PWR noding. Instead, it uses the levelizing model for drift flux.

Link 25 represents the flow from the third to the fourth tube node in SG-1.

Link 26 represents flow from the SG-1 tubes into the pump suction.

Links 27 and 47 are continuous-contact flowlinks that model the flow from the SG-1 pump suction node into RCP-1 and RCP-3 nodes, respectively.

Link 28 represents the flow from the RCP-1 node to cold leg 1. It uses the levelizing model for drift flux.

Link 29 represents the flow from cold leg 1 to the downcomer. It uses the levelizing model for drift flux.

Links 35 and 45 are critical flowlinks representing the feedwater flow for SGs 2 and 1, respectively. They are isolated on safety-related systems activation (S) signal.

Links 36 and 46 are critical flowlinks representing the main steam line for SGs 2 and 1, respectively. They are isolated on the reactor trip (R) signal.

Link 38 represents the flow from the RCP-4 to cold leg 4. It uses the levelizing model for drift flux.

Link 39 represents the flow from cold leg 4 to the downcomer. It uses the levelizing model for drift flux.

Link 48 represents the flow from the RCP-3 to cold leg 3. It uses the levelizing model for drift flux.

Link 49 represents the flow from cold leg 3 to the downcomer. It uses the levelizing model for drift flux.

Link 50 represents the flow from the bottom of CMT-1 through the isolation and check valves into the DVI piping.

Link 51 represents the flow from accumulator 1 attached to the CMT-1 side to the DVI piping.

Link 52 is a continuous-contact flowlink that represents the flow from the DVI piping on the CMT-1 side to the downcomer.

Link 53 is a continuous-contact flowlink that represents the flow from the top of the CMT-1 cold leg balance line to the top of CMT-1. This link uses the levelizing model for drift flux and one-way positive contact coefficient modification logic for vapor flow.

Link 54 is a continuous-contact flowlink that represents the flow from cold leg 3 into the CMT-1 balance line bottom node.

Link 56 represents the flow from the bottom of the IRWST to the CMT-1 side DVI piping.

Link 57 is a continuous-contact flowlink that represents the flow from the PRHR inlet piping uphill to downhill side. It uses the levelizing drift flux model and one-way positive contact coefficient modification logic for vapor flow.

Link 58 represents the flow from the top of the pressurizer to the piping upstream of the ADS 1-3 valves.

Link 59 is a critical flowlink representing ADS stage 1. It uses the Henry-Fauske/homogeneous equilibrium break flow model.

Link 60 represents the flow from the bottom of CMT-2 through the isolation and check valves into the DVI piping.

Link 61 represents the flow from accumulator 2 attached to the CMT-2 side to the DVI piping.

Link 62 is a continuous-contact flowlink that represents the flow from the DVI piping on the CMT-2 side to the downcomer.

Link 63 is a continuous-contact flowlink that represents the flow from the top of the CMT-2 cold leg balance line to the top of CMT-2. This link uses the levelizing model for drift flux and one-way positive contact coefficient modification logic for vapor flow.

Link 64 is a continuous-contact flowlink that represents the flow from cold leg 1 into the CMT-2 balance line bottom node.

Link 66 represents the flow from the bottom of the IRWST to the CMT-2 side DVI piping.

Link 67 represents the flow through the IRWST.

Links 68 through 70 are used to join the nodes that represent CMT-1.

Links 71 through 73 are used to join the nodes that represent CMT-2.

Link 74 is a continuous-contact flowlink that represents the flow from hot leg 2 into the PRHR inlet piping.

Link 75 is a homogeneous continuous-contact flowlink that represents flow from the PRHR inlet piping to the PRHR component top horizontal part.

Link 76 is a homogeneous continuous-contact flowlink that represents the flow out of the PRHR tubes into the PRHR outlet piping.

Link 77 represents flow from the PRHR outlet piping into the SG-2 outlet plenum. It is also an isolation valve that permits flow only after the S signal.

Link 80 is used to represent the break for single-sided breaks or one side for double-ended breaks. In double-ended breaks, one of the existing system flowlinks is reduced at break initiation to be a break link. All break links use the Henry-Fauske/homogeneous equilibrium break flow model.

Link 81 represents the top of the IRWST connected to the environment that is used to maintain the environment pressure in the IRWST.

Link 82 represents the fourth stage of ADS that connects the ADS-4, train 2 upstream piping off the PRHR inlet piping to the environment.

Link 83 represents the fourth stage of ADS that connects the ADS-4, train 1 upstream piping off hot leg 1 to the environment.

Links 84 and 85 are critical flowlinks representing ADS stage 2 and 3, respectively. They use the Henry-Fauske/homogeneous equilibrium break flow model.

Links 90 through 92 represent flow from two SG secondaries and the pressurizer to boundary fluid nodes for steady-state initialization. They are disconnected at break initiation.

Link 94 is a continuous-contact flowlink representing the flow from the PRHR inlet piping to the ADS-4, train 2 piping.

Link 95 is a continuous-contact flowlink representing the flow from the hot leg 1 piping to the ADS-4, train 1 piping.

Links 100 through 104 represent the core region reflux flow model. This model is identical to that used in standard PWR model calculations.

Links 112 through 115, 117 and 118 represent the flow between the successive fluid nodes in the PRHR tubes.

Links 153 and 163 represent the CMT-1 and CMT-2 balance line flows, respectively.

Link 158 connects the piping between the pressurizer and the ADS stages 1 through 3 valves to the containment node (FN 80) to prevent vacuum conditions in this area.

Links 201 and 202 are generalized reflux flowlinks used in the SG-2 tube uphill side fluid node stack.

Links 203 through 205 are generalized reflux flowlinks internal to CMT-1.

Links 206 through 208 are generalized reflux flowlinks internal to CMT-2.

Links 211 and 212 are generalized reflux flowlinks used in the SG-2 tube downhill side fluid node stack.

Links 221 and 222 are generalized reflux flowlinks used in the SG-1 tube uphill side fluid node stack.

Link 226 is a generalized reflux flowlink that represents cold leg balance line 1.

Link 227 is a generalized reflux flowlink that represents cold leg balance line 2.

Links 231 and 232 are generalized reflux flowlinks used in the SG-1 tube downhill side fluid node stack.

8.2.2.3 Metal Nodes

Node 1 represents the structural metal in the downcomer region of the vessel. It communicates with the downcomer fluid node (fluid node 1).

Node 2 represents the structural metal in the lower plenum region of the vessel. It communicates with the lower plenum fluid node (fluid node 2).

Nodes 3 through 6 represent the power channel vessel in the active core part (fluid nodes 3 through 6).

Node 7 represents the power channel structure near the upper plenum part (fluid node 7) of the reactor vessel.

Node 8 represents the upper head structure of the vessel. It communicates with the upper head fluid node 8.

Node 9 represents the pressurizer tank and surge line structures. This node communicates with the pressurizer fluid node 9.

Nodes 12 through 15 represent the SG-2 U-tubes. These nodes communicate with fluid nodes 12 through 15 and 30.

Nodes 22 through 25 represent the SG-1 U-tubes. These nodes communicate with fluid nodes 22 through 25 and 40.

Nodes 50 and 54 through 56 represent CMT-1. They communicate with fluid nodes 50 and 54 through 56, respectively.

Nodes 60 and 64 through 66 represent CMT-2. They communicate with fluid nodes 60 and 64 through 66, respectively.

Node 75 represents the bottom horizontal structure of the PRHR HX.

Nodes 111 through 114 represent the top horizontal structure of the PRHR HX.

Nodes 116 and 117 represent the vertical structure of the PRHR HX.

8.2.2.4 Heatlinks

The connection between the internal fluid (fluid node) and the metal containing the fluid (metal node) is modeled with heatlinks. Figure 8.2-3 shows also the connection between metal nodes and fluid nodes.

Link 1 models the heat transfer between the fluid and structural metal in the downcomer region (FN 1 and MN 1).

Heatlinks 3 through 6 model the heat transfer between the core region fluid nodes (FN 3-6) and the pressure vessel structure (MN 3-6).

Link 2 models the heat transfer between the fluid and structural metal in the lower plenum region of the vessel (FN 2 and MN 2).

Link 7 models the heat transfer between the fluid and structural metal in the upper plenum region of the vessel (FN 7 and MN 7). This heatlink uses the improved condensation model described in Section 2.

Link 8 models the heat transfer between the fluid and structural metal in the upper head region of the vessel (FN 8 and MN 8). This heatlink uses the improved condensation model described in Section 2.

Link 9 models the heat transfer between the fluid and structural metal in the pressurizer tank region and the surge line (FN 9 and MN 9). This heatlink uses the improved condensation model described in Section 2.

Links 12 through 15 model the heat transfer between the primary side of the SG-2 tubes and SG-2 tube metal (FN 12-15 and MN 12-15). These heatlinks use the improved condensation model described in Section 2.

Links 16 through 19 model the heat transfer between the secondary side of SG-2 (FN 30) and the SG-2 tube structures (MN 16-19).

Links 22 through 25 model the heat transfer between the primary side of the SG-1 tubes and SG-1 tube metal (FN 22-25 and MN 22-25). These heatlinks use the improved condensation model described in Section 2.

Links 26 through 29 model the heat transfer between the secondary side of SG-1 (FN 40) and the SG-1 tube structures (MN 26-29).

Links 41, 44, and 46 through 48 model the heat transfer between the PRHR primary fluid (FN 75, 111 through 114, 116, and 117) and the PRHR tube structure (MN 75, 111 through 114, 116, and 117). These heatlinks use the improved condensation model described in Section 2.

Links 50 and 54 through 56 model the heat transfer between the CMT-1 fluid and the CMT-1 structure (FN 50, 54 through 56 and MN 50, 54 through 56). These links use a constant heat transfer coefficient in the vapor region of a fluid node when condensation is predicted to occur.

Links 60 and 64 through 66 model the heat transfer between the CMT-2 fluid and the CMT-2 structure (FN 60, 64 through 66 and MN 60, 64 through 66). These links use a constant heat transfer coefficient in the vapor region of a fluid node when condensation is predicted to occur.

Links 67 through 70 and 72 through 74 model the heat transfer between the PRHR tube structure (MN 75, 111 through 114, 116, and 117) and the IRWST (FN 67). These links use the pool boiling limit on critical heat flux as described in Section 2.

Link 245 is a critical heatlink that models the total heat exchanged in the PRHR.

8.2.2.5 Core Nodes

The core is modeled as four axial nodes, with constant relative power levels to reproduce the uniform axial power shape produced by the OSU facility heater rods.

8.2.2.6 Pumps

Pump homologous curves for the test facility are input in a manner identical to that used in standard NOTRUMP analyses of PWRs. All models were retained with some improvements made as described in Section 2.

8.2.3 Selected Oregon State University Tests for Analysis

A total of seven OSU tests (six small-break LOCA tests and an inadvertent ADS actuation test) were selected for analysis with the NOTRUMP code. The selected tests cover the range of break locations and sizes that were tested in the OSU facility. All tests analyzed use only the passive emergency core cooling systems to mitigate the transient and to maintain core cooling. The tests include:

- SB18: 2-in. cold leg break in the bottom of cold leg 3. This is a repeat of the reference test for the OSU test matrix and simulates a typical small-break LOCA case.

- SB23: 0.5-in. cold leg break in the bottom of cold leg 3. This test is the smallest break performed for the facility and provides a break size comparison to the reference case.

- SB13: 2-in. break in DVI line 1. This test provides a different break location for the same size break as the reference case.

- SB12: double-ended DVI line break of DVI line 1. One half of the safety injection is lost to the containment. This break, along with test SB13, gives a break size sensitivity for the same break location.

- SB09: 2-in. cold leg balance line break is also a different break location for the same size break as the reference test.

- SB10: double-ended balance line break. This test, along with test SB09, gives another break size sensitivity at a different break location.

- SB14: inadvertent ADS actuation. This test provides the system response to the no-break LOCA event.

The combinations of the selected OSU tests exercise the NOTRUMP code over a wide range of break sizes and locations, which allows examination of different performance aspects of the AP600 passive emergency core cooling systems so that the code is adequately validated.

TABLE 8.2-1
OREGON STATE UNIVERSITY TEST SUMMARY MATRIX

Test No.	Break Size and Location	PRHR HX	CVS Pump	RNS Pump	ADS 4-1 (Hot Leg 1)	ADS 4-2 (Hot Leg 2)	Comments
SB01	2-in., cold leg 3, bottom of cold leg (CMT side)	On	Off	Off	50-percent flow area in AP600	100-percent flow area in AP600	Failure of one of two lines in ADS 4-1; reference cold-leg break case
SB06	4-in., cold leg 3, bottom of cold leg (CMT side)	On	Off	Off	50-percent flow area in AP600	100-percent flow area in AP600	Failure of one of two lines in ADS 4-1
SB09*	2-in., cold leg 3 to CMT-1 balance line	On	Off	Off	50-percent flow area in AP600	100-percent flow area in AP600	Same as SB01 except different break location; asymmetric behavior of CMTs
SB10*	DEG, cold leg 3 to CMT-1 balance line	On	Off	Off	50-percent flow area in AP600	100-percent flow area in AP600	Limiting break on balance line; asymmetric behavior of CMTs; failure of one of two lines in ADS 4-1
SB12*	DEG DVI-1 line break	On	Off	Off	100-percent flow area in AP600	100-percent flow area in AP600	Limiting break on DVI line; failure of one of two lines of ADS-1 and ADS-3
SB13*	2-in. DVI-1 line break	On	Off	Off	50-percent flow area in AP600	100-percent flow area in AP600	Same as SB01 except different break location
SB14*	Inadvertent ADS (no break)	On	Off	Off	50-percent flow area in AP600	100-percent flow area in AP600	No-break case with one failure of two lines in ADS 4-1
SB15	2-in., hot leg 2, bottom of pipe	On	Off	Off	50-percent flow area in AP600	100-percent flow area in AP600	Same as SB01 except break location

TABLE 8.2-1 (Continued)
OREGON STATE UNIVERSITY TEST SUMMARY MATRIX

Test No.	Break Size and Location	PRHR HX	CVS Pump	RNS Pump	ADS 4-1 (Hot Leg 1)	ADS 4-2 (Hot Leg 2)	Comments
SB18*	2-in., cold leg 3, bottom of cold leg (CMT side)	On	Off	Off	50-percent flow area in AP600	100-percent flow area in AP600	Repeat test of SB01; confirm behavior of system and instrumentation
SB19	2-in., cold leg 3, bottom of cold leg (CMT side)	On	Off	Off	50-percent flow area in AP600	100-percent flow area in AP600	Same as SB01 except containment backpressure simulated
SB21	4-in. top of and 4-in. bottom of cold leg 3 (CMT side)	On	Off	Off	50-percent flow area in AP600	100-percent flow area in AP600	Same as SB01 except larger break size; largest break size simulated in matrix tests
SB23*	1/2-in, cold leg 3, bottom of cold leg (CMT side)	On	Off	Off	50-percent flow area in AP600	100-percent flow area in AP600	Same as SB01 except smaller break size

Note:
* Tests chosen for NOTRUMP validatic .

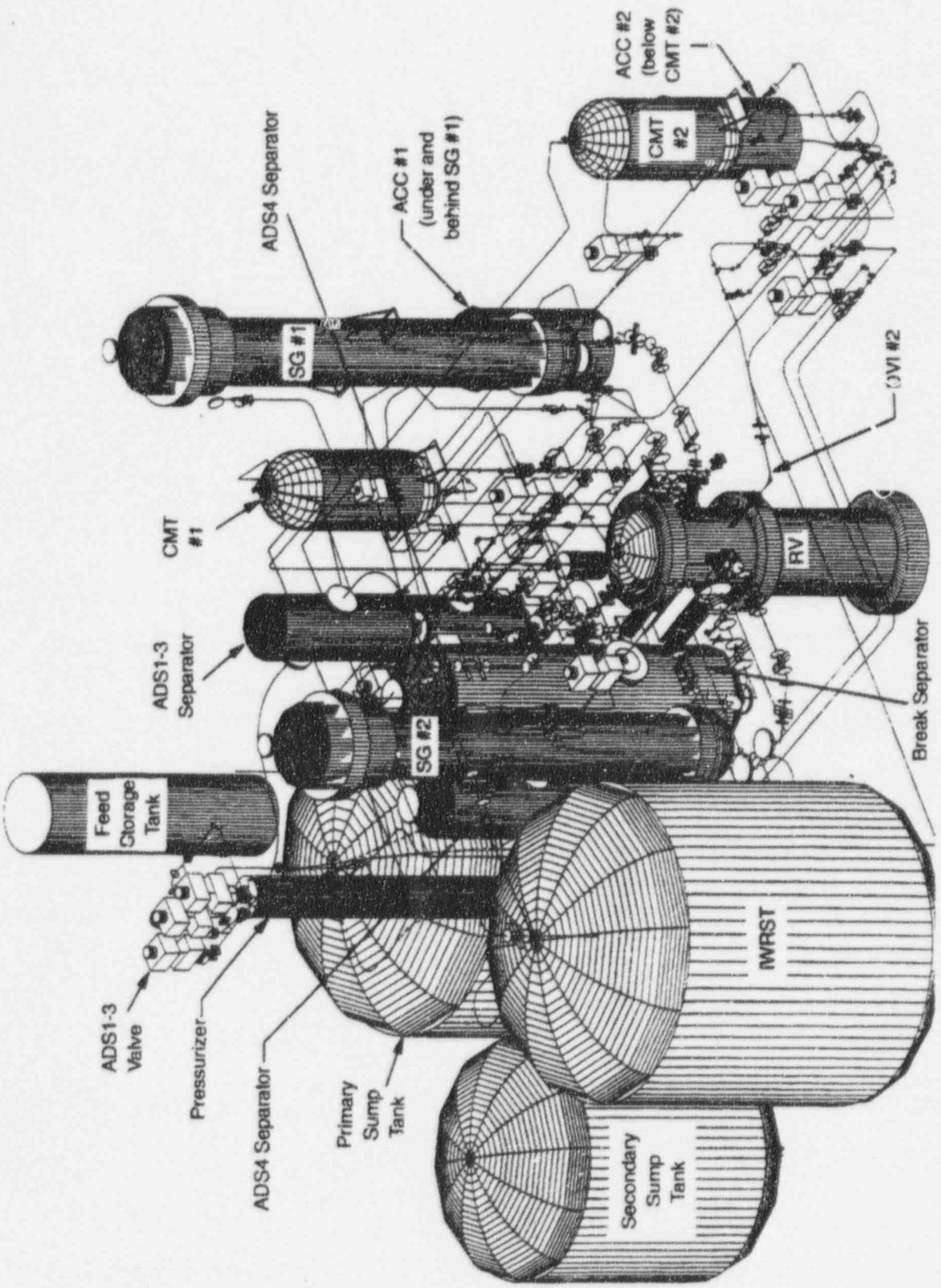

Figure 8.2-1 Isometric Drawing of the Oregon State University Test Facility

a,c

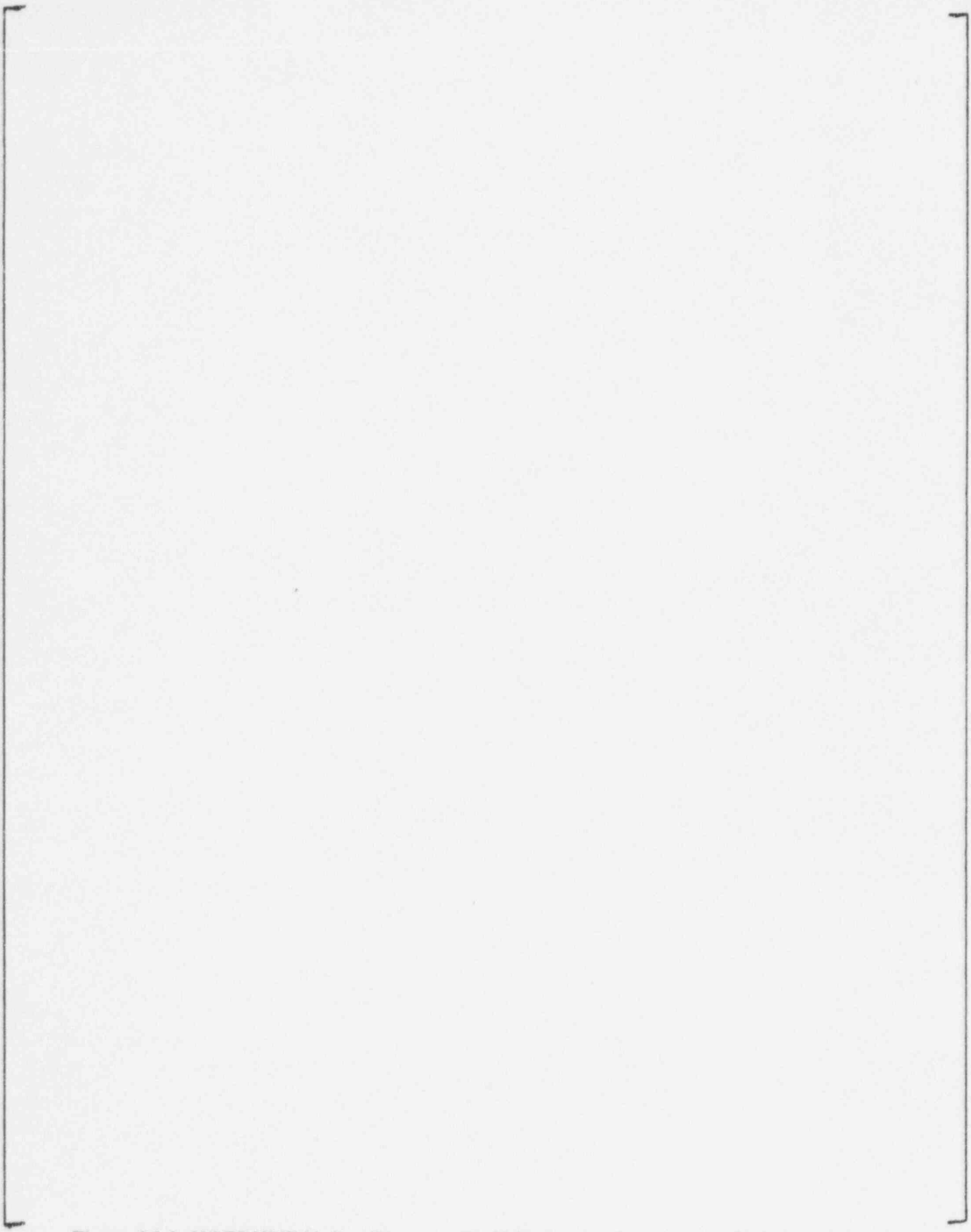

Figure 8.2-2 NOTRUMP Noding Diagram (Fluid Nodes) for Oregon State University Facility

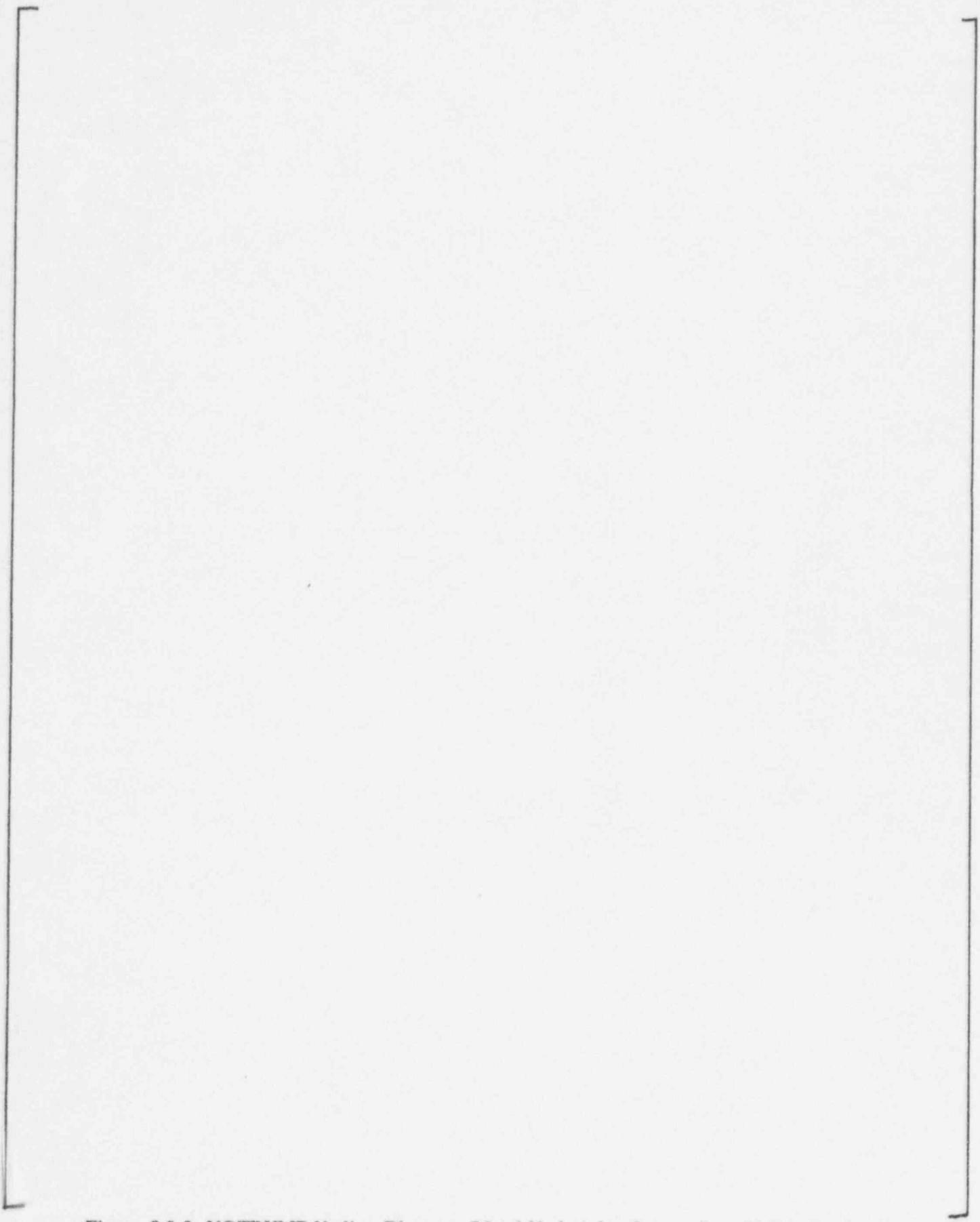

Figure 8.2-2 NOTRUMP Noding Diagram (Metal Nodes) for Oregon State University Facility

8.3 Comparisons of NOTRUMP to the Oregon State University Integral Systems Tests

NOTRUMP has been compared to seven of the OSU small-break LOCA tests as part of the final validation of the code. The tests cover the range of break size and break locations that are normally analyzed for the AP600 plant. The detailed comparisons of the code predictions to the data address the highly ranked PIRT phenomena identified in Table 1.3-1 and indicate how well NOTRUMP represents these phenomena for the different tests. The format used in the comparisons is to first describe the transient behavior observed in the test, and then compare the NOTRUMP prediction relative to the test data.

8.3.1 2-in. Cold Leg Break (SB18)

This test simulates a 2-in. break in the bottom of cold leg 3 and is performed without any nonsafety-related systems operating. A single failure of one of the two fourth- stage ADS valves on hot leg 1 is represented in the test.

8.3.1.1 Summary of Test and NOTRUMP Simulation Observations

The timing of the critical events for this transient in comparison with test results is reported in Table 8.3.1-1. Figure 8.3.1-1 shows primary system pressure during this test (as measured at the top of the pressurizer), with selected component actuations and plant responses shown in relation to primary system pressure. At the beginning of the test, the rod bundle heaters are shifted to power control mode, and the power increases to the maximum level (600 kW) for 140 seconds followed by a decaying power function simulating the total decay energy input of AP600 nuclear fuel. The simulation is started from a steady state-condition at a power level of 600 kW.

Blowdown Phase

The blowdown phase is initiated with the opening of the break. A reactor trip (R) signal occurs coincident with the break, and a safety signal (S) signal occurs 0.5 seconds later (the R and S signals occur simultaneously at time zero in the NOTRUMP simulation). The R and S signals initiate the following actions:

- The main steam line isolation valves (MSLIVs) close
- The main feedwater isolation valves (MFWIVs) shut off
- The CMT injection valves open
- The PRHR return flow valve opens
- The RCPs trip

The circulation flow through the CMTs and flow through the PRHR begin immediately after the CMT injection valves and the PRHR return flow valve are opened. Due to the rapid loss of pressure down to saturation pressure for the rod bundle and upper plenum, boiling begins and the upper plenum flashes. The flashing stops the rapid drop in primary system pressure and establishes a pseudo steady-state condition.

Natural Circulation Phase

After the primary system pressure reaches the pseudo steady-state condition at approximately [ ]^{a,b} seconds (75 seconds for NOTRUMP), the system transitions into the natural circulation phase. During the natural circulation phase, the rod bundle void fraction increases, which causes an increase in the void fraction in the upper plenum and hot legs.

The two-phase flow in the hot legs initiates the draindown of the SG U-tubes, since steam from the two-phase mixture collects at the top of the U-tubes. This stops the flow through the primary system.

When the CMT balance lines drain and the fluid near the top of the CMTs reaches saturation temperature, the CMTs convert from the circulation mode to the draindown mode of injection. This increases the cold injection flow and the rate of system pressure decay. This occurs at approximately [ ]^{a,b} seconds (420 seconds for NOTRUMP) for CMT-2 and [ ]^{a,b} seconds (385 seconds for NOTRUMP) for CMT-1. When system pressure drops to the saturation pressure for the upper head, the upper head begins to drain at [ ]^{a,b} seconds (75 seconds for NOTRUMP).

During the first [ ]^{a,b} seconds (548 seconds for NOTRUMP) of this event, [ ]^{a,b} lbm (1720 lbm for NOTRUMP) of water is discharged through the break while draining the pressurizer, the SG U-tubes, the upper head, the upper plenum above the hot leg, most of the cold legs, and approximately one quarter of the CMTs.

Automatic Depressurization System Phase

The ADS phase of the transient begins with the actuation of ADS-1 at [ ]^{a,b} seconds into the event (548 seconds for NOTRUMP). ADS-2 and ADS-3 occur within the next [ ]^{a,b} seconds.

ADS actuation increases the rate of primary system depressurization and results in a high level of injection flow from the accumulators. The rapid injection of cold fluid from the accumulators from approximately [ ]^{a,b} seconds into the event (535 to 770 seconds for NOTRUMP) temporarily reduces the boiling in the rod bundle and the void fractions in the rod bundle and the upper plenum. The pressurizer refills temporarily. When the accumulator discharge ends, the boiling intensity increases in the rod bundle, which results in increased void fractions.

During the period of ADS 1-3, which ends at ADS-4 actuation, approximately [ ]^{a,b} lbm (1025 lbm for NOTRUMP) of water is discharged from ADS-1, ADS-2, and ADS-3. The difference in ADS flow between the test and the simulation is due to the composition of the ADS flow. According to the test data, the flow is essentially liquid after approximately 250 seconds of two-phase flow, while the NOTRUMP simulation predicts two-phase flow out of the ADS until ADS-4 actuation. In addition, during the period of ADS 1-3, [ ]^{a,b} lbm of water (555 lbm for NOTRUMP) are discharged through the break. The higher break flow in NOTRUMP during this period is due to the accumulator water entering the cold legs and flowing out the break. The additional break flow calculated in the NOTRUMP simulation during the ADS phase compensates for the lower predicted ADS flow. After the accumulators empty and only the CMTs provide core injection, there is an increase in rod bundle void fraction. ADS-4 occurs at [ ]^{a,b} seconds, (1114 seconds for NOTRUMP) and the pressurizer water level falls. The fluid discharge through ADS-1, ADS-2, and ADS-3 essentially ends, and the fluid is discharged through ADS-4.

IRWST Injection Phase

At approximately [ ]^{a,b} seconds (1310 seconds for NOTRUMP), the system pressure has fallen below the pressure corresponding to the water elevation head of the IRWST. Flow from the IRWST enters the DVI line, and the IRWST injection phase begins. Shortly thereafter, the CMT flow drops significantly. The flow from the IRWST reduces the rod bundle boiling and partially refills the upper plenum above the hot-leg elevation. A steady flow of water is then flowing from the IRWST into the DVI line, through the rod bundle, and out of the primary system through ADS-4 and the break.

This test demonstrates that the rod bundle is fully covered by water or a two-phase mixture at all times during this event, and there is no indication of heater rod temperatures increasing due to lack of cooling. The NOTRUMP simulation also demonstrates no heater rod temperature increase.

8.3.1.2 Comparison of NOTRUMP Simulation to Test Data

Figure 8.3.1-2 shows the pressure at the top of the pressurizer for the test and the NOTRUMP simulation. Note that the test data shown for the low pressure region (right scale on figure) is taken from the narrow range pressure instrumentation while the high pressure region (left scale on figure) is taken from the wide range pressure instrumentation. The agreement between the test and the simulation is reasonable for the primary pressure response since the trends of the data are matched. The drop in pressure before ADS actuation is a result of vapor reaching and flowing through the break.

The primary system pressure decreases significantly at approximately [ ]^{a,b} seconds in the test as a result of ADS-1 actuation. For the NOTRUMP simulation, ADS-1 actuation occurs at 548 seconds. The trends of the pressure are the same once ADS-1 is actuated, with the timing of the remaining transient being shifted due to the difference in ADS-1 times between the test and the NOTRUMP simulation.

Figure 8.3.1-3 shows the collapsed liquid level in the pressurizer for the test and the NOTRUMP simulation. The break flow causes a rapid decrease in pressurizer level and empties the pressurizer at approximately [ ]^{a,b} seconds for the test and 50 seconds for the NOTRUMP simulation. The pressurizer level increases again with the opening of ADS-1 and the subsequent accumulator injection. The timing difference for the increase in pressurizer level between the test and the NOTRUMP simulation reflects the difference in ADS-1 actuation and accumulator injection times. In addition, substantially more mass accumulates in the pressurizer after ADS actuation in the test relative to the simulation.

Figure 8.3.1-4 shows the collapsed liquid levels in CMT-1 for the test and the NOTRUMP simulation. Figure 8.3.1-5 shows the collapsed liquid levels in CMT-2 for the test and the NOTRUMP simulation. In the test, CMT-1 transitions from the circulation mode to the draindown mode at about [ ]^{a,b} seconds and CMT-2 transitions at about [ ]^{a,b} seconds. In the simulation, CMT-1 transitions from

the circulation mode to the draindown mode at 385 seconds, and CMT-2 transitions at about 420 seconds. The delay in the transition to the draindown mode in NOTRUMP is a result of the temperature of the top fluid node in the simulation reaching saturation temperature at a later time compared to the relatively hot fluid layer near the top of the CMT in the test. In the simulation, the temperature of all of the fluid in the top fluid node, which represents 10 percent of the CMT volume, must reach saturation before flashing begins. Following the initial draindown period for the CMTs in the simulation, the levels increase when accumulator injection temporarily fills the cold legs and water flows up the balance line and into the CMT. The levels decrease again after the accumulators empty. The levels in both CMTs are predicted to increase following IRWST injection when the cold legs once again fill up and water flows up the CMT balance line into the CMTs. This behavior will be discussed further in subsequent paragraphs.

Figures 8.3.1-6 and 8.3.1-7 show the collapsed liquid levels in the hot side (upside) and the cold side (downside) of the SG-2 U-tubes for the test and the NOTRUMP simulation. Figures 8.3.1-8 and 8.3.1-9 show the same information for SG-1. There is reasonable agreement between the test and the simulation for the draining of the SG tubes. The balance line collapsed levels are shown in Figures 8.3.1-10 and 8.3.1-11. The levels remain at the top of the balance lines until the levels in the SG tubes decrease enough to allow vapor to reach the cold legs and migrate to the balance lines. Up to 1700 seconds, the general trends of the balance line collapsed levels are predicted by NOTRUMP, with a delay in the start of draining. This demonstrates that the PIRT items related to balance line-to-cold leg behavior and cold leg phase separation are predicted reasonably well. At approximately 1700 seconds, the balance lines are predicted to refill as the cold leg fills with water.

Figures 8.3.1-12 and 8.3.1-13 show the collapsed liquid levels in accumulator 1 and accumulator 2 for the test and the NOTRUMP simulation. In general, the predicted onset of full accumulator injection is delayed in comparison to the test results because of the delay in ADS-1 for the NOTRUMP simulation compared to the test.

The next series of plots, Figures 8.3.1-14 through 8.3.1-20, relate to the collapsed and two-phase levels at different locations in the vessel. For the test there is little change in the collapsed liquid level (see Figure 8.3.1-14) in the core, indicating low void fractions during the course of the test, as shown in Figure 8.3.1-17. NOTRUMP predicts higher void fractions, leading to a more substantial change in the collapsed liquid level during events such as accumulator injection. The level trends, however, are similar for the test and the simulation, with some differences in timing due to the shift in the ADS timing. In both the test and the simulation, the vessel levels initially decrease as inventory is lost from the system. The largest core collapsed level increase occurs when ADS-1 actuates, which lowers the system pressure, allowing the accumulators to inject at their maximum rate. Once the accumulators empty, the levels decrease as inventory is lost from the system. The levels drop until IRWST injection occurs following ADS-4 actuation. The collapsed and two-phase levels in the upper plenum are shown in Figures 8.3.1-15 and 8.3.1-16. Note that the test information for the collapsed upper plenum level does not represent the entire upper plenum. The instrumentation only provides information for the region just below the hot legs to the upper support plate. Valid instrumentation to measure the

entire upper plenum region level was unavailable. As a result, upper plenum collapsed level information below this region is unavailable for the test and Figure 8.3.1-15 indicates a straight line when the level drops below the bottom tap of the valid instrumentation. In addition, an accurate two-phase mixture level for the test data can not be calculated based on the available information. As such, only the NOTRUMP prediction for two-phase level is included in Figure 8.3.1-16. The upper plenum collapsed level plot shows that for the test, liquid accumulates in the upper plenum at ADS actuation. consistent with the increase in pressurizer mass. NOTRUMP shows less water flowing into the upper plenum. A plot of the core average void fraction for the test and the NOTRUMP simulation is provided (see Figure 8.3.1-17). This figure shows similar trends between the test and the simulation, with reduced voiding following the injection of the cold accumulator water and IRWST water.

Figure 8.3.1-18 shows the collapsed liquid level in the downcomer for the test and the NOTRUMP simulation. Although shifted in time, the predicted and test levels show the same trends, except following accumulator injection and ADS 1 actuation, when the test data indicates a level drop. This indication is questionable because the pressure difference from which the level is derived may be affected by the jet of flow issuing from the DVI line.

Figure 8.3.1-20 shows the collapsed liquid level in the upper head for the test and the corresponding NOTRUMP analysis. In the test, the upper head begins to drain at [ ]^{a,b} seconds, as the upper head fluid temperature quickly reaches the system saturation temperature. In the NOTRUMP simulation, the upper head starts to drain at about 75 seconds. One reason for this delay in draining is the time at which the upper head becomes saturated, which is affected by differences in system pressure, initial upper head temperature, and the upper head flow rates. The test indicates more mass in the upper head, consistent with the other indications in the upper plenum and pressurizer.

The next series of plots show the comparisons between the flows in the safety-related systems during the test and simulation.

Figure 8.3.1-21 shows the CMT-1 injection line mass flow rate for the test and the NOTRUMP simulation. Figure 8.3.1-22 shows the CMT-2 injection line mass flow rates. These figures show reasonable agreement between the test and the simulation with the test flow rate increasing sooner than the simulation because of the earlier start of drain of the CMTs in the test. The reasonable prediction of the CMT flows indicates that even though the timing of the CMT transition to draindown is different, the CMT balance line pressure drop and flow composition parameters identified in the PIRT are reasonably predicted by NOTRUMP.

Figure 8.3.1-23 shows the accumulator 1 injection line mass flow rates for the test and the NOTRUMP simulation. Figure 8.3.1-24 shows the accumulator 2 injection line mass flow rates. The prediction and the data are in reasonable agreement except for a slight shift in timing, demonstrating that this highly ranked PIRT item is reasonably predicted by NOTRUMP. The predicted onset of full

accumulator flow is delayed in comparison to the test results because of the delay in the actuation of ADS-1.

Figure 8.3.1-25 shows the IRWST-1 injection line mass flow rates for the test and the NOTRUMP simulation. Figure 8.3.1-26 shows the IRWST-2 injection line flow rates. The timing of IRWST injection is in good agreement between the test and the NOTRUMP simulation. The test reaches full flow at a slower rate than NOTRUMP due to slightly higher DVI line pressures in the test compared to the simulation. The agreement in IRWST flow initiation and flow rates after full flow is reached demonstrates that the highly ranked PIRT items of IRWST pool level and gravity draining are reasonably predicted by NOTRUMP.

Figure 8.3.1-27 shows the integrated mass flow through ADS stages 1 through 3 for the test and the NOTRUMP simulation. As discussed previously, the difference in the total integrated flow through ADS 1-3 results from fluid conditions in the pressurizer. According to the test data, ADS flow is liquid after a period of about 250 seconds of two-phase flow, while the NOTRUMP simulation predicts two-phase flow for the entire ADS 1-3 period. Figure 8.3.1-28 shows the integrated mass flow through ADS stage 4 for the test and the NOTRUMP simulation. These curves show reasonable agreement for the ADS flows once the delay in ADS actuation is accounted for. The agreement of these curves demonstrates that the PIRT highly ranked items related to ADS stage 4 (critical flow, two-phase pressure drop, and valve loss coefficients) are predicted well by NOTRUMP. Because of the difference in the pressurizer fluid conditions, which affects the composition of the ADS 1-3 flows, no conclusions can be drawn regarding the PIRT highly ranked items related to ADS stages 1-3.

Figure 8.3.1-29 shows the integrated mass flow out of the break for the test and the NOTRUMP simulation. The curves show reasonable agreement until ADS is actuated with the simulation slightly underpredicting the integrated flow rate. At the point of ADS actuation, the break flow is substantially reduced for the test. As discussed previously, the higher break flow in NOTRUMP during this period is due to the accumulator water entering the cold legs, allowing liquid to flow out the break. In the test, the accumulator injection increases the downcomer level but only a small amount of water enters the cold legs. As a result, there is little break flow following actuation of ADS in the test. Because of the difference in the flow composition at the break for the test and the simulation, no conclusions can be drawn for the PIRT highly ranked item of break critical flow.

Figure 8.3.1-30 shows the PRHR return line mass flow rate for the test and the corresponding NOTRUMP analysis. The simulation matches the data trends except in the time period from 100 to 250 seconds when the simulation underpredicts the flow. Figure 8.3.1-31 shows the PRHR inlet and outlet temperatures for the test and the NOTRUMP simulation. The simulation PRHR heat transfer is shown in Figure 8.3.1-32. There is no directly comparable data available from the test, so the plot only contains the simulation information. The PRHR heat transfer is expected to fall off in the test following ADS actuation, and it does so in the simulation. For the simulation, calculations for the PRHR nodes are turned off, and the nodes are removed from the system after ADS-3 is actuated (approximately 693 seconds for this simulation). This is done to enhance the speed of the calculations

given that the heat transfer is small. Once calculations for these nodes are turned off, the plotted value remains at the last calculated value, even though the actual heat transfer is zero. The PRHR inlet and outlet temperatures indicate that NOTRUMP underpredicts the PRHR heat transfer compared to the test.

Figure 8.3.1-33 shows temperatures at various elevations in CMT-1 for the test. Figure 8.3.1-34 shows temperatures for the four NOTRUMP fluid nodes representing CMT-1. The temperature profiles for CMT-2 are contained in Figures 8.3.1-35 and 8.3.1-36. A direct comparison between the NOTRUMP and test temperatures cannot be made because the NOTRUMP temperatures are averages over a region (the fluid node) while the test data are for distinct elevations; however, the trends can be compared. The agreement is reasonable between the test and the simulation with a slower heatup of the top node in the simulation because the fluid in the entire node must heat up. In contrast, the test data point is the temperature at a single elevation that heats up immediately when the hot layer of fluid passes it.

SG-related information is provided in Figures 8.3.1-37 through 8.3.1-39. Figure 8.3.1-37 shows the SG secondary pressures for the test and the NOTRUMP simulation. The NOTRUMP simulation secondary pressures are higher than the test for most of the transient. This is primarily due to not modeling the ambient heat losses; however, the effect of the higher pressures is insignificant on the primary-to-secondary heat transfer. The temperatures of the secondary side of the SGs are provided in Figure 8.3.1-38.

Figure 8.3.1-39 shows the collapsed SG levels for the test and the NOTRUMP simulation. The levels are initialized lower in the simulation than the test. The NOTRUMP simulation represents the secondary side as a single node, whereas the test represents a full recirculating SG design. This low level for the simulation is not important since the tubes remain covered with saturated water at all times, and therefore, the heat transfer characteristics are not significantly affected.

Figures 8.3.1-40 and 8.3.1-41 show the total DVI line flow rate for each of the DVI lines. The agreement between the test and the NOTRUMP simulation is reasonable for these parameters with the greatest difference being caused by the differences in timing between the test and the simulation.

Additional comparisons between the test and the NOTRUMP simulation that are provided include core inlet temperature (see Figure 8.3.1-42) and core outlet temperature (see Figure 8.3.1-43). Both the core inlet and outlet temperatures are higher for the simulation compared to the test.

The final two plots (see Figures 8.3.1-44 and 8.3.1-45), the integrated core inlet flow and the upper head bypass flow, only include the results of the simulation. There are no test data available for these items. They are included for completeness.

TABLE 8.3.1-1 SB18 SEQUENCE OF EVENTS			
Event	**Definition**	**OSU (seconds)**	**NOTRUMP (seconds)**
Break Opens		0	0
R Signal		0	0
S Signal		0.5	0
MFW Isolation Valve Closes		3.6	3.1
CMT Isolation Valves Open		6.1	5.6
RCPs Trip		9	6
CMT-1 Starts Draindown Phase	CMT level dropping and top of tank saturated	160	385
CMT-2 Starts Draindown Phase	CMT level dropping and top of tank saturated	355	420
ADS-1	CMT level 41in. + 15 sec	390	548
Accumulators Start		400	535
ADS-2	ADS-1 + 47 sec.	438	595
ADS-3	ADS-1 + 107 sec.	498	655
Accumulators Empty		665	770
ADS-4		950	1114
IRWST Injection		1226	1310

TABLE 8.3.1-2 FIGURES FOR OSU 2-IN. COLD LEG BREAK (SB18)	
Figure No.	**Title**
8.3.1-1	Facility Response Summary
8.3.1-2	Pressurizer Pressure
8.3.1-3	Pressurizer Level (Relative to Bottom Tap)
8.3.1-4	CMT-1 Level (Relative to Bottom Tap)
8.3.1-5	CMT-2 Level (Relative to Bottom Tap)
8.3.1-6	Steam Generator 2 Hot Side Collapsed Level (Relative to Bottom Tap)
8.3.1-7	Steam Generator 2 Cold Side Collapsed Level (Relative to Bottom Tap)
8.3.1-8	Steam Generator 1 Hot Side Collapsed Level (Relative to Bottom Tap)
8.3.1-9	Steam Generator 1 Cold Side Collapsed Level (Relative to Bottom Tap)
8.3.1-10	Cold Leg Balance Line 1 Levels (Relative to Bottom Tap)
8.3.1-11	Cold Leg Balance Line 2 Levels (Relative to Bottom Tap)
8.3.1-12	ACC-1 Level (Relative to Bottom Tap)
8.3.1-13	ACC-2 Level (Relative to Bottom Tap)
8.3.1-14	Core Collapsed Liquid Levels (Relative to Bottom of Lower Plenum)
8.3.1-15	Upper Plenum Collapsed Levels (Relative to Bottom of Lower Plenum)
8.3.1-16	NOTRUMP Upper Plenum 2-phase Level (Relative to Bottom of Lower Plenum)
8.3.1-17	Average Core Void Fraction
8.3.1-18	Collapsed Downcomer Levels (Relative to Bottom of Lower Plenum)
8.3.1-19	Not Applicable
8.3.1-20	Upper Head Collapsed Liquid Level (Relative to Bottom of Lower Plenum)
8.3.1-21	CMT-1 Injection Line Mass Flow
8.3.1-22	CMT-2 Injection Line Mass Flow
8.3.1-23	ACC-1 Injection Line Mass Flow
8.3.1-24	ACC-2 Injection Line Mass Flow
8.3.1-25	IRWST-1 Injection Line Mass Flow
8.3.1-26	IRWST-2 Injection Line Mass Flow
8.3.1-27	ADS Stage 1-3 Integrated Flows
8.3.1-28	ADS Stage 4 Integrated Total Flow
8.3.1-29	Integrated Break Flow
8.3.1-30	PRHR Return Line Mass Flow
8.3.1-31	PRHR Inlet and Exit Temperatures
8.3.1-32	NOTRUMP PRHR Heat Transfer Rate
8.3.1-33	Test CMT-1 Temperature Profile
8.3.1-34	NOTRUMP CMT-1 Temperature Profile
8.3.1-35	Test CMT-2 Temperature Profile

TABLE 8.3.1-2 (Cont.) FIGURES FOR OSU 2-IN. COLD LEG BREAK (SB18)	
Figure No.	**Title**
8.3.1-36	NOTRUMP CMT-2 Temperature Profile
8.3.1-37	Steam Generator Pressures
8.3.1-38	Steam Generator Secondary Fluid Temperatures
8.3.1-39	Steam Generator Secondary Liquid Levels (Relative to Top of Tube Sheet)
8.3.1-40	Total DVI Line 1 Flow
8.3.1-41	Total DVI Line 2 Flow
8.3.1-42	Core Inlet Temperatures
8.3.1-43	Core Outlet Temperatures
8.3.1-44	Integrated Core Inlet Flow
8.3.1-45	Upper Head Bypass Flow

Figures 8.3.1-1 through 8.3.1-45 are not included in the non-proprietary version of this report.

8.3.2 0.5-in. Cold Leg Break (SB23)

This test simulates a 0.5-in. break in the bottom of cold leg 3 and is performed without any nonsafety-related systems operating. A single failure of one of the two fourth-stage ADS valves on hot leg 1 is represented in the test.

8.3.2.1 Summary of Test and NOTRUMP Simulation Observations

The timing of the critical events for this transient in comparison with test results is reported in Table 8.3.2-1. Figure 8.3.2-1 shows primary system pressure during this test (as measured at the top of the pressurizer), with selected component actuation and plant responses shown in relation to primary system pressure. At the beginning of the test, the rod bundle heaters are shifted to power control mode and the power increases to the maximum level (600 kW) for 140 seconds followed by a decaying power function simulating the total decay energy input of AP600 nuclear fuel. The NOTRUMP simulation is initiated from a steady-state condition at a power level of 600 kW.

Initial simulations performed with the geometric break area yielded break flows that were approximately one half of those measured at the test facility. As a result, the break area was doubled for later simulations and reasonable agreement was obtained between the test data and the simulation break flows. Figure 8.3.2-29 shows the integrated break release information for the test simulation which used the modified NOTRUMP break modeling. This figure indicates that the adjusted break flow area reasonably represents the test break area. The reasons for this disparity in break flow performance have not been determined. The modified break area was used in all 0.5-in. simulations discussed below.

Two simulations are performed with the NOTRUMP code for the 0.5-in. cold leg break. The first is performed using the base model, which was created and used for all test simulations. The results obtained with this model show a significant delay in the prediction of ADS actuation compared to the test facility response for the 0.5 in. break. A few figures are provided to show the results of this simulation. Figure 8.3.2-2A presents the pressurizer pressure response for this simulation. A period of system re-pressurization is predicted to occur following system saturation prior to ADS actuation, which the test data did not exhibit. The reason for the re-pressurization can be traced to NOTRUMP's prediction of high core inlet temperature and excess steam generation compared to the test. This is partially caused by underpredicted PRHR heat removal and excessive thermal mixing in the CMT. This re-pressurization results in delayed CMT draining and subsequently delayed ADS actuation. ADS actuation is eventually achieved for the NOTRUMP simulation, without core uncovery, as seen in Figure 8.3.2-14A, which shows the predicted two-phase upper plenum mixture level. IRWST injection is also predicted to occur, as seen in Figure 8.3.2-26A, which indicates that a stable, long-term source of RCS makeup is attained that precludes possible core uncovery. As a consequence of the results obtained with the base model, the model was adjusted to provide a more accurate representation of the test facility for the 0.5-in. cold leg break, particularly to more accurately predict the core inlet

conditions. The model adjustments were primarily related to PRHR heat removal capabilities and CMT thermal stratification prediction improvements.

The adjusted model is used for a second simulation of the 0.5 in. break. This second simulation modifies the PRHR performance to more accurately reflect the test facility PRHR response. This is accomplished by artificially increasing the heat transfer area used to 125 percent of nominal. The initial CMT temperatures are also reduced, relative to the test data, to delay the predicted heating of the lower CMT node due to numerical diffusion that occurs as a result of the coarse CMT noding used in the NOTRUMP OSU facility model. These modifications lower the core inlet temperature and subsequently delay the onset of system saturation sufficiently to better predict ADS actuation. The subsequent detailed descriptions of the NOTRUMP code simulation are based on the adjusted model results. The reason for doing this is to more properly evaluate the other models important to the NOTRUMP predictions, recognizing that for this case the PRHR and CMT models failed to perform adequately.

Blowdown Phase

The blowdown phase is initiated with the opening of the break. An R signal occurs coincident with the break, and an S signal occurs 0.5 seconds later (the R and S signals occur simultaneously at time zero in the NOTRUMP simulation). The R and S signals initiate the following actions:

- The MSLIVs close
- The MFWIVs close
- The CMT injection valves open
- The PRHR return flow valve opens
- The RCPs trip

Note that this test indicates that a brief period of steam relief is required from the pressurizer to prevent system overpressurization. This is a result of the combination of the switch to power control mode, which increases heater rod output at transient initiation time, and the size of the simulated break. These two factors result in a brief pressure excursion in the primary system of the test facility. This period is not explicitly modeled in the simulation; however, the NOTRUMP steady-state pressurizer level was adjusted to account for the brief in-surge of liquid into the pressurizer to more accurately predict the time the pressurizer empties.

The circulation flow through the CMTs and flow through the PRHR begin immediately after the CMT injection valves and the PRHR return flow valve are opened. Due to the size of the simulated break, the depressurization rate is much smaller than for larger breaks. As a result, flashing of the rod bundle and upper plenum does not appear to occur until the ADS activation phase. Flashing first occurs in the upper head region and results in a decrease in the predicted RCS depressurization rate. Due to the size of the simulated break, a true pseudo steady-state condition, in which the RCS pressure stabilizes to slightly above the SG secondary pressures, was not observed. Instead, a continuous

depressurization of the primary system was observed as a result of the effectiveness of the PRHR and break in removing the energy being added by the heater rods. This condition can be defined as a stable subcooled natural circulation phase however; this condition continues to be defined as pseudo steady-state.

Natural Circulation Phase

After the primary system pressure reaches the pseudo steady-state condition at approximately [ ]^{a,b} seconds (200 seconds for NOTRUMP), the system transitions into the natural circulation phase. During the natural circulation phase, no significant voiding in the RCS vessel, other than the upper head, is predicted or observed to occur. The test information indicates that the SG-1 tubes begin to drain at approximately 1200 seconds, indicating a source of vapor flow has been encountered. This could be the result of flashing in the upper plenum, hot leg or SG, none of which are observed in the NOTRUMP simulations. SG-2 does not begin draining until near actuation of the ADS in both the test and NOTRUMP simulations.

This source of vapor in the SG-1 tubes initiates the draindown of the SG-1 U-tubes, since steam from the two-phase mixture collects at the top of the U-tubes. This ultimately serves to break natural circulation flow through this RCS loop. The NOTRUMP code continues to predict the existence of natural circulation flow in both RCS loops, indicating that no significant vapor generation source exists prior to ADS actuation that could provide vapor to the RCS hot legs and SGs. When system pressure drops to the saturation pressure for the upper head, the upper head begins to drain at [ ]^{a,b} seconds (800 seconds for NOTRUMP).

When the CMT balance lines begin to drain (resulting from balance line flashing), the CMTs have the ability to convert from circulation mode to intermittent circulation/draindown mode of injection. CMT draining can not commence prior to saturation of the upper regions. For the test, this can occur more rapidly than for the NOTRUMP code since NOTRUMP must saturate the fluid in the entire volume occupied by the upper fluid node. Sustained CMT draining can not occur without a continuous vapor source. This source is typically vapor flow from the cold leg balance lines into the CMTs.

The intermittent circulation/draindown mode of CMT injection increases the cold injection flow and the rate of system pressure decay. This occurs at approximately [ ]^{a,b} seconds (1165 seconds for NOTRUMP) for CMT-2 and [ ]^{a,b} seconds (1145 seconds for NOTRUMP) for CMT-1. Due to the depressurization characteristics observed in this test, a period of coincident CMT and accumulator flow was observed in both the test [ ]^{a,b} seconds and NOTRUMP simulation (1138 seconds) prior to ADS actuation due to the effectiveness of the passive systems in removing the heat being added from the primary heat sources (heater rods, RCS metal, and SG secondaries).

During the first [ ]^{a,b} seconds (2276 seconds for NOTRUMP) of this event, [ ]^{a,b} lbm (870 lbm for NOTRUMP) of water is discharged through the break while draining the pressurizer, upper head,

portions of the CMT balance lines, and approximately one quarter of the CMTs. In the test, the draining of SG-1 occurs during this period, which is not observed in the NOTRUMP simulation.

Automatic Depressurization System Phase

The ADS phase of the transient begins with the actuation of ADS-1 at [ ]^{a,b} seconds into the event (2276 seconds for NOTRUMP). ADS-2 and ADS-3 occur within the next [ ]^{a,b} seconds.

ADS actuation increases the rate of primary system depressurization and results in significant system flashing as well as a high level of injection flow from the accumulators. The rapid injection of cold fluid from the accumulators from approximately [ ]^{a,b} seconds into the event (2341 to 2583 seconds for NOTRUMP) temporarily minimizes the boiling in the rod bundle and the void fractions in the rod bundle and upper plenum. The pressurizer refills temporarily. When the accumulator discharge ends, the boiling intensity increases in the rod bundle, which results in increased void fractions.

During the period of ADS 1-3, which ends at ADS-4 actuation, approximately [ ]^{a,b} lbm (2250 lbm for NOTRUMP) of water is discharged from ADS-1, ADS-2, and ADS-3. Also during the period of ADS 1-3, [ ]^{a,b} lbm of water (110 lbm for NOTRUMP) are discharged through the break. The higher break flow in NOTRUMP during this period is due to the accumulator water entering the cold legs and flowing out the break. In the test, the accumulator injection increases the downcomer level but does not allow significant amounts of liquid to enter the cold legs. As a result, there is little break flow following actuation of ADS in the test. After the accumulators empty, and only the CMTs provide core injection, there is an increase in rod bundle void fraction. ADS-4 occurs at [ ]^{a,b} seconds, (2891 seconds for NOTRUMP) and the pressurizer water level falls. The fluid discharge through ADS-1, ADS-2, and ADS-3 essentially ends, and the fluid is discharged through ADS-4.

IRWST Injection Phase

At approximately [ ]^{a,b} seconds (3245 seconds for NOTRUMP), the system pressure has fallen below the pressure corresponding to the water elevation head of the IRWST. Flow from the IRWST enters the DVI line, and the IRWST injection phase begins. Shortly thereafter, CMT flow drops significantly. Flow from the IRWST reduces rod bundle boiling and partially refills the upper plenum above the hot leg elevation. Water then steadily flows from the IRWST into the DVI line, through the rod bundle, and out of the primary system through ADS-4 and the break.

This test demonstrates that the rod bundle is fully covered by water or a two-phase mixture at all times during this event, and there is no indication of heater rod temperatures increasing due to lack of cooling. The NOTRUMP simulation also demonstrates no heater rod temperature increase.

8.3.2.2 Comparison of NOTRUMP Simulation to Test Data

Figure 8.3.2-2 shows the pressure at the top of the pressurizer for the test and the NOTRUMP simulation. Note that the test data shown for the low pressure region (right scale on figure) is taken from the narrow range pressure instrumentation while the high pressure region (left scale on figure) is taken from the wide range pressure instrumentation. The agreement between the test and the simulation is reasonable for the primary pressure response since the trends of the data are matched. RCS depressurization prior to ADS actuation is driven primarily by heat removal via the PRHR HX.

The primary system pressure decreases significantly at approximately [ ]^{a,b} seconds in the test as a result of ADS-1 actuation. For the NOTRUMP simulation, ADS-1 actuation occurs at 2276 seconds. The trends of the pressure are the same following ADS-1 actuation between the test and the NOTRUMP simulation. The only observed difference in the pressure response is a direct result of the delay in achieving ADS-4 actuation in the NOTRUMP simulation, the cause of which is discussed later.

Figure 8.3.2-3 shows the collapsed liquid level in the pressurizer for the test and the NOTRUMP simulation. The break flow causes a gradual decrease in pressurizer level and empties the pressurizer at approximately [ ]^{a,b} seconds for the test and 550 seconds for the NOTRUMP simulation. The pressurizer level increases again with the opening of ADS-1 and the subsequent accumulator injection.

Figure 8.3.2-4 shows the collapsed liquid levels in CMT-1 for the test and the NOTRUMP simulation. Figure 8.3.2-5 shows the collapsed liquid levels in CMT-2 for the test and the NOTRUMP simulation. In the test, CMT-1 transitions from the circulation mode to the draindown mode at about [ ]^{a,b} seconds, and CMT-2 transitions at about [ ]^{a,b} seconds. In the NOTRUMP simulation, CMT-1 transitions from the circulation mode to the draindown mode at 1145 seconds, and CMT-2 transitions at about 1165 seconds. The differences in the transition to the draindown mode between NOTRUMP and the test are due to differences in the occurrence of upper CMT saturation and subsequent phase separation. The NOTRUMP simulation also forms a sustained level in the cold leg balance lines at approximately 1150 and 1180 seconds for CMT-1 and CMT-2, respectively; whereas the test forms an initial level at approximately the same time period but subsequently collapses the vapor space (see Figures 8.3.2-10 and 8.3.2-11). This results in the availability of a liquid source to the CMTs and in the test indicating CMT refill until a sustained balance line draining occurs at approximately 2000 seconds. The availability of vapor results in the formation of a sustained saturation layer in the CMT and provides a means for continuous draining to occur. The NOTRUMP simulation CMT levels temporarily stabilize during the accumulator injection phase as the cold legs temporarily refill and water flows up the balance line and into the CMTs. This interruption of the CMT draining process results in a delay in the receipt of the ADS-4 actuation signal. The CMTs re-commence draining following the emptying of the accumulators. The levels in both CMTs increase late in the simulation following IRWST injection when the cold legs once again fill up and water flows up the CMT balance line into the CMTs. Although the test plots do not show this for the period presented, they eventually demonstrate the same phenomenon after 4000 seconds.

Figures 8.3.2-6 and 8.3.2-7 show the collapsed liquid levels in the hot side (upside) and the cold side (downside) of the SG-1 U-tubes for the test and the NOTRUMP simulation. Figures 8.3.2-8 and 8.3.2-9 show the same information for SG-2. Typically the draining of the SG tubes affects the time of transition from the circulation mode to the draindown mode in the CMTs. Until the SG tube levels decrease sufficiently to allow the formation of cold leg levels, the cold leg balance lines primarily remain filled. Once a level is formed in the cold legs, sustained balance line draining occurs, allowing a sustained vapor source to reach the CMTs. The transition from the circulation mode to the draindown mode in the CMTs does not occur until the upper CMT saturates and the cold leg balance line liquid flow into the CMT ceases. The SG tube levels decrease slower in the NOTRUMP simulation compared to the test, causing a delay in cold leg draining and a corresponding delay in the balance line draining. In the simulation, the NOTRUMP code does not predict the onset of draining of either SG tube bundle until after ADS actuation. The test indicates that a vapor source exists in RCS loop 1, thereby allowing the SG-1 tubes to drain. In the simulation, the upper CMT and upper balance line nodes heat and subsequently saturate without the draining of the SG tubes or cold legs due to the prolonged CMT circulation period. The collapsed balance line levels are shown in Figures 8.3.2-10 and 8.3.2-11.

The prediction of the balance line drain times demonstrates that the PIRT items related to balance line-to-cold leg behavior and cold leg phase separation are predicted reasonably well. The comparison of Figures 8.3.2-10 and 8.3.2-11 and the prediction of CMT levels in Figures 8.3.2-4 and 8.3.2-5 indicate that even though the timing of the CMT transition to drain-down is different, the CMT balance line pressure drop and flow composition parameters identified in the PIRT are reasonably predicted by NOTRUMP.

Figures 8.3.2-12 and 8.3.2-13 show the collapsed liquid levels in accumulator 1 and accumulator 2 for the test and the NOTRUMP simulation. Both the test and the simulation indicate a period of coincident accumulator/CMT injection prior to ADS actuation. This differs from the trends seen in larger break sizes but is consistent with that observed in the simulation of the SPES 1-in. cold leg break. In general, the predicted accumulator injection following ADS actuation is similar between the simulation and the test.

The next series of plots, Figures 8.3.2-14 through 8.3.2-20, relate to the collapsed and two-phase levels at different locations in the vessel. For the test there is little change in the collapsed liquid level (see Figure 8.3.2-14) in the core, indicating small void fractions during the course of the test, as shown in Figure 8.3.2-17. NOTRUMP predicts slightly higher void fractions leading to a more substantial change in the collapsed liquid level during events such as accumulator injection. The level trends, however, are similar for the test and the simulation, with some differences in timing due to the shift in the ADS-4 actuation. In both the test and the simulation, no significant decrease in vessel levels occurs until sufficient inventory is depleted from the system and saturation of the vessel regions begin. Due to the nature of the 0.5-in. cold leg break, the NOTRUMP simulation indicates that the majority of the RCS remains subcooled prior to ADS actuation. The core collapsed level in the test and the NOTRUMP simulation, does not decrease until after ADS actuation occurs. The levels decrease until

IRWST injection occurs following ADS-4 actuation. Similar trends occur in the collapsed and two-phase levels in the upper plenum (see Figures 8.3.2-15 and 8.3.2-16). It should be noted that the test information for the collapsed upper plenum level does not represent the entire upper plenum. The instrumentation only provides information for the region just below the hot legs to the upper support plate. Valid instrumentation with which to measure the entire upper plenum region, was unavailable. As a result, upper plenum collapsed level information below this region is unavailable for the test and Figure 8.3.2-15 indicates a straight line when the level drops below the bottom tap of the valid instrumentation. In addition, an accurate two-phase mixture level for the test data can not be calculated based on the available information. As such, only the NOTRUMP prediction for two-phase level is included in Figure 8.3.2-16. A plot of the core average void fraction for the test and the NOTRUMP simulation is provided (see Figure 8.3.2-17). This figure shows similar trends between the test and the simulation, with reduced voiding during the injection of the cold accumulator water and IRWST water.

Figure 8.3.2-18 shows the collapsed liquid level in the downcomer for the test and the NOTRUMP simulation. The trends seen in the downcomer level are similar up to the point of ADS-4 actuation and subsequent IRWST injection. Because ADS-4 actuation and subsequent IRWST injection is delayed relative to the test in the NOTRUMP simulation, the collapsed downcomer levels diverge at this point. However, following IRWST injection, the observed and predicted levels re-converge. The delay in ADS-4 is the result of CMT refill, which occurs during the accumulator injection period for the NOTRUMP simulation. Elimination of this delay would result in excellent agreement between the test and NOTRUMP simulation. Again there is reasonable agreement between the test and the simulation, demonstrating that the highly ranked PIRT items related to the levels in the core, upper plenum, and downcomer are predicted reasonably well by NOTRUMP.

Figure 8.3.2-20 presents the collapsed liquid level in the upper head for the test and the corresponding NOTRUMP simulation. In the test and simulation, the upper head drains as the upper head fluid temperature reaches saturation conditions. This occurs at [ ]^{a,b} seconds in the test and 695 seconds in the NOTRUMP simulation. Upper head draining is affected by differences in initial upper head temperature and the upper head flow rates. Once upper head draining begins, the characteristics are reasonably represented by NOTRUMP.

The next series of plots show the comparisons between the flows in the safety-related systems during the test and simulation.

Figures 8.3.2-21 and 8.3.2-22 show the CMT-1 and CMT-2 injection line mass flow rates, respectively, for the test and the NOTRUMP simulation. These figures show reasonable agreement between the test and the simulation.

Figures 8.3.2-23 and 8.3.2-24 show the accumulator 1 and accumulator 2 injection line mass flow rates, respectively, for the test and the NOTRUMP simulation. The prediction and the data are in

reasonable agreement, demonstrating that this highly ranked PIRT item is reasonably predicted by NOTRUMP.

Figures 8.3.2-25 and 8.3.2-26 show the IRWST-1 and IRWST-2 injection line mass flow rates, respectively, for the test and the NOTRUMP simulation. Subsequent to the initial delay in IRWST injection as a result in the ADS-4 actuation delay for the NOTRUMP simulation, the trends observed between the test and NOTRUMP are in reasonable agreement. The test and the simulation results are similar, with the test reaching full flow at a slower rate due to slightly higher DVI line pressures in the test compared to the simulation. The agreement in IRWST flow rates demonstrates that the highly ranked PIRT items of IRWST pool level and gravity draining are reasonably predicted by NOTRUMP.

Figure 8.3.2-27 shows the integrated mass flow through ADS 1-3 for the test and the NOTRUMP simulation. The differences between the test and NOTRUMP simulation are due primarily to the differences in the ADS-4 actuation times. This results in additional inventory being depleted via the ADS 1-3 valves in NOTRUMP as they remain effective for a longer period of time. Accounting for this ADS delay, this demonstrates that the PIRT highly ranked items related to ADS 1-3 (critical flow, two-phase pressure drop, and valve loss coefficients) are well represented by the NOTRUMP code. Figure 8.3.2-28 shows the integrated mass flow through ADS-4 for the test and the NOTRUMP simulation. These curves show reasonable agreement for the ADS flows once the delay in ADS-4 actuation is accounted for. The agreement of these curves demonstrates that the PIRT highly ranked items related to ADS-4 (critical flow, two-phase pressure drop, and valve loss coefficients) are predicted well by NOTRUMP.

Figure 8.3.2-29 shows the integrated mass flow out of the break for the test and the NOTRUMP simulation. The curves show reasonable agreement until ADS is actuated, with the simulation slightly underpredicting the integrated flow rate. At the point of ADS actuation, the break flow is substantially reduced for the test and NOTRUMP simulation. Some additional break flow is predicted to occur in the simulation as a result of accumulator water entering the cold legs, allowing liquid to flow out the break. In the test, the accumulator injection increases the downcomer level, but only a small amount of water enters the cold legs. As a result, there is little additional break flow following actuation of ADS in the test. Again, it must be noted that the NOTRUMP break area was adjusted to achieve the results observed at the facility. The cause of these differences has not been determined.

Figure 8.3.2-30 shows the PRHR return line mass flow rate for the test and the corresponding NOTRUMP analysis. These are in reasonable agreement. Figure 8.3.2-31 shows the PRHR inlet and outlet temperatures for the test and the NOTRUMP simulation. These show that the same general trends are followed. It should be noted, however, that the heat transfer surface area was increased by 25 percent to achieve this agreement. For the simulation, calculations for the PRHR nodes are turned off and the nodes are removed from the system after ADS-3 is actuated (approximately 2382.7 seconds for this simulation). This is done to enhance code execution and does not have a significant impact on the results since the predicted PRHR heat transfer following ADS-3 actuation is small. Once calculations for these nodes are turned off, the plotted value remains at the last calculated value, even

though the actual heat transfer is zero. Figure 8.3.7-32 presents the NOTRUMP PRHR heat removal rate for this simulation. There is no directly comparable data available from the test, so the plot only contains the simulation information.

Figure 8.3.2-33 shows temperatures at various elevations in CMT-1 for the test and Figure 8.3.2-34 shows temperatures for the four NOTRUMP fluid nodes representing CMT-1. A direct comparison between Figures 8.3.2-33 and 8.3.2-34 cannot be made because the NOTRUMP temperatures are averages over a region while the test data are for distinct elevations; however, the trends can be compared. The agreement is reasonable between the test and the simulation with the differences in the heatup and saturation of the top node resulting in different CMT drain performance. The temperature profiles for CMT-2 are contained in Figures 8.3.2-35 and 8.3.2-36. Relating this information to the CMT-related PIRT items, the temperature agreement at the top of the tank indicates reasonable NOTRUMP code prediction for the natural circulation between the CMT and the cold leg balance line. Due to the nature of this test, the prediction of thermal stratification in the CMT is relatively important since it ultimately affects core inlet temperatures and subsequently the time at which core voiding is predicted to occur. The NOTRUMP code significantly underpredicts the time at which the CMT injection temperature increases resulting in significantly warmer conditions in the DVI line and subsequently the lower plenum and core. This indicates that thermal stratification is not well represented by NOTRUMP for breaks as small as the 0.5 in. cold leg break.

SG-related information is provided in Figures 8.3.2-37 through 8.3.2-39. Figure 8.3.2-37 shows the SG secondary pressures for the test and the NOTRUMP simulation. The NOTRUMP simulation secondary pressures are higher than the test for most of the transient. This is primarily due to not modeling the ambient heat losses; however, the effect of the higher pressures is insignificant on the primary to secondary heat transfer. The temperatures of the secondary side of the SGs are provided in Figure 8.3.2-38.

Figure 8.3.2-39 shows the collapsed SG levels for the test and the NOTRUMP simulation. The levels are initialized lower in the simulation than the test. The NOTRUMP simulation represents the secondary side as a single node, whereas the test represents a full recirculating SG design. This low level for the simulation is not important since the tubes remain covered with saturated water at all times, and therefore, the heat transfer characteristics are not significantly affected.

Figures 8.3.2-40 and 8.3.2-41 show the total DVI line flow rates for each of the DVI lines. The agreement between the test and the NOTRUMP simulation is reasonable for these parameters, with the greatest difference being caused by the differences in timing between the test and the simulation.

Additional comparisons between the test and the NOTRUMP simulation that are provided include core inlet temperature (see Figure 8.3.2-42) and core outlet temperature (see Figure 8.3.2-43). Both the core inlet and outlet temperatures are higher for the simulation compared to the test and may be indicative of higher simulated flows through the core than observed for the test, as well as the lack of a thermal stratification model.

The final two plots (see Figures 8.3.2-44 and 8.3.2-45), the integrated core inlet flow, and the upper head bypass flow only include the results of the simulation. There are no test data available for these items. They are included for completeness.

TABLE 8.3.2-1 SB23 SEQUENCE OF EVENTS			
Event	**Definition**	**OSU (seconds)**	**NOTRUMP (seconds)**
Break Opens		0	0
R Signal		0	0
S Signal		0.5	0
MFW Isolation Valve Closes		3.6	3.1
CMT Isolation Valves Open		6.1	5.6
RCPs Trip		8.8	6
CMT-1 Starts Draindown Phase	CMT level dropping and top of tank saturated	1190	1145
CMT-2 Starts Draindown Phase	CMT level dropping and top of tank saturated	2270	1165
ADS-1	CMT level 41 in. + 15 sec	2262	2276
Accumulators Start	Low Flow Period (Pre-ADS) High Flow Period (Post-ADS)	1340 2280	1138 2341
ADS-2	ADS-1 + 47 sec.	2310	2323
ADS-3	ADS-1 + 107 sec.	2372	2383
Accumulators Empty		2700	2583
ADS-4		2575	2891
IRWST Injection		2980	3245

TABLE 8.3.2-2 FIGURES FOR OSU 0.5-IN. COLD LEG BREAK (SB23)	
Figure No.	**Title**
8.3.2-1	Facility Response Summary
8.3.2-2	Pressurizer Pressure
8.3.2-2A	Pressurizer Pressure (Base NOTRUMP Model)
8.3.2-3	Pressurizer Level (Relative to Bottom Tap)
8.3.2-4	CMT-1 Level (Relative to Bottom Tap)
8.3.2-5	CMT-2 Level (Relative to Bottom Tap)
8.3.2-6	Steam Generator 2 Hot Side Collapsed Level (Relative to Bottom Tap)
8.3.2-7	Steam Generator 2 Cold Side Collapsed Level (Relative to Bottom Tap)
8.3.2-8	Steam Generator 1 Hot Side Collapsed Level (Relative to Bottom Tap)
8.3.2-9	Steam Generator 1 Cold Side Collapsed Level (Relative to Bottom Tap)
8.3.2-10	Cold Leg Balance Line 1 Levels (Relative to Bottom Tap)
8.3.2-11	Cold Leg Balance Line 2 Levels (Relative to Bottom Tap)
8.3.2-12	ACC-1 Level (Relative to Bottom Tap)
8.3.2-13	ACC-2 Level (Relative to Bottom Tap)
8.3.2-14	Core Collapsed Liquid Levels (Relative to Bottom of Lower Plenum)
8.3.2-14A	Core Mixture Level (Base NOTRUMP Model)
8.3.2-15	Upper Plenum Collapsed Levels (Relative to Bottom of Lower Plenum)
8.3.2-16	NOTRUMP Upper Plenum 2-phase Level (Relative to Bottom of Lower Plenum)
8.3.2-17	Average Core Void Fraction
8.3.2-18	Collapsed Downcomer Levels (Relative to Bottom of Lower Plenum)
8.3.2-19	Not Applicable
8.3.2-20	Upper Head Collapsed Liquid Level (Relative to Bottom of Lower Plenum)
8.3.2-21	CMT-1 Injection Line Mass Flow
8.3.2-22	CMT-2 Injection Line Mass Flow
8.3.2-23	ACC-1 Injection Line Mass Flow
8.3.2-24	ACC-2 Injection Line Mass Flow
8.3.2-25	IRWST-1 Injection Line Mass Flow
8.3.2-26	IRWST-2 Injection Line Mass Flow
8.3.2-26A	IRWST Injection Line Mass Flows (Base NOTRUMP Model)
8.3.2-27	ADS Stage 1-3 Integrated Flows
8.3.2-28	ADS Stage 4 Integrated Total Flow
8.3.2-29	Integrated Break Flow
8.3.2-30	PRHR Return Line Mass Flow
8.3.2-31	PRHR Inlet and Exit Temperatures
8.3.2-32	NOTRUMP PRHR Heat Transfer Rate
8.3.2-33	Test CMT-1 Temperature Profile

TABLE 8.3.2-2 (Cont.) FIGURES FOR OSU 0.5-IN. COLD LEG BREAK (SB23)	
Figure No.	**Title**
8.3.2-34	NOTRUMP CMT-1 Temperature Profile
8.3.2-35	Test CMT-2 Temperature Profile
8.3.2-36	NOTRUMP CMT-2 Temperature Profile
8.3.2-37	Steam Generator Pressures
8.3.2-38	Steam Generator Secondary Fluid Temperatures
8.3.2-39	Steam Generator Secondary Liquid Levels (Relative to Top of Tube Sheet)
8.3.2-40	Total DVI Line 1 Flow
8.3.2-41	Total DVI Line 2 Flow
8.3.2-42	Core Inlet Temperatures
8.3.2-43	Core Outlet Temperatures
8.3.2-44	Integrated Core Inlet Flow
8.3.2-45	Upper Head Bypass Flow

Figures 8.3.2-1 through 8.3.2-45 are not included in the non-proprietary version of this report.

8.3.3 2-in. Direct Vessel Injection Line Break (SB13)

This test simulates a 2-in. break in DVI line 1 and is performed without any nonsafety-related systems operating. A single failure of one of the two fourth-stage ADS valves on hot leg 1 is represented in the test.

8.3.3.1 Summary of Test and NOTRUMP Simulation Observations

The timing of the critical events for this transient in comparison with the test results is reported in Table 8.3.1-1. Figure 8.3.1-1 shows primary system pressure during this test (as measured at the top of the pressurizer), with selected component actuations and plant responses shown in relation to primary system pressure. At the beginning of the test, the reactor heaters are shifted to power control mode, and the power increases to the maximum level (600 kW) for 140 seconds followed by a decaying power function simulating the total decay energy input of APó00 nuclear fuel. The simulation is started from a steady-state condition at a power level of 600 kW.

Blowdown Phase

The blowdown phase is initiated with the opening of the break. An R signal occurs coincident with the break, and an S signal occurs 0.5 seconds later (the R and S signals occur simultaneously at time zero in the NOTRUMP simulation). The R and S signals initiate the following actions:

- The MSLIVs close
- The MFWIVs shut off
- The CMT injection valves open
- The PRHR return flow valve opens
- The RCPs trip

The circulation flow through the CMTs and flow through the PRHR begin immediately after the CMT injection valves and the PRHR return flow valve are opened. Due to the rapid loss of pressure down to saturation pressure for the rod bundle and upper plenum, boiling begins and the upper plenum flashes. The flashing stops the rapid drop in primary system pressure and establishes a pseudo steady-state condition.

Natural Circulation Phase

After the primary system pressure reaches the pseudo steady-state condition at approximately [ ]^{a,b} seconds (65 seconds for NOTRUMP), the system transitions into the natural circulation phase. During the natural circulation phase, the rod bundle void fraction increases, which causes voiding in the upper plenum and hot legs

The two-phase flow in the hot legs initiates the draindown of the SG U-tubes by allowing steam from the two-phase mixture to collect at the top of the U-tubes.

When the CMT balance lines drain and the fluid near the top of the CMTs reaches saturation temperature, the CMTs convert from the circulation mode to the draindown mode of injection. This occurs at approximately [ ]^{a,b} seconds (234 seconds for NOTRUMP) for CMT-1 and [ ]^{a,b} seconds (255 seconds for NOTRUMP) for CMT-2. When system pressure drops to the saturation pressure for the upper head, the upper head begins to drain at [ ]^{a,b} seconds (65 seconds for NOTRUMP).

During the first [ ]^{a,b} seconds (334 seconds for NOTRUMP) of this event, [ ]^{a,b} lbm (1958 lbm for NOTRUMP) of water is discharged through the break while draining the pressurizer, the SG U-tubes, the upper head, the upper plenum above the hot leg, most of the cold legs, and approximately one quarter of the CMTs.

Automatic Depressurization System Phase

The ADS phase of the transient begins with the actuation of ADS-1 at [ ]^{a,b} seconds into the event (334 seconds for NOTRUMP). ADS-2 and ADS-3 occur within the next [ ]^{a,b} seconds.

The ADS actuation increases the rate of primary system depressurization and results in accumulator injection. The accumulators inject from approximately [ ]^{a,b} seconds (353 to 540 seconds for NOTRUMP). Immediately following ADS actuation, boiling increases in the rod bundle and the void fractions in the rod bundle and upper plenum increase. Once the cold fluid from the accumulators reaches the rod bundle, boiling is temporarily reduced along with the void fractions through the rod bundle and the upper plenum. The pressurizer refills temporarily. When the accumulator discharge ends, the boiling intensity increases, which results in increased void fractions.

During the period of ADS 1-3, which ends at ADS-4 actuation, [ ]^{a,b} lbm (300 lbm for NOTRUMP) of water is discharged from ADS-1, ADS-2, and ADS-3. The difference in ADS flow between the test and the simulation is due to the composition of the ADS flow. According to the test data, the flow is two-phase throughout this period, while the NOTRUMP simulation predicts all vapor flow for approximately one third of the period. In addition, during the period of ADS 1-3, [ ]^{a,b} lbm of water (880 lbm for NOTRUMP) are discharged through the break. After the accumulators empty and only the CMTs provide core injection, there is an increase in rod bundle void fraction. ADS-4 occurs at [ ]^{a,b} seconds (594 seconds for NOTRUMP) and the pressurizer water level falls. The fluid discharge through ADS-1, ADS-2, and ADS-3 essentially ends, and fluid discharge through ADS-4 begins.

IRWST Injection Phase

At approximately [ ]^{a,b} seconds (860 seconds for NOTRUMP), the pressure in DVI line 1 with the break on it has fallen below the pressure corresponding to the water elevation head of the IRWST.

Flow from the IRWST enters DVI line 1 and the IRWST injection phase begins. This occurs about 100 seconds later for DVI line 2. Shortly after IRWST injection begins, the CMT flow drops significantly. The flow from the IRWST reduces the rod bundle boiling slightly. A steady flow of water then flows from the IRWST into the DVI line, through the rod bundle, and out of the primary system through ADS-4 and the break.

This test demonstrates that the rod bundle is fully covered by water or a two-phase mixture at all times during this event, and there is no indication of heater rod temperatures increasing due to lack of cooling. The NOTRUMP simulation also demonstrates no heater rod temperature increase.

8.3.3.2 Comparison of NOTRUMP Simulation to Test Data

Figure 8.3.3-2 shows the pressure at the top of the pressurizer for the test and the NOTRUMP simulation. Note that the test data shown for the low pressure region (right scale on figure) is taken from the narrow range pressure instrumentation while the high pressure region (left scale on figure) is taken from the wide range pressure instrumentation. The agreement between the test and the simulation is reasonable for the primary pressure response since the trends of the data are matched. The simulation pressure is lower than the test for the initial phase of the transient out to ADS-1. The lower simulation pressure in this period is due to the pressurizer draining earlier, resulting in an earlier formation of a hot leg level and vapor flow into the PRHR. This enhances the PRHR heat removal in the simulation, allowing the pressure to decrease below the test pressure.

The primary system pressure decreases significantly at approximately [ ]^{a,b} seconds in the test as a result of ADS-1 actuation. For the NOTRUMP simulation, ADS-1 actuation occurs at 334 seconds. The trends of the pressure are the same once ADS-1 is actuated.

Figure 8.3.3-3 shows the collapsed liquid level in the pressurizer for the test and the NOTRUMP simulation. The break flow causes a rapid decrease in pressurizer level and empties the pressurizer at approximately [ ]^{a,b} seconds in the test (50 seconds for NOTRUMP). The pressurizer level increases again with the opening of ADS-1 and the subsequent accumulator injection. Substantially more mass accumulates in the pressurizer for the test than is predicted in the simulation. This affects ADS flows as will be discussed later.

Figure 8.3.3-4 shows the collapsed liquid levels in CMT-1 for the test and the NOTRUMP simulation. Figure 8.3.3-5 shows the collapsed liquid levels in CMT-2 for the test and the NOTRUMP simulation. In the test, CMT-1 transitions from the circulation mode to the draindown mode at [ ]^{a,b} seconds and CMT-2 transitions at about [ ]^{a,b} seconds. In the simulation, CMT-1 transitions from the circulation mode to the draindown mode at about 234 seconds and CMT-2 transitions at about 255 seconds. The delay in the transition to the draindown mode in NOTRUMP is a result of the temperature of the top fluid node in the simulation reaching saturation temperature at a later time compared to the relatively hot fluid layer near the top of the CMT in the test. In the simulation, the

temperature of all of the fluid in the top fluid node, which represents 10 percent of the CMT volume, must reach saturation before flashing begins.

Figures 8.3.3-6 and 8.3.3-7 show the collapsed liquid levels in the hot side (upside) and the cold side (downside) of the SG-2 U-tubes for the test and the NOTRUMP simulation. Figures 8.3.3-8 and 8.3.3-9 show the same information for SG-1. There is reasonable agreement between the test and the simulation for the draining of the tubes with the simulation draining earlier than the test. The balance line collapsed liquid levels are shown in Figures 8.3.3-10 and 8.3.3-11. The levels remain at the top of the balance lines until the levels in the SG tubes decrease enough to allow vapor to reach the cold legs and migrate to the balance lines. These plots show reasonable agreement between the test and the simulation, which demonstrates that the PIRT items related to balance line-to-cold leg behavior and cold leg phase separation are predicted reasonably well by NOTRUMP.

Figures 8.3.3-12 and 8.3.3-13 show the collapsed liquid levels in accumulator 1 and accumulator 2 for the test and the NOTRUMP simulation. The predicted onset of accumulator injection is nearly the same in the NOTRUMP simulation as compared to the test due to the similar timing of ADS-1 actuation.

The next series of plots, Figures 8.3.3-14 through 8.3.3-20, relate to the collapsed and two-phase levels at different locations in the vessel. There is reasonable agreement between the NOTRUMP simulation and the test. Figure 8.3.3-14 shows the core collapsed liquid level for the test and the NOTRUMP simulation. In both cases, the level initially decreases as inventory is lost from the system. Once significant boiling occurs in the core, the collapsed level drops. This occurs for a short period of time following actuation of ADS-1. The collapsed level increases a short time later when the cold accumulator water, which is injected because of the decreasing pressure, reaches the core region and lowers the void fraction. Once the accumulators empty, the levels decrease as inventory is lost from the system. The levels drop until IRWST injection occurs following ADS-4 actuation. The collapsed and two-phase levels in the upper plenum are shown in Figures 8.3.3-15 and 8.3.3-16. Note that the test information for the collapsed upper plenum level does not represent the entire upper plenum. The instrumentation only provides information for the region just below the hot legs to the upper support plate. Valid instrumentation to measure the entire upper plenum region level was unavailable. As a result, upper plenum collapsed level information below this region is unavailable for the test and Figure 8.3.3-15 indicates a straight line when the level drops below the bottom tap of the valid instrumentation. In addition, an accurate two-phase mixture level for the test data can not be calculated based on the available information. As such, only the NOTRUMP prediction for two-phase level is included in Figure 8.3.4-16. The test data indicates that liquid accumulates in the upper plenum following ADS actuation, consistent with the increase in pressurizer mass. A plot of the core average void fraction for the test and the NOTRUMP simulation is provided (see Figure 8.3.3-17). This figure shows similar trends between the test and the simulation with void collapse following the injection of the cold accumulator water and IRWST water.

Figures 8.3.3-18 and 8.3.3-19 provide plots of the collapsed level in the downcomer for the test and the NOTRUMP simulation. The prediction and the test levels show similar trends, with the prediction being higher for much of the transient.

The agreement between the test and the simulation for the core, upper plenum, and downcomer levels demonstrates that these highly ranked PIRT items are reasonably predicted by NOTRUMP.

Figure 8.3.3-20 shows the collapsed liquid level in the upper head for the test and the corresponding NOTRUMP analysis. Both start to drain at [ ]^{a,b} seconds when the temperature of the fluid in the head reaches saturation. The test indicates more mass in the upper head for the test, consistent with the other indications in the upper plenum and pressurizer.

The next series of plots show the comparisons between the flows in the safety-related systems during the test and simulation.

Figure 8.3.3-21 shows the CMT-1 injection line mass flow rate for the test and the NOTRUMP simulation. Figure 8.3.3-22 shows the CMT-2 injection line mass flow rates. The flows from CMT-1 are higher during circulation phase than the CMT-2 flows because of the break located on DVI line 1. The prediction and the data are in reasonable agreement, demonstrating that the CMT balance line pressure drop and flow composition parameters identified in the PIRT are reasonably predicted by NOTRUMP.

Figure 8.3.3-23 shows the accumulator 1 injection line mass flow rates for the test and the NOTRUMP simulation. Figure 8.3.3-24 shows the accumulator 2 injection line mass flow rates. The prediction and the data are in reasonable agreement, demonstrating that this highly ranked PIRT item is reasonably predicted by NOTRUMP.

Figure 8.3.3-25 shows the IRWST-1 injection line mass flow rates for the test and the NOTRUMP simulation. Figure 8.3.3-26 shows the IRWST-2 injection line flow rates. The timing of IRWST injection is earlier in the simulation compared to the test due to the earlier ADS-4 actuation in NOTRUMP. Once the difference in ADS-4 actuation time is accounted for, the predicted IRWST flows show reasonable agreement with the test data. The agreement in IRWST flow rates demonstrates that the highly ranked PIRT items of IRWST pool level and gravity draining are reasonably predicted by NOTRUMP.

Figure 8.3.3-27 shows the integrated mass flow through ADS stages 1 through 3 for the test and the NOTRUMP simulation. As noted previously, the difference in the total integrated flow through ADS 1-3 results from fluid conditions in the pressurizer. According to the test data, ADS flow is two-phase throughout the ADS 1-3 period, while the NOTRUMP simulation predicts all vapor flow for approximately one third of the period. Figure 8.3.3-28 shows the integrated mass flow through ADS stage 4 for the test and the NOTRUMP simulation. These curves show reasonable agreement once the delay in ADS-4 actuation is accounted for. The agreement of these curves demonstrates that the PIRT

highly ranked items related to ADS stage 4 (critical flow, two-phase pressure drop, and valve loss coefficients) are predicted well by NOTRUMP. Because of the difference in the pressurizer fluid conditions, which affects the composition of the ADS 1-3 flows, no conclusions can be drawn regarding the PIRT highly ranked items related to ADS stages 1-3.

Figure 8.3.3-29 shows the integrated mass flow out of the break for the test and the NOTRUMP simulation. The simulation shows higher break flow early in the transient. This is caused by NOTRUMP predicting a lower temperature in the DVI node with the break on it compared to the test. The lower temperature in the simulation results in higher density and increased break flow. Even with the difference, the agreement is reasonable for this PIRT item.

Figure 8.3.3-30 shows the PRHR return line mass flow rate for the test and the corresponding NOTRUMP analysis. The NOTRUMP initially overpredicts the flow rate, in the first 40 seconds of the transient, then underpredicts the flow rate in the next 100 seconds. After approximately 140 seconds, there is good agreement between the simulation and the test.

Figure 8.3.3-31 shows the PRHR inlet and outlet temperatures for the test and the NOTRUMP simulation. These show that the same general trends are followed; however, the simulation removes less energy from the primary system via the PRHR HX than is removed in the test. The simulation PRHR heat transfer is shown in Figure 8.3.3-32. There is no directly comparable data available from the test, so the plot only contains the simulation information. The PRHR heat transfer is expected to fall off in the test following ADS actuation, and it does so in the simulation. For the simulation, calculations for the PRHR nodes are turned off and the nodes are removed from the system shortly after ADS-3 is actuated (445 seconds for this simulation). This is done to enhance the speed of the calculations given that the expected heat transfer is small. Once calculations for these nodes are turned off, the plotted value remains at the last calculated value even though the actual heat transfer is zero. That is why the NOTRUMP simulation plot shows a constant value after 445 seconds.

Figure 8.3.3-33 shows temperatures at various elevations in CMT-1 for the test. Figure 8.3.3-34 shows temperatures for the four NOTRUMP fluid nodes representing CMT-1. The temperature profiles for CMT-2 are contained in Figures 8.3.3-35 and 8.3.3-36. A direct comparison between the NOTRUMP and test temperatures cannot be made because the NOTRUMP temperatures are averages over a region (the fluid node) while the test data are for distinct elevations; however, the trends can be compared. The agreement is reasonable between the test and the simulation with a slower heatup of the top node in the simulation because the fluid in the entire node must heat up. In contrast, the test data point is the temperature at a single elevation that heats up immediately when the hot layer of fluid passes it.

SG-related information is provided in Figures 8.3.3-37 through 8.3.3-39. Figure 8.3.3-37 shows the SG secondary pressures for the test and the NOTRUMP simulation. The NOTRUMP simulation pressures are higher than the test for most of the transient. This is primarily due to not modeling the ambient heat losses; however, the effect of the higher pressures is insignificant on the primary-to-

secondary heat transfer. The temperatures of the secondary side of the SGs are provided in Figure 8.3.3-38.

Figure 8.3.3-39 shows the collapsed SG levels for the test and the NOTRUMP simulation. The levels are initialized lower in the simulation than the test. The NOTRUMP simulation represents the secondary side as a single node whereas the test represents a full recirculating SG design. This low level for the simulation is not important since the tubes remain covered with water at all times and therefore the heat transfer characteristics are not significantly affected.

Figures 8.3.3-40 and 8.3.3-41 show the total DVI line flow rate for each of the DVI lines. The agreement between the test and the NOTRUMP simulation is reasonable for these parameters.

Additional comparisons between the test and the NOTRUMP simulation that are provided include core inlet temperature (see Figure 8.3.3-42) and core outlet temperature (see Figure 8.3.3-43). The core inlet temperatures are higher for the simulation for most of the transient. The core outlet temperatures show good agreement.

The final two plots (see Figures 8.3.3-44 and 8.3.3-45), the integrated core inlet flow and the upper head bypass flow, only include the results of the simulation. There are no test data available for these items. They are included for completeness.

TABLE 8.3.3-1
SB13 SEQUENCE OF EVENTS

Event	Definition	OSU (seconds)	NOTRUMP (seconds)
Break Opens		0	0
R Signal		0	0
S Signal		0.5	0
MFW Isolation Valve Closes		3.6	3.1
CMT Isolation Valves Open		6.1	5.6
RCPs Trip		8	6
CMT-1 Starts Draindown Phase	CMT level dropping and top of tank saturated	125	234
CMT-2 Starts Draindown Phase	CMT level dropping and top of tank saturated	150	255
ADS-1	CMT level 41in. + 15 sec	319	334
Accumulators Start		346	353
ADS-2	ADS-1 + 47 sec.	366	381
ADS-3	ADS-1 + 107 sec.	426	441
Accumulators Empty		620	540
ADS-4		668	594
IRWST Injection		870	860

TABLE 8.3.3-2 FIGURES FOR OSU 2-IN. DVI LINE BREAK (SB13)	
Figure No.	**Title**
8.3.3-1	Facility Response Summary
8.3.3-2	Pressurizer Pressure
8.3.3-3	Pressurizer Level (Relative to Bottom Tap)
8.3.3-4	CMT-1 Level (Relative to Bottom Tap)
8.3.3-5	CMT-2 Level (Relative to Bottom Tap)
8.3.3-6	Steam Generator 2 Hot Side Collapsed Level (Relative to Bottom Tap)
8.3.3-7	Steam Generator 2 Cold Side Collapsed Level (Relative to Bottom Tap)
8.3.3-8	Steam Generator 1 Hot Side Collapsed Level (Relative to Bottom Tap)
8.3.3-9	Steam Generator 1 Cold Side Collapsed Level (Relative to Bottom Tap)
8.3.3-10	Cold Leg Balance Line 1 Levels (Relative to Bottom Tap)
8.3.3-11	Cold Leg Balance Line 2 Levels (Relative to Bottom Tap)
8.3.3-12	ACC-1 Level (Relative to Bottom Tap)
8.3.3-13	ACC-2 Level (Relative to Bottom Tap)
8.3.3-14	Core Collapsed Liquid Levels (Relative to Bottom of Lower Plenum)
8.3.3-15	Upper Plenum Collapsed Levels (Relative to Bottom of Lower Plenum)
8.3.3-16	NOTRUMP Upper Plenum 2-phase Level (Relative to Bottom of Lower Plenum)
8.3.3-17	Average Core Void Fraction
8.3.3-18	Collapsed Downcomer Levels (Relative to Bottom of Lower Plenum)
8.3.3-19	Not Applicable
8.3.3-20	Upper Head Collapsed Level (Relative to Bottom of Lower Plenum)
8.3.3-21	CMT-1 Injection Line Mass Flow
8.3.3-22	CMT-2 Injection Line Mass Flow
8.3.3-23	ACC-1 Injection Line Mass Flow
8.3.3-24	ACC-2 Injection Line Mass Flow
8.3.3-25	IRWST-1 Injection Line Mass Flow
8.3.3-26	IRWST-2 Injection Line Mass Flow
8.3.3-27	ADS Stage 1-3 Integrated Flows
8.3.3-28	ADS Stage 4 Integrated Total Flow
8.3.3-29	Integrated Break Flow
8.3.3-30	PRHR Return Line Mass Flow
8.3.3-31	PRHR Inlet and Exit Temperatures
8.3.3-32	NOTRUMP PRHR Heat Transfer Rate
8.3.3-33	Test CMT-1 Temperature Profile
8.3.3-34	NOTRUMP CMT-1 Temperature Profile
8.3.3-35	Test CMT-2 Temperature Profile

TABLE 8.3.3-2 (Cont.) FIGURES FOR OSU 2-IN. DVI LINE BREAK (SB13)	
Figure No.	**Title**
8.3.3-36	NOTRUMP CMT-2 Temperature Profile
8.3.3-37	Steam Generator Pressures
8.3.3-38	Steam Generator Secondary Fluid Temperatures
8.3.3-39	Steam Generator Secondary Liquid Levels (Relative to Top of Tube Sheet)
8.3.3-40	Total DVI Line 1 Flow
8.3.3-41	Total DVI Line 2 Flow
8.3.3-42	Core Inlet Temperatures
8.3.3-43	Core Outlet Temperatures
8.3.3-44	Integrated Core Inlet Flow
8.3.3-45	Upper Head Bypass Flow

Figures 8.3.3-1 through 8.3.3-45 are not included in the non-proprietary version of this report.

8.3.4 Double-Ended Guillotine Direct Vessel Injection Line Break (SB12)

This test simulates a double-ended guillotine (DEG) break in direct vessel injection line 1 and is performed without any nonsafety-related systems operating. A single failure of one ADS-1 valve and one ADS-3 valve is represented in the test.

8.3.4.1 Summary of Test and NOTRUMP Simulation Observations

The timing of the critical events for this transient in comparison with test results is reported in Table 8.3.4-1. Figure 8.3.4-1 shows primary system pressure during this test (as measured at the top of the pressurizer), with selected component actuations and plant responses shown in relation to primary system pressure. At the beginning of the test, the rod bundle heaters are shifted to power control mode, and the power increases to the maximum level (600 kW) for 140 seconds followed by a decaying power function simulating the total decay energy input of AP600 nuclear fuel. The simulation is started from a steady-state condition at a power level of 600 kW.

Blowdown Phase

The blowdown phase is initiated with the opening of the break. An R signal occurs coincident with the break, and an S signal occurs 0.5 seconds later (the R and S signals occur simultaneously at time zero in the NOTRUMP simulation). The R and S signals initiate the following actions:

- The MSLIVs close
- The MFWIVs shut off
- The CMT injection valves open
- The PRHR return flow valve opens
- The RCPs trip

The circulation flow through the CMTs and flow through the PRHR begin immediately after the CMT injection valves and the PRHR return flow valve are opened. Due to the rapid loss of pressure down to saturation pressure for the rod bundle and upper plenum, boiling begins and the upper plenum flashes. The flashing stops the rapid drop in primary system pressure and establishes a brief pseudo steady-state condition.

Natural Circulation Phase

After the primary system pressure reaches the pseudo steady-state condition, the system transitions into the natural circulation phase. During the natural circulation phase, the rod bundle void fraction increases, which causes an increase in the void fraction in the upper plenum and hot legs.

The two-phase flow in the hot legs initiates the draindown of the SG U-tubes, since steam from the two-phase mixture collects at the top of the U-tubes. This stops the natural circulation flow through the primary system.

When the CMT balance lines start to drain and the fluid near the top of the CMTs reaches saturation temperature, the CMTs convert from the circulation mode to the draindown mode of injection. This occurs at approximately [ ]^{a,b} seconds (30 seconds for NOTRUMP) for CMT-1 and [ ]^{a,b} seconds (150 seconds for NOTRUMP) for CMT-2. The injection flow from CMT-1 exits the system through the break due to the break location. The draining of CMT-1 causes ADS-1 actuation at [ ]^{a,b} seconds into the event (89 seconds for NOTRUMP). When system pressure drops to the saturation pressure for the upper head, the upper head begins to drain at [ ]^{a,b} seconds (40 seconds for NOTRUMP).

Due to the large break size and location, the system rapidly depressurizes and accumulator 1 begins injecting water within [ ]^{a,b} seconds (6 seconds for NOTRUMP). The water from accumulator 1 enters DVI line 1 and exits the system through the break. Accumulator 2 begins injecting water into DVI line 2 at [ ]^{a,b} seconds for both the test and the simulation.

During the first [ ]^{a,b} seconds (89 seconds for NOTRUMP) of this event, [ ]^{a,b} lbm (1218 lbm for NOTRUMP) of water are discharged through the break on the vessel side. The higher break flow in the simulation is due to the code predicting a higher system pressure than the test in the first 100 seconds of the transient and a slightly lower temperature for the fluid in the vicinity of the vessel side of the break.

Automatic Depressurization System Phase

The ADS phase of the transient begins with the actuation of ADS-1 at [ ]^{a,b} seconds into the event (89 seconds for NOTRUMP). ADS-2 and ADS-3 occur within the next [ ]^{a,b} seconds.

The ADS actuation increases the rate of primary system depressurization and results in a high level of injection flow from the accumulators. The injection of cold water from accumulator 2 occurs from [ ]^{a,b} seconds into the transient (107 to 307 seconds for NOTRUMP). After the cold water injected from accumulator 2 flows into the core, there is a reduction in the boiling in the rod bundle and the void fractions through the rod bundle and the upper plenum. The pressurizer partially refills.

During the period of ADS 1-3, which ends at ADS-4 actuation, approximately [ ]^{a,b} lbm (56 lbm for NOTRUMP) of water are discharged from ADS-1, ADS-2, and ADS-3. The difference in the ADS flow between the test and the simulation is due to the composition of the flow. According to the test data, the flow is two-phase for most of the period, while the NOTRUMP simulation predicts all vapor out of the ADS for the entire period until ADS-4 actuation. In addition, during the period of ADS 1-3, [ ]^{a,b} lbm of water (199 lbm for NOTRUMP) are discharged through the break. ADS-4

occurs at [ ]^{a,b} seconds (269 seconds for NOTRUMP). The fluid discharge through ADS-1, ADS-2, and ADS-3 decreases and eventually ends, and the fluid is discharged through ADS-4.

IRWST Injection Phase

At approximately [ ]^{a,b} seconds (380 seconds for NOTRUMP), the system pressure has fallen below the pressure corresponding to the water elevation head of the IRWST. Flow from the IRWST enters DVI line 2 and the IRWST injection phase begins. The flow from the IRWST reduces the rod bundle boiling and partially refills the upper plenum above the hot-leg elevation. A steady flow of water then flows from the IRWST into the DVI line, through the rod bundle, and out of the primary system through ADS-4 and the break.

This test demonstrates that the rod bundle is fully covered by water or a two-phase mixture at all times during this event, and there is no indication of heater rod temperatures increasing due to lack of cooling. The NOTRUMP simulation also demonstrates no heater rod temperature increase.

8.3.4.2 Comparison of NOTRUMP Simulation to Test Data

Figure 8.3.4-2 shows the pressure at the top of the pressurizer for the test and the NOTRUMP simulation. Note that the test data shown for the low pressure region (right scale on figure) is taken from the narrow range pressure instrumentation while the high pressure region (left scale on figure) is taken from the wide range pressure instrumentation. The pressure decreases initially due to the blowdown through the break. The depressurization rate slows (and stops for NOTRUMP) when the primary system becomes saturated. Following actuation of ADS-1 at [ ]^{a,b} seconds in the test (89 seconds for NOTRUMP), the depressurization rate increases significantly. NOTRUMP predicts a higher pressure for most of the time prior to ADS-1 actuation. The agreement between the test data and the prediction is reasonable for the primary pressure response since the trends of the data are similar.

Figure 8.3.4-3 shows the collapsed liquid level in the pressurizer for the test and the NOTRUMP simulation. The break flow causes a rapid decrease in pressurizer level and empties the pressurizer at approximately [ ]^{a,b} seconds for the test and 10 seconds for the NOTRUMP simulation. The pressurizer level increases again after a delay following ADS actuation for both the test and the simulation; however, the delay between ADS actuation and the increase in the pressurizer level is longer for the simulation. The pressurizer collapsed level decreases rapidly in the simulation following ADS-4 actuation, while the test data indicates that the pressurizer empties at a slower rate.

Figure 8.3.4-4 shows the collapsed liquid levels in CMT-1 for the test and the NOTRUMP simulation. Figure 8.3.4-5 shows the collapsed liquid levels in CMT-2 for the test and the corresponding NOTRUMP analysis. In the test, CMT-1, which is attached to the broken DVI line begins draining out the break at [ ]^{a,b} seconds. NOTRUMP starts the drain slightly earlier at 30 seconds, but matches the draindown behavior closely. CMT-2 transitions to draindown at about [ ]^{a,b} seconds (150 seconds

in the simulation). The delay in the transition to the draindown mode for CMT-2 in NOTRUMP compared to the test is a result of the top fluid node in the simulation reaching saturation temperature at a later time compared to the relatively hot fluid layer near the top of the CMT in the test. This delay also affects the draindown behavior because the draindown starts prior to accumulator 2 injection for the test, and after the start of accumulator 2 injection in the simulation. In the simulation, there is no significant CMT-2 injection until the accumulator empties since the accumulator injection prevents the start of CMT-2 injection.

Figures 8.3.4-6 and 8.3.4-7 show the collapsed liquid levels in the hot side (upside) and the cold side (downside) of the SG-2 U-tubes for the test and the NOTRUMP simulation. Figures 8.3.4-8 and 8.3.4-9 show the same information for SG-1. There appears to be erroneous data for the lower levels for SG-2 for the test as there is no reason for the tubes not to completely drain. While the final absolute levels are questionable, these data are believed to be adequate for comparing the time of tube draining. The NOTRUMP levels drain slightly earlier than the test data, however, the comparison is reasonable. The balance line collapsed levels are shown in Figures 8.3.4.10 and 8.3.4.11. The level behavior is similar for balance line 1 until the draindown starts. After the start of draindown, the test level stops draining and after a 100 seconds of relatively stable level, refills. The test eventually drains significantly at approximately 300 seconds. This difference in draining behavior between the test and the simulation does not significantly affect the transient because the draining of CMT-1 is well predicted for actuation of ADS-1 and the behavior of balance line 1 is not important after the CMT drains. There is good agreement between the test and the simulation for balance line 2. The general trends of the balance line level are predicted by NOTRUMP, demonstrating that the PIRT items related to balance line-to-cold leg behavior and cold leg phase separation are predicted reasonably well.

Figures 8.3.4-12 and 8.3.4-13 show the collapsed liquid levels in accumulator 1 and accumulator 2 for the test and the NOTRUMP simulation. The comparison between the test and the NOTRUMP simulation is good for both accumulators.

The next series of plots, Figures 8.3.4-14 through 8.3.4-20, relate to the collapsed and two-phase levels at different locations in the vessel. The trends of the simulation plots are in good agreement with the test. In both cases, the core level initially decreases as inventory is lost from the system. The levels increase following accumulator injection. Once the accumulators empty, the levels continue to increase as a result of CMT-2 injection and IRWST-2 injection. There is not much change throughout the transient in the collapsed and two-phase levels in the upper plenum (see Figures 8.3.4-15 and 8.3.4-16). Note that the test information for the collapsed upper plenum level does not represent the entire upper plenum. The instrumentation only provides information for the region just below the hot legs to the upper support plate. Valid instrumentation to measure the entire upper plenum region level was unavailable. As a result, upper plenum collapsed level information below this region is unavailable for the test and Figure 8.3.4-15 indicates a straight line when the level drops below the bottom tap of the valid instrumentation. In addition, an accurate two-phase mixture level for the test data can not be calculated based on the available information. As such, only the NOTRUMP

prediction for two-phase level is included in Figure 8.3.4-16. A plot of the core average void fraction is provided as Figure 8.3.4-17. This figure shows lower predicted void fractions during the ADS period.

Figures 8.3.4-18 shows the collapsed liquid level in the downcomer for the test and the NOTRUMP simulation. Again there is reasonable agreement between the test and the simulation, with NOTRUMP predicting a slightly higher collapsed liquid level. These comparisons demonstrate that the highly ranked PIRT items related to the levels in the core, upper plenum, and downcomer are predicted reasonably well by NOTRUMP.

Figure 8.3.4-20 shows the collapsed liquid level in the upper head for the test and the corresponding NOTRUMP analysis. In the test, the upper head begins to drain at [ ]^{a,b} seconds, as the upper head fluid temperature reaches the system saturation temperature. In the NOTRUMP simulation, the upper head starts to drain at about 40 seconds. The test indicates more mass in the upper head, consistent with the other indications in the upper plenum and pressurizer.

The next series of plots show the comparisons between the flows in the safety-related systems during the test and simulation.

Figures 8.3.4-21 and 8.3.4-22 show the CMT injection line mass flow rates for CMT-1 and CMT-2 for the simulation only. The test data are invalid and is not provided because the flows are greater than the maximum flow rate of the flow meter for almost the entire draining period. After the draining period, the data are invalid because the meters cannot measure steam flow. The flow rates in the test and the simulation for CMT-1 must be in reasonable agreement since there is good agreement in the CMT-1 levels.

Figure 8.3.4-23 shows the accumulator 1 injection line mass flow rates for the test and the NOTRUMP simulation. Figure 8.3.4-24 shows the accumulator 2 injection line mass flow rates. For accumulator 1, there are differences in the plots between the test and the simulation, however the trends are matched with both starting injection within [ ]^{a,b} seconds and then stopping injection for a brief time around 100 seconds before eventually injecting again. Figure 8.3.4-24 shows good agreement between the test data and the prediction, demonstrating that this highly ranked PIRT item is reasonably well predicted by NOTRUMP.

Figure 8.3.4-25 shows the IRWST-1 injection line mass flow rates for the test and the NOTRUMP simulation. Figure 8.3.4-26 shows the IRWST-2 injection line flow rates. For injection line 1, which is attached to the broken DVI line, NOTRUMP predicts a delay in the start of IRWST injection. Once the test and the simulation are both injecting, the test shows a slightly higher flow rate. For injection line 2, the start of IRWST injection is predicted well by NOTRUMP. For this line, the test reaches full flow at a slower rate than NOTRUMP due to slightly higher DVI line pressures in the test compared to the simulation. The agreement in IRWST flow rates demonstrates that the highly ranked PIRT items of IRWST pool level and gravity draining are reasonably well predicted by NOTRUMP.

Figure 8.3.4-27 shows the integrated mass flow through ADS stages 1 through 3 for the test and the NOTRUMP simulation. As was discussed previously, the difference in the total integrated flow from ADS 1-3 results in the fluid conditions in the pressurizer. According to the test data, the flow is two-phase for most of the period, while the NOTRUMP simulation predicts all vapor out of the ADS for the entire period until ADS-4 actuation. Figure 8.3.4-28 shows the integrated mass flow through ADS stage-4 for the test and the NOTRUMP simulation. These curves show that the ADS stage-4 flow is underpredicted by NOTRUMP immediately after the valves are opened. For ADS stage-4, the simulation shows mostly vapor passing through the valves, however the test data indicates that when the valves first open, a significant amount of liquid passes through the valves. After the initial difference in flows between the test and the simulation, the flows match reasonably well as indicated by the parallel behavior of the integrated flow curves. This agreement in the slope of the curves demonstrates that the PIRT highly ranked items related to ADS stage-4 (critical flow, two-phase pressure drop, and valve loss coefficients) are predicted well by NOTRUMP. Because of the difference in the pressurizer fluid conditions, which affects the composition of the ADS 1-3 flows, no conclusions can be drawn regarding the PIRT highly ranked items related to ADS stages 1-3.

Figure 8.3.4-29 shows the integrated mass flow out of the break for the test and the NOTRUMP simulation. The higher break flow in the simulation is due to the code predicting a higher system pressure than the test in the first 100 seconds of the transient and a slightly lower temperature for the fluid in the vicinity of the vessel side of the break. The higher break flow observed in the NOTRUMP calculation leads to a lower mass in the pressurizer and more rapid pressurizer draining. This, in turn, leads to a high steam quality ADS flow. Although the integrated break flow is overpredicted by NOTRUMP, the general trends of the test break flow are similar to the prediction. This demonstrates that the PIRT highly ranked item of break critical flow can be predicted by NOTRUMP.

Figure 8.3.4-30 shows the PRHR return line mass flow rate for the test and the corresponding NOTRUMP analysis. These are in reasonable agreement. Figure 8.3.4-31 shows the PRHR inlet and outlet temperatures for the test and the NOTRUMP simulation. These indicate that NOTRUMP underpredicts the heat transfer. The heat transfer is shown for the simulation in Figure 8.3.4-32. There is no directly comparable data available from the test so the plot only contains the simulation information. The PRHR heat transfer is expected to fall off significantly in the test following ADS actuation, and it does so in the simulation. For the simulation, calculations for the PRHR nodes are turned off and the nodes are removed from the system after ADS-3 is actuated (250 seconds for this simulation). This is done to enhance the speed of the calculations given that the expected heat transfer is small. Once calculations for these nodes are turned off, the plotted values for inlet flow and inlet and outlet temperatures remain at the last calculated value, even though the actual heat transfer is zero.

Figure 8.3.4-33 shows temperatures at various elevations in CMT-1 for the test. Figure 8.3.4-34 shows temperatures for the four NOTRUMP fluid nodes representing CMT-1. The temperature profiles for CMT-2 are contained in Figures 8.3.4-35 and 8.3.4-36. A direct comparison between the test temperatures and the NOTRUMP temperatures cannot be made because the NOTRUMP

temperatures are averages over a region while the test data are for distinct elevations; however, the trends can be compared. The temperatures for CMT-1 show reasonable agreement. The temperatures for CMT-2 also show reasonable agreement with a slower heatup of the top node in the simulation because the fluid in the entire node must heat up. In contrast, the test data point is the temperature at a single elevation that heats up immediately when the hot layer of fluid passes it.

SG-related information is provided in Figures 8.3.4-37 through 8.3.4-39. Figure 8.3.4-37 shows the SG pressures for the test and the NOTRUMP simulation. The NOTRUMP simulation secondary pressures are higher than the test for most of the transient. This is primarily due to not modeling the ambient heat losses; however, the effect of the higher pressures is insignificant. The temperatures of the secondary side of the SGs are provided in Figure 8.3.4-38.

Figure 8.3.4-39 shows the collapsed SG levels for the test and the NOTRUMP simulation. The levels are initialized lower in the simulation than the test. The NOTRUMP simulation represents the secondary side as a single node, whereas the test represents a full recirculating SG design. This low level for the simulation is not important since the tubes remain covered with water at all times, and therefore, the heat transfer characteristics are not significantly affected.

Figures 8.3.4-40 and 8.3.4-41 show the total DVI line flow rate for each of the DVI lines for the simulation only. The test data are invalid and are not provided because some of the flows added together to get the total flow are greater than the maximum measurement capability of the flow meter.

Additional comparisons between the test and the NOTRUMP simulation that are provided include core inlet temperature (see Figure 8.3.4-42) and core outlet temperature (see Figure 8.3.4-43). The core inlet temperature is higher in the simulation after the first 300 seconds of the transient, while the outlet temperature is predicted reasonably well.

The final two plots (see Figures 8.3.4-44 and 8.3.4-45), the integrated core inlet flow and the upper head bypass flow, only include the results of the simulation. There are no test data available for these items. They are included for completeness.

TABLE 8.3.4-1 SB12 SEQUENCE OF EVENTS			
Event	**Definition**	**OSU (seconds)**	**NOTRUMP (seconds)**
Break Opens		0	0
R Signal		0.5	0
S Signal		0.5	0
MFW Isolation Valve Closes		3.6	3.1
CMT Isolation Valves Open		6	5.6
RCPs Trip		8	6
CMT-1 Starts Draindown Phase	CMT level dropping and top of tank saturated	60	30
CMT-2 Starts Draindown Phase	CMT level dropping and top of tank saturated	70	150
ADS-1	CMT level 41 in. + 15 sec	91	89
Accumulators Start	Accumulator 1 Accumulator 2	2 107	6 107
ADS-2	ADS-1 + 47 sec	139	136
ADS-3	ADS-1 + 107 sec	200	196
Accumulators Empty	Accumulator 1 Accumulator 2	240 317	274 307
ADS-4		255	269
IRWST Injection	IRWST-1 IRWST-2	250 360	317 380

TABLE 8.3.4-2 FIGURES FOR OSU DOUBLE-ENDED DIRECT VESSEL INJECTION LINE BREAK (SB12)	
Figure No.	**Title**
8.3.4-1	Facility Response Summary
8.3.4-2	Pressurizer Pressure
8.3.4-3	Pressurizer Level (Relative to Bottom Tap)
8.3.4-4	CMT-1 Level (Relative to Bottom Tap)
8.3.4-5	CMT-2 Level (Relative to Bottom Tap)
8.3.4-6	Steam Generator 2 Hot Side Collapsed Level (Relative to Bottom Tap)
8.3.4-7	Steam Generator 2 Cold Side Collapsed Level (Relative to Bottom Tap)
8.3.4-8	Steam Generator 1 Hot Side Collapsed Level (Relative to Bottom Tap)
8.3.4-9	Steam Generator 1 Cold Side Collapsed Level (Relative to Bottom Tap)
8.3.4-10	Cold Leg Balance Line 1 Levels (Relative to Bottom Tap)
8.3.4-11	Cold Leg Balance Line 2 Levels (Relative to Bottom Tap)
8.3.4-12	ACC-1 Level (Relative to Bottom Tap)
8.3.4-13	ACC-2 Level (Relative to Bottom Tap)
8.3.4-14	Core Collapsed Liquid Levels (Relative to Bottom of Lower Plenum)
8.3.4-15	Upper Plenum Collapsed Levels (Relative to Bottom of Lower Plenum)
8.3.4-16	NOTRUMP Upper Plenum 2-phase Levels (Relative to Bottom of Lower Plenum)
8.3.4-17	Average Core Void Fraction
8.3.4-18	Collapsed Downcomer Levels (Relative to Bottom of Lower Plenum)
8.3.4-19	Not Applicable
8.3.4-20	Upper Head Collapsed Liquid Level (Relative to Bottom of Lower Plenum)
8.3.4-21	NOTRUMP CMT-1 Injection Line Mass Flow
8.3.4-22	NOTRUMP CMT-2 Injection Line Mass Flow
8.3.4-23	ACC-1 Injection Line Mass Flow
8.3.4-24	ACC-2 Injection Line Mass Flow
8.3.4-25	IRWST-1 Injection Line Mass Flow
8.3.4-26	IRWST-2 Injection Line Mass Flow
8.3.4-27	ADS Stage 1-3 Integrated Flows
8.3.4-28	ADS Stage 4 Integrated Total Flow
8.3.4-29	Integrated Break Flow Vessel Side Only
8.3.4-30	PRHR Return Line Mass Flow
8.3.4-31	PRHR Inlet and Exit Temperatures
8.3.4-32	NOTRUMP PRHR Heat Transfer Rate
8.3.4-33	Test CMT 1 Temperature Profile
8.3.4-34	NOTRUMP CMT 1 Temperature Profile
8.3.4-35	Test CMT 2 Temperature Profile

TABLE 8.3.4-2 (Cont.) FIGURES FOR OSU DOUBLE-ENDED DIRECT VESSEL INJECTION LINE BREAK (SB12)	
Figure No.	**Title**
8.3.4-36	NOTRUMP CMT 2 Temperature Profile
8.3.4-37	Steam Generator Pressures
8.3.4-38	Steam Generator Secondary Fluid Temperatures
8.3.4-39	Steam Generator Secondary Liquid Levels (Relative to Top of Tube Sheet)
8.3.4-40	NOTRUMP Total DVI Line 1 Flow
8.3.4-41	NOTRUMP Total DVI Line 2 Flow
8.3.4-42	Core Inlet Temperatures
8.3.4-43	Core Outlet Temperatures
8.3.4-44	Integrated Core Inlet Flow
8.3.4-45	Upper Head Bypass Flow

Figures 8.3.4-1 through 8.3.4-45 are not included in the non-proprietary version of this report.

8.3.5 2-in. Cold Leg Balance Line Break (SB09)

This test simulates a 2-in. break in cold leg 3 to CMT-1 balance line and is performed without any nonsafety-related systems operating. A single failure of one of the two fourth-stage ADS valves on hot leg 1 is represented in the test.

8.3.5.1 Summary of Test and NOTRUMP Simulation Observations

The timing of the critical events for this transient in comparison with test results is reported in Table 8.3.5-1. Figure 8.3.5-1 shows primary system pressure during this test (as measured at the top of the pressurizer), with selected component actuations and plant responses shown in relation to primary system pressure. At the beginning of the test, the rod bundle heaters are shifted to power control mode, and the power is maintained at the maximum level (600 kW) for 140 seconds followed by a decaying power function simulating the total decay energy input of AP600 nuclear fuel. The simulation is started from a steady-state condition at a power level of 600 kW.

Blowdown Phase

The blowdown phase is initiated with the opening of the break. An R signal occurs coincident with the break, and an S signal occurs 0.5 seconds later (the R and S signals occur simultaneously at time zero in the NOTRUMP simulation). The R and S signals initiate the following actions:

- The MSLIVs close
- The MFWIVs shut off
- The CMT injection valves open
- The PRHR return flow valve opens
- The RCPs trip

The circulation flow through the CMTs and flow through the PRHR begin immediately after the CMT injection valves and the PRHR return flow valve are opened. Due to the rapid loss of pressure down to saturation pressure for the rod bundle and upper plenum, boiling begins and the upper plenum flashes. The flashing stops the rapid drop in primary system pressure and establishes a pseudo steady-state condition.

Natural Circulation Phase

After the primary system pressure reaches the pseudo steady-state condition at approximately [ ]^{a,b} seconds (75 seconds for NOTRUMP), the system transitions into the natural circulation phase. During the natural circulation phase, the rod bundle void fraction increases, which causes an increase in the void fraction in the upper plenum and hot legs.

The two-phase flow in the hot legs initiates the draindown of the SG U-tubes, since steam from the two-phase mixture collects at the top of the U-tubes. This stops the flow through the primary system.

When the CMT balance lines drain and the fluid near the top of the CMTs reaches saturation temperature, the CMTs convert from the circulation mode to the draindown mode of injection. This increases the cold injection flow and the rate of system pressure decay. This occurs at approximately [ ]^{a,b} seconds (470 seconds for NOTRUMP) for CMT-2 and [ ]^{a,b} seconds (900 seconds for NOTRUMP) for CMT-1. When system pressure drops to the saturation pressure for the upper head, the upper head begins to drain at [ ]^{a,b} seconds (120 seconds for NOTRUMP).

During the first [ ]^{a,b} seconds (648 seconds for NOTRUMP) of this event, [ ]^{a,b} lbm (1800 lbm for NOTRUMP) of water is discharged through the break while draining the pressurizer, the SG U-tubes, the upper head, the upper plenum above the hot leg, most of the cold legs, and approximately one quarter of the CMTs.

Automatic Depressurization System Phase

The ADS phase of the transient begins with the actuation of ADS-1 at [ ]^{a,b} seconds into the event (648 seconds for NOTRUMP). ADS-2 and ADS-3 occur within the next [ ]^{a,b} seconds.

ADS actuation increases the rate of primary system depressurization and results in a high level of injection flow from the accumulators. The rapid injection of cold fluid from the accumulators from approximately [ ]^{a,b} seconds into the event (560 to 863 seconds for NOTRUMP) temporarily reduces the boiling in the rod bundle and the void fractions in the rod bundle and the upper plenum. The pressurizer refills temporarily. When the accumulator discharge ends, the boiling intensity increases in the rod bundle, which results in increased void fractions.

During the period of ADS 1-3, which ends at ADS-4 actuation, approximately [ ]^{a,b} lbm (1060 lbm for NOTRUMP) of water are discharged from ADS-1, ADS-2, and ADS-3. The difference in ADS flow between the test and the simulation is due to the composition of the ADS flow. According to the test data, the flow is essentially liquid after approximately 200 seconds of two-phase flow, while the NOTRUMP simulation predicts two-phase flow out of the ADS until ADS-4 actuation. In addition, during the period of ADS 1-3, [ ]^{a,b} lbm of water (300 lbm for NOTRUMP) are discharged through the break. The higher break flow in NOTRUMP during this period is due to the accumulator water filling the cold legs, allowing liquid to flow up the balance line and out the break. The additional break flow calculated in the NOTRUMP simulation during the ADS phase compensates for the lower predicted ADS flow. After the accumulators empty and only the CMTs provide core injection, there is an increase in rod bundle void fraction. ADS-4 occurs at [ ]^{a,b} seconds, (1180 seconds for NOTRUMP) and the pressurizer water level falls. The fluid discharge through ADS-1, ADS-2, and ADS-3 essentially ends, and the fluid is discharged through ADS-4.

IRWST Injection Phase

At approximately [ ]^{a,b} seconds (1235 seconds for NOTRUMP), the system pressure has fallen below the pressure corresponding to the water elevation head of the IRWST. Flow from the IRWST enters the DVI line, and the IRWST injection phase begins. Shortly thereafter, the CMT flow drops significantly. The flow from the IRWST reduces the rod bundle boiling and partially refills the upper plenum above the hot-leg elevation. A steady flow of water is then flowing from the IRWST into the DVI line, through the rod bundle, and out of the primary system through ADS-4.

This test demonstrates that the rod bundle is fully covered by water or a two-phase mixture at all times during this event, and there is no indication of heater rod temperatures increasing due to lack of cooling. The NOTRUMP simulation also demonstrates no heater rod temperature increase.

8.3.5.2 Comparison of NOTRUMP Simulation to Test Data

Figure 8.3.5-2 shows the pressure at the top of the pressurizer for the test and the NOTRUMP simulation. Note that the test data shown for the low pressure region (right scale on figure) is taken from the narrow range pressure instrumentation while the high pressure region (left scale on figure) is taken from the wide range pressure instrumentation. The agreement between the test and the simulation is reasonable for the primary pressure response since the trends of the data are matched. The drop in pressure before ADS actuation is a result of vapor reaching and flowing through the break. The simulation pressure is higher than the test for most of the transient, due primarily to the delay in the NOTRUMP ADS actuation.

The primary system pressure decreases significantly at approximately [ ]^{a,b} seconds in the test as a result of ADS-1 actuation. For the NOTRUMP simulation, ADS-1 actuation occurs at 648 seconds. The trends of the pressure transient are the same once ADS-1 is actuated, with the timing of the remaining transient being shifted due to the difference in ADS-1 times between the test and the NOTRUMP simulation.

Figure 8.3.5-3 shows the collapsed liquid level in the pressurizer for the test and the NOTRUMP simulation. The break flow causes a rapid decrease in pressurizer level and empties the pressurizer at approximately [ ]^{a,b} seconds for the test and 80 seconds for the NOTRUMP simulation. The pressurizer level increases again with the opening of ADS-1 and the subsequent accumulator injection. The timing difference for the increase in pressurizer level between the test and the NOTRUMP simulation reflects the difference in ADS-1 actuation and subsequent accumulator injection times. In addition, substantially more mass accumulates in the pressurizer after ADS actuation in the test relative to the simulation..

Figure 8.3.5-4 shows the collapsed liquid levels in CMT-1 for the test and the NOTRUMP simulation. Figure 8.3.5-5 shows the collapsed liquid levels in CMT-2 for the test and the corresponding NOTRUMP analysis. In the test, CMT-1, the CMT attached to the balance line with the break on it,

transitions from the circulation mode to the draindown mode at about [ ]^{a,b} seconds and CMT-2 transitions at about [ ]^{a,b} seconds. In the simulation, CMT-1 transitions from the circulation mode to the draindown mode at 900 seconds, and CMT-2 transitions at about 470 seconds. For CMT-1, the start of the draindown period is delayed compared to the start of draindown of CMT-2 as a result of the break on the balance line attached to CMT-1. The break maintains a lower pressure on the balance line side of CMT-1, minimizing the circulation flow, which is low for the first few hundred seconds of both the test and the simulation. The break also vents some vapor instead of letting it all flow to the CMT after the SG tubes drain.

The delay in the transition to the draindown mode in NOTRUMP compared to the test is a result of the temperature of the top fluid node in the simulation reaching saturation temperature at a later time compared to the relatively hot fluid layer near the top of the CMT in the test. In the simulation, the temperature of all of the fluid in the top fluid node, which represents 10 percent of the CMT volume, must reach saturation before flashing begins. Following the initial draindown period for CMT-2 in the simulation, the level increases when accumulator injection temporarily fills the cold legs and water flows up the balance line and into the CMT. The level decreases again after the accumulators empty. The levels in both CMTs are predicted to increase following IRWST injection when the cold legs fill up and water flows up the CMT balance line into the CMTs. This behavior will be discussed further in subsequent paragraphs.

Figures 8.3.5-6 and 8.3.5-7 show the collapsed liquid levels in the hot side (upside) and the cold side (downside) of the SG-2 U-tubes for the test and the NOTRUMP simulation. Figures 8.3.5-8 and 8.3.5-9 show the same information for SG-1. There is reasonable agreement between the test and the simulation for the draining of the SG tubes. The balance line collapsed levels are shown in Figures 8.3.5-10 and 8.3.5-11. The levels remain at the top of the balance lines until the levels in the SG tubes decrease enough to allow vapor to reach the cold legs and migrate to the balance lines. Up to 1500 seconds, the general trends of the collapsed balance line level are predicted by NOTRUMP, demonstrating that the PIRT items related to balance line-to-cold leg behavior and cold leg phase separation are predicted reasonably well. Just prior to 1500 seconds, the balance lines are predicted to refill as the cold leg fills with water.

Figures 8.3.5-12 and 8.3.5-13 show the collapsed liquid levels in accumulator 1 and accumulator 2 for the test and the NOTRUMP simulation. In general, the predicted onset of full accumulator injection is delayed in comparison to the test results because of the delay in ADS-1 for the NOTRUMP simulation compared to the test.

The next series of plots, Figures 8.3.5-14 through 8.3.5-20, relate to the collapsed and two-phase levels at different locations in the vessel. For the test, there is little change in the collapsed liquid level (see Figure 8.3.5-14) in the core, indicating low void fractions during the course of the test, as shown in Figure 8.3.5-17. NOTRUMP predicts higher void fractions, leading to a more substantial change in the collapsed liquid level during events such as accumulator injection. The level trends, however, are similar for the test and the simulation, with some differences in timing due to the shift in the ADS

timing. In both the test and the simulation, the vessel levels initially decrease as inventory is lost from the system. The largest core collapsed level increase occurs when ADS-1 actuates, which lowers the system pressure, allowing the accumulators to inject at their maximum rate. Once the accumulators empty, the levels decrease as inventory is lost from the system. The levels drop until IRWST injection occurs following ADS-4 actuation. The collapsed and two-phase levels in the upper plenum are shown in Figures 8.3.5-15 and 8.3.5-16. Note that the test information for the collapsed upper plenum level does not represent the entire upper plenum. The instrumentation only provides information for the region just below the hot legs to the upper support plate. Valid instrumentation to measure the entire upper plenum region level was unavailable. As a result, upper plenum collapsed level information below this region is unavailable for the test and Figure 8.3.5-15 indicates a straight line when the level drops below the bottom tap of the valid instrumentation. In addition, an accurate two-phase mixture level for the test data can not be calculated based on the available information. As such, only the NOTRUMP prediction for two-phase level is included in Figure 8.3.5-16. The test data indicates that liquid accumulates in the upper plenum at ADS actuation, consistent with the increase in pressurizer mass. NOTRUMP shows less water flowing into the upper plenum. A plot of the core average void fraction for the test and the NOTRUMP simulation is provided (see Figure 8.3.5-17). This figure shows similar trends between the test and the simulation, with significant void collapse following the injection of the cold accumulator water (500 to 900 seconds) and IRWST water.

Figure 8.3.5-18 shows the collapsed liquid level in the downcomer for the test and the NOTRUMP simulation. Although shifted in time, the predicted and test levels show the same trends, except following accumulator injection and ADS 1 actuation, when the test data indicates a level drop. This indication is questionable because the pressure difference from which the level is derived may be affected by the jet of flow issuing from the DVI line.

Figure 8.3.5-20 shows the collapsed liquid level in the upper head for the test and the corresponding NOTRUMP analysis. In the test, the upper head begins to drain at [ ]^{a,b} seconds, as the upper head fluid temperature quickly reaches the system saturation temperature. In the NOTRUMP simulation, the upper head starts to drain at about 130 seconds. One reason for this delay in draining is the time at which the upper head becomes saturated, which is affected by differences in system pressure, initial upper head temperature, and the upper head flow rates. The test indicates more mass in the upper head, consistent with the other indications in the upper plenum and pressurizer.

The next series of plots show the comparisons between the flows in the safety-related systems during the test and simulation.

Figure 8.3.5-21 shows the CMT-1 injection line mass flow rate for the test and the NOTRUMP simulation. Figure 8.3.5-22 shows the CMT-2 injection line mass flow rates. The flow from CMT-1 is lower than the CMT-2 flow early in the transient because of the break on the balance line attached to CMT-1. Because of the break location, there is little circulation flow in CMT-1 in the first [ ]^{a,b} seconds of the test. The NOTRUMP-predicted circulation flow in CMT-2 is lower than the data from 0 to 400 seconds, but subsequent drain flow is predicted well. The reasonable prediction of the CMT

flows indicates that even though the timing of the CMT transition to draindown is different, the CMT balance line pressure drop and flow composition parameters identified in the PIRT are reasonably predicted by NOTRUMP.

Figure 8.3.5-23 shows the accumulator 1 injection line mass flow rates for the test and the NOTRUMP simulation. Figure 8.3.5-24 shows the accumulator 2 injection line mass flow rates. The prediction and the data are in reasonable agreement except for a slight shift in timing, demonstrating that this highly ranked PIRT item is reasonably predicted by NOTRUMP. The predicted onset of full accumulator flow is delayed in comparison to the test results because of the delay in the actuation of ADS-1.

Figure 8.3.5-25 shows the IRWST-1 injection line mass flow rates for the test and the NOTRUMP simulation. Figure 8.3.5-26 shows the IRWST-2 injection line flow rates. The timing of IRWST injection is in good agreement between the test and the NOTRUMP simulation. The test reaches full flow at a slower rate than NOTRUMP due to slightly higher DVI line pressures in the test compared to the simulation. The agreement in IRWST flow initiation and the flow rates after full flow is reached, demonstrate that the highly ranked PIRT items of IRWST pool level and gravity draining are reasonably predicted by NOTRUMP.

Figure 8.3.5-27 shows the integrated mass flow through ADS stages 1 through 3 for the test and the NOTRUMP simulation. As discussed previously, the difference in the total integrated flow through ADS 1-3 results from fluid conditions in the pressurizer. According to the test data, ADS flow is liquid after a brief period of about 200 seconds of two-phase flow, while the NOTRUMP simulation predicts two-phase flow for the entire ADS 1-3 period. Figure 8.3.5-28 shows the integrated mass flow through ADS stage 4 for the test and the NOTRUMP simulation. These curves show reasonable agreement for the ADS flows once the delay in ADS actuation is accounted for. The agreement of these curves demonstrates that the PIRT highly ranked items related to ADS stage 4 (critical flow, two-phase pressure drop, and valve loss coefficients) are predicted well by NOTRUMP. Because of the difference in the pressurizer fluid conditions, which affects the composition of the ADS 1-3 flows, no conclusions can be drawn regarding the PIRT highly ranked items related to ADS stages 1-3.

Figure 8.3.5-29 shows the integrated mass flow out of the break for the test and the NOTRUMP simulation. The curves show good agreement until ADS is actuated. At that point, the break flow is substantially reduced for the test. As discussed previously, the higher break flow in NOTRUMP during this period is due to the accumulator water filling the cold legs, allowing liquid to flow up the balance line and out the break. In the test, the accumulator injection increases the downcomer level but does not appear to fill up the cold legs. As a result, there is little break flow following actuation of ADS in the test. Prior to ADS actuation, the curves that the PIRT highly ranked item of break critical flow is reasonably predicted by NOTRUMP. Because of the difference in the flow composition at the break for the test and the simulation after ADS actuation, no conclusions can be drawn regarding critical break flow after this time.

Figure 8.3.5-30 shows the PRHR return line mass flow rate for the test and the corresponding NOTRUMP analysis. The simulation matches the data trends except in the time period from 100 to 250 seconds when the simulation underpredicts the flow. Figure 8.3.5-31 shows the PRHR inlet and outlet temperatures for the test and the NOTRUMP simulation. The simulation PRHR heat transfer is shown in Figure 8.3.3-32. There is no directly comparable data available from the test, so the plot only contains the simulation information. The PRHR heat transfer is expected to fall off in the test following ADS actuation, and it does so in the simulation. For the simulation, calculations for the PRHR nodes are turned off, and the nodes are removed from the system after ADS-3 is actuated (approximately 775 seconds for this simulation). This is done to enhance the speed of the calculations given that the heat transfer is small. Once calculations for these nodes are turned off, the plotted value remains at the last calculated value, even though the actual heat transfer is zero. The PRHR inlet and outlet temperatures indicate that NOTRUMP underpredicts the PRHR heat transfer compared to the test.

Figure 8.3.5-33 shows temperatures at various elevations in CMT-1 for the test. Figure 8.3.5-34 shows temperatures for the four NOTRUMP fluid nodes representing CMT-1. The temperature profiles for CMT-2 are contained in Figures 8.3.5-35 and 8.3.5-36. A direct comparison between the NOTRUMP and test temperatures cannot be made because the NOTRUMP temperatures are averages over a region (the fluid node) while the test data are for distinct elevations; however, the trends can be compared. The agreement is reasonable between the test and the simulation with a slower heatup of the top node in the simulation because the fluid in the entire node must heat up. In contrast, the test data point is the temperature at a single elevation that heats up immediately when the hot layer of fluid passes it.

The temperature profiles for CMT-1 are indicative of the lack of circulation prior to draindown of the tank. Relating this information to the CMT-related PIRT items, the temperature agreement at the top of the tank indicates reasonable NOTRUMP code prediction for the natural circulation between the CMT and the cold leg balance line.

SG-related information is provided in Figures 8.3.5-37 through 8.3.5-39. Figure 8.3.5-37 shows the SG secondary pressures for the test and the NOTRUMP simulation. The NOTRUMP simulation secondary pressures are higher than the test for most of the transient. This is primarily due to not modeling the ambient heat losses; however, the effect of the higher pressures is insignificant on the primary-to-secondary heat transfer. The temperatures of the secondary side of the SGs are provided in Figure 8.3.5-38.

Figure 8.3.5-39 shows the collapsed SG levels for the test and the NOTRUMP simulation. The levels are initialized lower in the simulation than the test. The NOTRUMP simulation represents the secondary side as a single node, whereas the test represents a full recirculating SG design. This low level for the simulation is not important since the tubes remain covered with saturated water at all times, and therefore, the heat transfer characteristics are not significantly affected.

Figures 8.3.5-40 and 8.3.5-41 show the total DVI line flow rate for each of the DVI lines. The agreement between the test and the NOTRUMP simulation is reasonable for these parameters with the greatest difference being caused by the differences in timing between the test and the simulation.

Additional comparisons between the test and the NOTRUMP simulation that are provided include core inlet temperature (see Figure 8.3.5-42) and core outlet temperature (see Figure 8.3.5-43). The core inlet temperature is higher for the simulation, while the outlet temperature is predicted reasonably well for most of the test.

The final two plots (see Figures 8.3.5-44 and 8.3.5-45), the integrated core inlet flow and the upper head bypass flow, only include the results of the simulation. There are no test data available for these items. They are included for completeness.

TABLE 8.3.5-1
SB09 SEQUENCE OF EVENTS

Event	Definition	OSU (seconds)	NOTRUMP (seconds)
Break Opens		0	0
R Signal		0	0
S Signal		0.5	0
MFW Isolation Valve Closes		3.6	3.1
CMT Isolation Valves Open		6.1	5.6
RCPs Trip		8	6
CMT-1 Starts Draindown Phase	CMT level dropping and top of tank saturated	770	900
CMT-2 Starts Draindown Phase	CMT level dropping and top of tank saturated	380	470
ADS-1	CMT level 41in. + 15 sec	525	648
Accumulators Start		510	560
ADS-2	ADS-1 + 47 seconds	572	695
ADS-3	ADS-1 +107 seconds	632	755
Accumulators Empty		810	863
ADS-4		950	1180
IRWST Injection		1230	1235

TABLE 8.3.5-2 FIGURES FOR OSU 2-IN. COLD LEG BALANCE LINE BREAK (SB09)	
Figure No.	**Title**
8.3.5-1	Facility Response Summary
8.3.5-2	Pressurizer Pressure
8.3.5-3	Pressurizer Level (Relative to Bottom Tap)
8.3.5-4	CMT-1 Level (Relative to Bottom Tap)
8.3.5-5	CMT-2 Level (Relative to Bottom Tap)
8.3.5-6	Steam Generator 2 Hot Side Collapsed Level (Relative to Bottom Tap)
8.3.5-7	Steam Generator 2 Cold Side Collapsed Level (Relative to Bottom Tap)
8.3.5-8	Steam Generator 1 Hot Side Collapsed Level (Relative to Bottom Tap)
8.3.5-9	Steam Generator 1 Cold Side Collapsed Level (Relative to Bottom Tap)
8.3.5-10	Cold Leg Balance Line 1 Levels (Relative to Bottom Tap)
8.3.5-11	Cold Leg Balance Line 2 Levels (Relative to Bottom Tap)
8.3.5-12	ACC-1 Level (Relative to Bottom Tap)
8.3.5-13	ACC-2 Level (Relative to Bottom Tap)
8.3.5-14	Core Collapsed Liquid Levels (Relative to Bottom of Lower Plenum)
8.3.5-15	Upper Plenum Collapsed Levels (Relative to Bottom of Lower Plenum)
8.3.5-16	NOTRUMP Upper Plenum 2-phase Levels (Relative to Bottom of Lower Plenum)
8.3.5-17	Average Core Void Fraction
8.3.5-18	Collapsed Downcomer Levels (Relative to Bottom of Lower Plenum)
8.3.5-19	Not Applicable
8.3.5-20	Upper Head Collapsed Level (Relative to Bottom of Lower Plenum)
8.3.5-21	CMT-1 Injection Line Mass Flow
8.3.5-22	CMT-2 Injection Line Mass Flow
8.3.5-23	ACC-1 Injection Line Mass Flow
8.3.5-24	ACC-2 Injection Line Mass Flow
8.3.5-25	IRWST-1 Injection Line Mass Flow
8.3.5-26	IRWST-2 Injection Line Mass Flow
8.3.5-27	ADS Stage 1-3 Integrated Flows
8.3.5-28	ADS Stage 4 Integrated Total Flow
8.3.5-29	Integrated Break Flow
8.3.5-30	PRHR Return Line Mass Flow
8.3.5-31	PRHR Inlet and Exit Temperatures
8.3.5-32	NOTRUMP PRHR Heat Transfer Rate
8.3.5-33	Test CMT-1 Temperature Profile
8.3.5-34	NOTRUMP CMT-1 Temperature Profile
8.3.5-35	Test CMT-2 Temperature Profile

TABLE 8.3.5-2 (Cont.) FIGURES FOR OSU 2-IN. COLD LEG BALANCE LINE BREAK (SB9)	
Figure No.	**Title**
8.3.5-36	NOTRUMP CMT-2 Temperature Profile
8.3.5-37	Steam Generator Pressures
8.3.5-38	Steam Generator Secondary Fluid Temperatures
8.3.5-39	Steam Generator Secondary Liquid Levels (Relative to Top of Tube Sheet)
8.3.5-40	Total DVI Line 1 Flow
8.3.5-41	Total DVI Line 2 Flow
8.3.5-42	Core Inlet Temperatures
8.3.5-43	Core Outlet Temperatures
8.3.5-44	Integrated Core Inlet Flow
8.3.5-45	Upper Head Bypass Flow

Figures 8.3.5-1 through 8.3.5-45 are not included in the non-proprietary version of this report.

8.3.6 Double-Ended Guillotine Cold Leg Balance Line Break (SB10)

This test simulates a DEG break in the cold leg 3 to CMT-1 balance line and is performed without any nonsafety-related systems operating. A single failure of one of the two fourth-stage ADS valves on hot leg 1 is represented in the test.

8.3.6.1 Summary of Test and NOTRUMP Simulation Observations

The timing of the critical events for this transient in comparison with test results is reported in Table 8.3.6-1. Figure 8.3.6-1 shows primary system pressure during this test (as measured at the top of the pressurizer), with selected component actuations and plant responses shown in relation to primary system pressure. At the beginning of the test, the rod bundle heaters are shifted to power control mode, and the power is maintained at the maximum level (600 kW) for 140 seconds followed by a decaying power function simulating the total decay energy input of AP600 nuclear fuel. The simulation is started from a steady-state condition at a power level of 600 kW.

Blowdown Phase

The blowdown phase is initiated with the opening of the break. An R signal occurs coincident with the break, and an S signal occurs 0.5 seconds later (the R and S signals occur simultaneously at time zero in the NOTRUMP simulation). The R and S signals initiate the following actions:

- The MSLIVs close
- The MFWIVs shut off
- The CMT injection valves open
- The PRHR return flow valve opens
- The RCPs trip

The circulation flow through the CMTs and flow through the PRHR begin immediately after the CMT injection valves and the PRHR return flow valve are opened. Due to the rapid loss of pressure down to saturation pressure for the rod bundle and upper plenum, boiling begins and the upper plenum flashes. The flashing stops the rapid drop in primary system pressure and establishes a brief pseudo steady-state condition.

Natural Circulation Phase

After the primary system pressure reaches the pseudo steady-state condition at approximately [ ]^{a,b} seconds (20 seconds for NOTRUMP), the system transitions into the natural circulation phase. During the natural circulation phase, the rod bundle void fraction increases, which causes an increase in the void fraction in the upper plenum and hot legs.

The two-phase flow in the hot legs initiates the draindown of the SG U-tubes, since steam from the two-phase mixture collects at the top of the U-tuoes. This stops the natural circulation flow through the primary system.

For this test, CMT-1, which is attached to the broken balance line, remains full until the DVI line pressure is less than the hydrostatic head in the CMT. After this time, the CMT drains via gravity. This occurs at approximately [ ]^{a,b} seconds in the test, and afterward, the tank slowly drains. The NOTRUMP simulation does not show appreciable draining of CMT-1.

For CMT-2, the transition from circulation mode to draindown mode occurs when the balance line drains and the fluid near the top of the CMT reaches saturation temperature. This increases the cold injection flow and the rate of system pressure decay. This occurs at [ ]^{a,b} seconds (150 seconds for NOTRUMP). When system pressure drops to the saturation pressure for the upper head, the upper head begins to drain at [ ]^{a,b} seconds (40 seconds for NOTRUMP).

Due to the relatively large break size, the rapid depressurization of the RCS initiates accumulator injection early in the transient, but at relatively low flow rates. The accumulators begin injecting at [ ]^{a,b} seconds (103 seconds for NOTRUMP).

During the first [ ]^{a,b} seconds (354 seconds for NOTRUMP) of this event, [ ]^{a,b} lbm (2410 lbm for NOTRUMP) of water are discharged through the break while draining the pressurizer, the SG U-tubes, the upper head, the upper plenum above the hot leg, most of the cold legs, and approximately one quarter of CMT-2. The higher break flow in the simulation is due to the code predicting a lower temperature for the fluid in the vicinity of the break and a higher cold leg level on cold leg 3, allowing liquid to flow out the break for a longer period of time than the test.

Automatic Depressurization System Phase

The ADS phase of the transient begins with the actuation of ADS-1 at [ ]^{a,b} seconds into the event (354 seconds for NOTRUMP). ADS-2 and ADS-3 occur within the next [ ]^{a,b} seconds.

The ADS actuation increases the rate of primary system depressurization and results in a high level of injection flow from the accumulators. The rapid injection of cold fluid from the accumulators from approximately [ ]^{a,b} seconds into the transient (103 to 424 seconds for NOTRUMP) temporarily reduces the boiling in the rod bundle and the void fractions through the rod bundle and the upper plenum. The pressurizer refills temporarily. When the accumulator discharge ends, the boiling intensity increases in the rod bundle, which results in increased void fractions.

During the period of ADS 1-3, which ends at ADS-4 actuation, approximately [ ]^{a,b} lbm (175 lbm for NOTRUMP) of water are discharged from ADS-1, ADS-2, and ADS-3. The difference in the ADS flow between the test and the simulation is due to the composition of the flow. According to the test data, the flow is essentially liquid after approximately 200 seconds of two-phase flow, while the

NOTRUMP simulation predicts all vapor out of the ADS for the first 270 seconds, followed by two-phase flow until ADS-4 actuation. In addition, during the period of ADS 1-3, [ ]^{a,b} lbm of water (613 lbm for NOTRUMP) are discharged through the break. The reasons for the additional break flow in the simulation are noted above. The NOTRUMP-predicted cold leg 3 level remains high enough to allow liquid to flow to the break until shortly after the accumulators empty at 424 seconds. The additional break flow observed in the NOTRUMP simulation during the ADS phase compensates for the lower predicted ADS flow. After the accumulators empty and only the CMTs provide core injection, there is an increase in rod bundle void fraction. ADS-4 occurs at [ ]^{a,b} seconds (841 seconds for NOTRUMP) and the pressurizer water level falls. The fluid discharge through ADS-1, ADS-2, and ADS-3 essentially ends, and the fluid is discharged through ADS-4.

IRWST Injection Phase

At approximately [ ]^{a,b} seconds (870 seconds for NOTRUMP), the system pressure has fallen below the pressure corresponding to the water elevation head of the IRWST. Flow from the IRWST enters the DVI line and the IRWST injection phase begins. Shortly thereafter, the CMT flow drops significantly. The flow from the IRWST reduces the rod bundle boiling and partially refills the upper plenum above the hot-leg elevation. A steady flow of water then flows from the IRWST into the DVI line, through the rod bundle, and out of the primary system through ADS-4 and the break.

This test demonstrates that the rod bundle is fully covered by water or a two-phase mixture at all times during this event, and there is no indication of heater rod temperatures increasing due to lack of cooling. The NOTRUMP simulation also demonstrates no heater rod temperature increase.

8.3.6.2 Comparison of NOTRUMP Simulation to Test Data

Figure 8.3.6-2 shows the pressure at the top of the pressurizer for the test and the NOTRUMP simulation. Note that the test data shown for the low pressure region (right scale on figure) is taken from the narrow range pressure instrumentation while the high pressure region (left scale on figure) is taken from the wide range pressure instrumentation. NOTRUMP predicts a more rapid depressurization prior to ADS.

The pressure decreases initially due to the blowdown through the break, then stabilizes once the primary system becomes saturated. After a short period with the stable pressure, the PRHR heat transfer increases and the pressure decreases significantly prior to ADS actuation. The primary system pressure continues to decrease at approximately [ ]^{a,b} seconds in the test when ADS-1 actuates. For the NOTRUMP simulation, ADS-1 actuation does not occur until approximately 354 seconds

Figure 8.3.6-3 shows the collapsed liquid level in the pressurizer for the test and the NOTRUMP simulation. The break flow causes a rapid decrease in pressurizer level and empties the pressurizer at approximately [ ]^{a,b} seconds for the test and 55 seconds for the NOTRUMP simulation. The pressurizer level increases again after ADS-1 is actuated for both the test and the simulation; however,

the delay between ADS-1 actuation and the level increase in the pressurizer is longer for the simulation. In addition, substantially less mass is predicted to collect in the pressurizer. The timing difference for the increase in pressurizer level between the test and the NOTRUMP simulation reflects the difference in ADS-1 actuation and the difference in delay time until the level starts to increase significantly.

Figure 8.3.6-4 shows the collapsed liquid levels in CMT-1 for the test and the NOTRUMP simulation. Figure 8.3.6-5 shows the collapsed liquid levels in CMT-2 for the test and the corresponding NOTRUMP analysis. In the test, CMT-1, which is attached to the broken balance line begins draining into the DVI line at [ ]^{a,b} seconds. NOTRUMP does not predict draining for the duration of the simulation (this will be discussed further when CMT fluid temperatures are compared). CMT-2 transitions to draindown at about [ ]^{a,b} seconds (160 seconds in the simulation). The small delay in the transition to the draindown mode in NOTRUMP compared to the test is a result of the top fluid node in the simulation reaching saturation temperature at a later time compared to the relatively hot fluid layer near the top of the CMT in the test. The level in CMT-2 is predicted to increase following IRWST injection when the cold leg fills up and water flows up the balance line into the CMT.

Figures 8.3.6-6 and 8.3.6-7 show the collapsed liquid levels in the hot side (upside) and the cold side (downside) of the SG-2 U-tubes for the test and the NOTRUMP simulation. Figures 8.3.6-8 and 8.3.6-9 show the same information for SG-1. There appears to be erroneous data for the upper and lower levels for the test as all levels should start at the same elevation and be at the same elevation after the tubes are drained. While the absolute levels are questionable, these data are adequate for comparing the time of tube draining. The NOTRUMP levels drain before the test data. The balance line collapsed level for the balance line from cold leg 1 to CMT-2 is shown in Figure 8.3.6-11. Because of the location of the break, the level in the balance line attached to CMT-1 is not provided. As seen on Figure 8.3.6-11, the balance line drains quickly for the test and the simulation. The lower level of the test data shown on Figure 8.3.6-11 appears to be in error as this balance line should drain completely for such a large break. While the lower level for the data may be in error, the indication of the time of balance line draining is believed to be adequate for comparison purposes. The balance line collapsed level in both the test and the simulation increases following IRWST injection. The general trends of the balance line level are predicted by NOTRUMP, demonstrating that the PIRT items related to balance line-to-cold leg behavior and cold leg phase separation are predicted reasonably well.

Figures 8.3.6-12 and 8.3.6-13 show the collapsed liquid levels in accumulator 1 and accumulator 2 for the test and the NOTRUMP simulation. The comparison between the test and the NOTRUMP simulation is good.

The next series of plots, Figures 8.3.6-14 through 8.3.6-20, relate to the collapsed and two-phase levels at different locations in the vessel. NOTRUMP predicts slightly lower collapsed liquid levels, but the trends are in good agreement with the test. In both cases, the levels initially decrease as inventory is lost from the system. The levels increase once the accumulators inject. Once the accumulators empty,

the levels decrease slightly then stabilize as CMT-2 provides injection. The stable levels continue until IRWST injection occurs following ADS-4 actuation. The collapsed and two-phase levels in the upper plenum are shown in Figures 8.3.6-15 and 8.3.6-16. Note that the test information for the collapsed upper plenum level does not represent the entire upper plenum. The instrumentation only provides information for the region just below the hot legs to the upper support plate. Valid instrumentation to measure the entire upper plenum region level was unavailable. As a result, upper plenum collapsed level information below this region is unavailable for the test and Figure 8.3.6-15 indicates a straight line when the level drops below the bottom tap of the valid instrumentation. In addition, an accurate two-phase mixture level for the test data can not be calculated based on the available information. As such, only the NOTRUMP prediction for two-phase level is included in Figure 8.3.6-16. A plot of the core average void fraction is provided (see Figure 8.3.6-17). This figure shows similar trends between the test and the simulation, with some void collapse following the injection of the cold accumulator water and IRWST water.

Figures 8.3.6-18 shows the collapsed liquid level in the downcomer for the test and the NOTRUMP simulation. Again there is reasonable agreement between the test and the simulation, with NOTRUMP predicting slightly lower collapsed liquid levels, demonstrating that the highly ranked PIRT items related to the levels in the core, upper plenum, and downcomer are predicted reasonably well by NOTRUMP.

Figure 8.3.6-20 shows the collapsed liquid level in the upper head for the test and the corresponding NOTRUMP analysis. In the test, the upper head begins to drain at [ ]^{a,b} seconds, as the upper head fluid temperature quickly reaches the system saturation temperature. In the NOTRUMP simulation, the upper head starts to drain at about 40 seconds. One reason for this delay in draining is the time at which the upper head becomes saturated, which is affected by differences in system pressure, initial upper head temperature, upper head flow rates, and the upper head flow rates. The test indicates more mass in the upper head, consistent with the other indications in the upper plenum and pressurizer.

The next series of plots show the comparisons between the flows in the safety-related systems during the test and simulation.

Figure 8.3.6-21 shows the CMT-1 (attached to broken balance line) injection mass flow rate for the test and the NOTRUMP simulation. Figure 8.3.6-22 shows the CMT-2 injection line mass flow rates. The flow from CMT-1 is essentially zero in the simulation except for momentary fluctuations, while the test shows a small drain rate after [ ]^{a,b} seconds. The CMT-2 flow rates show good agreement, with the simulation slightly lagging the test due to the slight delay in the transition from circulation mode to draindown mode.

Figure 8.3.6-23 shows the accumulator 1 injection line mass flow rates for the test and the NOTRUMP simulation. Figure 8.3.6-24 shows the accumulator 2 injection line mass flow rates. The shape of the curves is in reasonable agreement, demonstrating that this highly ranked PIRT item is reasonably predicted by NOTRUMP.

Figure 8.3.6-25 shows the IRWST-1 injection line mass flow rates for the test and the NOTRUMP simulation. Figure 8.3.6-26 shows the IRWST-2 injection line flow rates. The timing of IRWST injection is in good agreement between the test and the NOTRUMP simulation. The test reaches full flow at a slower rate than NOTRUMP due to slightly higher DVI line pressures in the test compared to the simulation from approximately 1000 to 1400 seconds. The agreement in IRWST flow rates demonstrates that the highly ranked PIRT items of IRWST pool level and gravity draining are reasonably predicted by NOTRUMP.

Figure 8.3.6-27 shows the integrated mass flow through ADS stages 1 through 3 for the test and the NOTRUMP simulation. As discussed previously, the difference in the total integrated flow from ADS 1-3 is a result of differences in actual and predicted fluid conditions in the pressurizer. According to the test data, the ADS flow is essentially liquid after approximately 200 seconds of two-phase flow, while the NOTRUMP simulation predicts all vapor out of the ADS for the first 270 seconds, followed by two-phase flow until ADS-4 actuation. As a result, substantially more mass is ejected through the ADS than is predicted by NOTRUMP. Figure 8.3.6-28 shows the integrated mass flow through ADS stage 4 for the test and the NOTRUMP simulation. These curves show reasonable agreement, which demonstrates that the PIRT highly ranked items related to ADS stage 4 (critical flow, two-phase pressure drop, and valve loss coefficients) are predicted well by NOTRUMP. Because of the difference in the pressurizer fluid conditions, which affects the composition of the ADS 1-3 flows, no conclusions can be drawn regarding the PIRT highly ranked items related to ADS stages 1-3.

Figure 8.3.6-29 shows the integrated mass flow out of the break for the test and the NOTRUMP simulation. The higher break flow in the simulation is due to the code predicting a lower temperature for the fluid in the vicinity of the break and a higher level in cold leg 3, allowing liquid to flow out the break for a longer period of time than the test. The NOTRUMP-predicted cold leg 3 level remains high enough to allow liquid to flow to the break until shortly after the accumulators empty at 424 seconds. The additional break flow observed in the NOTRUMP simulation during the ADS phase compensates for the lower predicted ADS flow. Because of the difference in the flow composition at the break for the test and the simulation, no conclusions can be drawn for the PIRT highly ranked item of break critical flow.

Figure 8.3.6-30 shows the PRHR return line mass flow rate for the test and the corresponding NOTRUMP analysis. These are in reasonable agreement, with the simulation values slightly lower than the test data. Figure 8.3.6-31 shows the PRHR inlet and outlet temperatures for the test and the NOTRUMP simulation. These indicate that NOTRUMP underpredicts the heat transfer. The heat transfer is shown for the simulation in Figure 8.3.6-32. There is no directly comparable data available from the test so the plot only contains the simulation information. The PRHR heat transfer is expected to fall off significantly in the test following ADS actuation, and it does so in the simulation. For the simulation, calculations for the PRHR nodes are turned off, and the nodes are removed from the system after ADS-3 is actuated (465 seconds for this simulation). This is done to enhance the speed of the calculations given that the expected heat transfer is small. Once calculations for these nodes are

turned off, the plotted values for inlet flow and inlet and outlet temperatures remain at the last calculated value, even though the actual heat transfer is zero.

Figure 8.3.6-33 shows temperatures at various elevations in CMT-1 for the test. Figure 8.3.6-34 shows temperatures for the four NOTRUMP fluid nodes representing CMT-1, which has the break in the balance line. The temperature profiles for CMT-2 are contained in Figures 8.3.6-35 and 8.3.6-36. A direct comparison between the test temperatures and the NOTRUMP temperatures cannot be made because the NOTRUMP temperatures are averages over a region while the test data are for distinct elevations; however, the trends can be compared. The temperatures for CMT-1 show little change as a result of there being little flow from this tank due to the break location. Eventually, however, a vapor bubble forms and the tank begins to drain. NOTRUMP predicts no draining because the upper node does not saturate. The temperatures for CMT-2 show reasonable agreement with a slower heatup of the top fluid node in the simulation because the fluid in the entire node must heat up. In contrast, the test data point is the temperature at a single elevation that heats up immediately when the hot layer of fluid passes it.

SG-related information is provided in Figures 8.3.6-37 through 8.3.6-39. Figure 8.3.6-37 shows the SG pressures for the test and the NOTRUMP simulation. The NOTRUMP simulation secondary pressures are higher than the test for most of the transient. This is primarily due to not modeling the ambient heat losses; however, the effect of the higher pressures is insignificant on the primary-to-secondary heat transfer. The temperatures of the secondary side of the SGs are provided in Figure 8.3.6-38.

Figure 8.3.6-39 shows the collapsed SG levels for the test and the NOTRUMP simulation. The levels are initialized lower in the simulation than the test. The NOTRUMP simulation represents the secondary side as a single node, whereas the test represents a full recirculating SG design. This low level for the simulation is not important since the tubes remain covered with water at all times, and therefore, the heat transfer characteristics are not significantly affected.

Figures 8.3.6-40 and 8.3.6-41 show the total DVI line flow rate for each of the DVI lines. There is good agreement between the test and the NOTRUMP simulation.

Additional comparisons between the test and the NOTRUMP simulation that are provided include core inlet temperature (see Figure 8.3.6-42) and core outlet temperature (see Figure 8.3.6-43). The core inlet temperature is higher in the simulation for most of the transient, while the outlet temperature is predicted reasonably well for most of the transient.

The final two plots (see Figures 8.3.6-44 and 8.3.6-45), the integrated core inlet flow and the upper head bypass flow, only include the results of the simulation. There are no test data available for these items. They are included for completeness.

TABLE 8.3.6-1 SB10 SEQUENCE OF EVENTS			
Event	**Definition**	**OSU (seconds)**	**NOTRUMP (seconds)**
Break Opens		0	0
R Signal		0.5	0
S Signal		0.5	0
MFW Isolation Valve Closes		3.6	3.1
CMT Isolation Valves Open		6.1	5.6
RCPs Trip		6	6
CMT-1 Starts Draindown Phase	CMT level dropping and top of tank saturated	970	-
CMT-2 Starts Draindown Phase	CMT level dropping and top of tank saturated	115	160
ADS-1	CMT level 41 in. + 15 sec	253	354
Accumulators Start		146	103
ADS-2	ADS-1 + 47 sec	302	401
ADS-3	ADS-1 + 107 sec	360	461
Accumulators Empty		474	424
ADS-4		752	841
IRWST Injection		785	870

TABLE 8.3.6-2 FIGURES FOR OSU DOUBLE-ENDED BALANCE LINE BREAK (SB10)	
Figure No.	**Title**
8.3.6-1	Facility Response Summary
8.3.6-2	Pressurizer Pressure
8.3.6-3	Pressurizer Level (Relative to Bottom Tap)
8.3.6-4	CMT-1 Level (Relative to Bottom Tap)
8.3.6-5	CMT-2 Level (Relative to Bottom Tap)
8.3.6-6	Steam Generator 2 Hot Side Collapsed Level (Relative to Bottom Tap)
8.3.6-7	Steam Generator 2 Cold Side Collapsed Level (Relative to Bottom Tap)
8.3.6-8	Steam Generator 1 Hot Side Collapsed Level (Relative to Bottom Tap)
8.3.6-9	Steam Generator 1 Cold Side Collapsed Level (Relative to Bottom Tap)
8.3.6-10	Not Applicable
8.3.6-11	Cold Leg Balance Line 2 Levels (Relative to Bottom Tap)
8.3.6-12	ACC-1 Level (Relative to Bottom Tap)
8.3.6-13	ACC-2 Level (Relative to Bottom Tap)
8.3.6-14	Core Collapsed Liquid Levels (Relative to Bottom of Lower Plenum)
8.3.6-15	Upper Plenum Collapsed Levels (Relative to Bottom of Lower Plenum)
8.3.6-16	NOTRUMP Upper Plenum 2-phase Levels (Relative to Bottom of Lower Plenum)
8.3.6-17	Average Core Void Fraction
8.3.6-18	Collapsed Downcomer Levels (Relative to Bottom of Lower Plenum)
8.3.6-19	Not Applicable
8.3.6-20	Upper Head Collapsed Liquid Level (Relative to Bottom of Lower Plenum)
8.3.6-21	CMT-1 Injection Line Mass Flow
8.3.6-22	CMT-2 Injection Line Mass Flow
8.3.6-23	ACC-1 Injection Line Mass Flow
8.3.6-24	ACC-2 Injection Line Mass Flow
8.3.6-25	IRWST-1 Injection Line Mass Flow
8.3.6-26	IRWST-2 Injection Line Mass Flow
8.3.6-27	ADS Stage 1-3 Integrated Flows
8.3.6-28	ADS Stage 4 Integrated Total Flow
8.3.6-29	Integrated Break Flow Loop Side of Break Only
8.3.6-30	PRHR Return Line Mass Flow
8.3.6-31	PRHR Inlet and Exit Temperatures
8.3.6-32	NOTRUMP PRHR Heat Transfer Rate
8.3.6-33	Test CMT 1 Temperature Profile
8.3.6-34	NOTRUMP CMT 1 Temperature Profile
8.3.6-35	Test CMT 2 Temperature Profile

TABLE 8.3.6-2 (Cont.) FIGURES FOR OSU DOUBLE-ENDED BALANCE LINE BREAK (SB10)	
Figure No.	**Title**
8.3.6-36	NOTRUMP CMT 2 Temperature Profile
8.3.6-37	Steam Generator Pressures
8.3.6-38	Steam Generator Secondary Fluid Temperatures
8.3.6-39	Steam Generator Secondary Liquid Levels (Relative to Top of Tube Sheet)
8.3.6-40	Total DVI Line 1 Flow
8.3.6-41	Total DVI Line 2 Flow
8.3.6-42	Core Inlet Temperatures
8.3.6-43	Core Outlet Temperatures
8.3.6-44	Integrated Core Inlet Flow
8.3.6-45	Upper Head Bypass Flow

Figures 8.3.6-1 through 8.3.6-45 are not included in the non-proprietary version of this report.

8.3.7 Inadvertent Automatic Depressurization System Actuation (SB14)

This test simulates the inadvertent actuation of the ADS without any nonsafety-related systems operating. A single failure of one of two fourth-stage ADS valves on hot leg 1 is represented in the test.

8.3.7.1 Summary of Test and NOTRUMP Simulation Observations

The timing of the critical events for this transient in comparison with test results is reported in Table 8.3.7-1. Figure 8.3.7-1 shows primary system pressure during this test (as measured at the top of the pressurizer), with selected component actuation and plant responses shown in relation to primary system pressure. At the beginning of the test, the rod bundle heaters are shifted to power control mode and the power increases to the maximum level (600 kW) for 140 seconds followed by a decaying power function simulating the total decay energy input of AP600 nuclear fuel. The NOTRUMP simulation is initiated from a steady-state condition at a power level of 600 kW.

Blowdown Phase

Since the transient being analyzed is the inadvertent actuation of the ADS system, no specific blowdown or natural circulation phase exists to be discussed. The transient initiation is similar to other simulations in that the sequence of events, related to safeguards systems actuation, are consistent with all other simulations. An R signal occurs coincident with the break, and an S signal occurs 0.5 seconds later (the R and S signals occur simultaneously at time zero in the NOTRUMP simulation). The R and S signals initiate the following actions:

- The MSLIVs close
- The MFWIVs shut off
- The CMT injection valves open
- The PRHR return flow valve opens
- The RCPs trip

The circulation flow through the CMTs and flow through the PRHR begin immediately after the CMT injection valves and the PRHR return flow valve are opened. Since the break being analyzed is caused by the inadvertent opening of the ADS system, the phenomenon normally occurring during the remainder of the blowdown and natural circulations phases, of a typical small LOCA response, will occur during the ADS phase. As such, the phenomena will be discussed during the ADS System Phase discussion which follows.

Natural Circulation Phase

The phenomena normally occurring during this phase of the transient will occur during the ADS phase due to the nature of the break being analyzed. As such, these phenomena will be discussed in the following section.

Automatic Depressurization System Phase

The ADS phase of the transient begins with the actuation of ADS-1 at [ ]^{a,b} seconds into the event (0 seconds for NOTRUMP). ADS-2 and ADS-3 occur within the next [ ]^{a,b} seconds.

The ADS actuation results in a rapid depressurization of the primary system. This transient differs from that observed for other break locations in that the pressurizer mixture level initially increases following break initiation. This break location results in the largest discharge of RCS fluid to the IRWST, since the ADS valves perform both the break and depressurization system functions. The rapid RCS depressurization following ADS actuation results in rapid saturation and voiding of hot RCS locations such as the core, upper plenum, upper head, hot legs and steam generator tubes. This saturation process temporarily stops the depressurization process until the ADS valves and the passive safety systems provide an adequate source of heat removal/absorption. As a result of the system voiding, primary system natural circulation is short lived as steam collects in the SG U-tube regions. Subsequently, the cold legs and cold leg balance lines drain providing a means by which the CMTs can saturate and ultimately commence draining. The CMT draindown is temporarily interrupted as the RCS depressurizes to the injection pressure of the accumulator tanks. The rapid injection of cold fluid from the accumulators from approximately [ ]^{a,b} seconds (121 to 336 seconds for NOTRUMP) temporarily reduces boiling in the rod bundle, and reduces void fractions in the rod bundle and the upper plenum. This rapid accumulator injection also results in the NOTRUMP simulation predicting the refill of the cold leg balance lines which delays the draindown of the CMTs. This phenomenon was not observed in the test. Once the accumulator discharge period ends, the boiling intensity increases in the rod bundle, which results in increased void fractions. In addition, following the termination of the accumulator discharge period, the NOTRUMP simulation allows the cold leg balance lines to once again drain thereby allowing the CMTs to resume draining. The CMT flows also increases after the accumulators empty, thereby minimizing the increase in predicted and observed core voiding.

During the period of ADS 1-3, which ends at ADS-4 actuation, approximately [ ]^{a,b} lbm (3335 lbm for NOTRUMP) of water is discharged from ADS-1, ADS-2, and ADS-3. ADS-4 occurs at [ ]^{a,b} seconds, (952 seconds for NOTRUMP) and the pressurizer water level decreases. The fluid discharge through ADS-1, ADS-2, and ADS-3 essentially ends, and the fluid is discharged through ADS-4.

IRWST Injection Phase

At approximately [ ]^{a,b} seconds (1040 seconds for NOTRUMP), the system pressure has fallen below the pressure corresponding to the water elevation head of the IRWST. Flow from the IRWST enters the DVI line, and the IRWST injection phase begins. Shortly thereafter, the CMT flow drops significantly. The flow from the IRWST reduces the rod bundle boiling and partially refills the upper plenum above the hot leg elevation. Water then flows steadily from the IRWST, into the DVI line, through the rod bundle, and out of the primary system through ADS-4.

This test demonstrates that the rod bundle is fully covered by water or a two-phase mixture at all times during this event, and there is no indication of heater rod temperatures increasing due to lack of cooling. The NOTRUMP simulation also demonstrates no heater rod temperature increase.

8.3.7.2 Comparison of NOTRUMP Simulation to Test Data

Figure 8.3.7-2 shows the pressure at the top of the pressurizer for the test and the NOTRUMP simulation. Note that the test data shown for the low pressure region (right scale on figure) is taken from the narrow range pressure instrumentation while the high pressure region (left scale on figure) is taken from the wide range pressure instrumentation. NOTRUMP predicts a slightly higher system pressure but the agreement is reasonable since the trends of the data are closely followed.

The primary system pressure decreases significantly at transient initiation due to the inadvertent actuation of the ADS system. The trends of the pressure are the same following ADS-1 actuation between the test and the NOTRUMP simulation. The only observed difference in the pressure response is a direct result of the delay in achieving ADS-4 actuation in the NOTRUMP simulation, the cause of which will be discussed later.

Figure 8.3.7-3 shows the collapsed liquid level in the pressurizer for the test and the NOTRUMP simulation. The break flow causes an initial increase in pressurizer level since the break flow path is through the pressurizer to the ADS Stages 1 through 3 valves. As the passive systems become effective, the pressurizer level initially falls; however, during the accumulator injection period, the pressurizer level again increases. The NOTRUMP pressurizer level decrease following ADS-4 actuation is more pronounced than the decrease in the test data as a result of oscillatory surge line flow behavior.

Figure 8.3.7-4 shows the collapsed liquid levels in CMT-1 for the test and the NOTRUMP simulation. Figure 8.3.7-5 shows the collapsed liquid levels in CMT-2 for the test and the NOTRUMP simulation. In the test, CMT-1 transitions from the circulation mode to the draindown mode at about [ ]^{a,b} seconds and CMT-2 transitions at about [ ]^{a,b} seconds. In the NOTRUMP simulation, CMT-1 transitions from the circulation mode to the draindown mode at 211 seconds and CMT-2 transitions at 176 seconds. The differences in the transition to the draindown mode between NOTRUMP and the test are due to differences in the occurrence of upper CMT saturation and subsequent phase separation.

The NOTRUMP simulation also forms a sustained level in the cold leg balance lines at approximately 76 seconds for both CMT-1 and CMT-2 whereas the test forms an initial level at approximately the [ ]^{a,b} and [ ]^{a,b} seconds respectively (see Figures 8.3.7-10 and 8.3.7-11). However, the entire NOTRUMP upper fluid node volume must reach saturation conditions prior to allowing the CMTs to transition to draindown mode. Figures 8.3.7.33 through 8.3.7-36 indicate the upper CMT region quickly saturates in the test thereby allowing earlier CMT draining, while the NOTRUMP top fluid node heats up more slowly. Once saturation occurs, the available source of vapor flow allows for continued CMT draindown since the cold leg balance line levels have decreased sufficiently. The simulation CMT levels temporarily increase during the accumulator injection phase as the cold legs momentarily refill and water flows up the balance line and into the CMTs. This interruption of the CMT draining process ultimately results in a delay in the receipt of the ADS-4 actuation signal. The CMTs re-commence draindown following the end of the accumulator discharge period. The NOTRUMP CMT levels are predicted to increase late in the simulation, following IRWST injection, when the cold legs once again refill and water flows up the CMT balance line into the CMTs. Although the test data provided does not show this for the time period shown, the test data exhibits the same phenomenon after 3000 seconds.

Figures 8.3.7-6 and 8.3.7-7 show the collapsed liquid levels in the hot side (upside) and the cold side (downside) of the SG-2 U-tubes for the test and the NOTRUMP simulation. Figures 8.3.7-8 and 8.3.7-9 show the same information for SG-1. These plots indicate that system saturation is predicted to occur rapidly resulting in early draining of the SG tubes, consistent with the test results. Once the SG tube levels decrease sufficiently to allow the formation of cold leg levels, the cold leg balance lines also have an available vapor source enabling them to commence sustained balance line draining. This, in turn, provides a sustained vapor source to the CMTs allowing them to transition from circulation mode to the draindown mode. For the NOTRUMP code, CMT draindown can not occur until the top CMT node saturates and cold leg balance line liquid flow into the CMT ceases. The collapsed balance line levels are shown in Figures 8.3.7-10 and 8.3.7-11. The previously noted cold leg refilling predicted by NOTRUMP can be see in these plots.

The prediction of the balance line drain times demonstrates that the PIRT items related to balance line-to-cold leg behavior and cold leg phase separation are predicted reasonably well. The comparison of Figures 8.3.7-10 and 8.3.7-11 and the prediction of CMT levels in Figures 8.3.7-4 and 8.3.7-5, indicate that even though the timing of the CMT transition to draindown is different, the CMT balance line pressure drop and flow composition parameters identified in the PIRT are reasonably predicted by NOTRUMP.

Figures 8.3.7-12 and 8.3.7-13 show the collapsed liquid levels in Accumulator 1 and Accumulator 2 for the test and the NOTRUMP simulation. Both the test and NOTRUMP simulation indicate a continuous injection period as a result of the sustained depressurization which results from ADS actuation. The accumulator injection is well matched between the NOTRUMP simulation and the test data.

The next series of plots, Figures 8.3.7-14 through 8.3.7-20, relate to the collapsed and two-phase levels at different locations in the vessel. Both the test and NOTRUMP simulations indicate early voiding in the core and upper plenum region as a result of the inadvertent actuation of the ADS system valves. In general, the NOTRUMP simulations predicts similar or higher void fractions to those observed in the test. As such, the level trends are also similar, with some differences in timing due to the shift in the ADS-4 actuation. Due to the nature of the Inadvertent ADS actuation, the largest change in vessel levels occur during the accumulator injection period. Following accumulator empty time, the levels decrease slightly until IRWST injection occurs following ADS-4 actuation. Similar trends occur in the collapsed and two-phase levels in the upper plenum (see Figures 8.3.7-15 and 8.3.7-16). It should be noted that the test information for the collapsed upper plenum level does not represent the entire upper plenum. The region covered by the instrumentation only provides information for the region just below the hot legs to the upper support plate. Valid instrumentation, with which to measure the entire upper plenum region, was unavailable. As a result, upper plenum collapsed level information below this region is unavailable for the test and Figure 8.3.4-15 indicates a straight line when the level drops below the bottom tap of the valid instrumentation. In addition, an accurate two-phase mixture level for the test data can not be calculated based on the available information. As such, only the NOTRUMP prediction for two-phase level is included in Figure 8.3.4-16. A plot of the core average void fraction for the test and the NOTRUMP simulation is provided (see Figure 8.3.7-17). This figure shows similar trends between the test and the simulation, with reduced voiding during the injection of the cold accumulator water and IRWST water.

Figure 8.3.7-18 shows the collapsed liquid level in the downcomer for the test and the NOTRUMP simulation. The trends seen in the downcomer level are similar to those observed in the test. The NOTRUMP simulation predicts a higher refill of the downcomer region during the accumulator injection phase than observed in the test facility. As a result, liquid flows into the cold legs, cold leg balance lines, and ultimately the CMTs which results in a delay in ADS-4 actuation. Since the occurrence of ADS 4 actuation and subsequent IRWST injection is delayed in the simulation relative to the test, the collapsed downcomer levels diverge at this point. There is reasonable agreement between the test and the simulation, demonstrating that the highly ranked PIRT items related to the levels in the core, upper plenum, and downcomer are predicted reasonably well by NOTRUMP.

Figure 8.3.7-20 shows the collapsed liquid level in the upper head for the test and the corresponding NOTRUMP analysis. In both the test and NOTRUMP simulations, the upper head drains as the upper head fluid temperature reaches saturation conditions. This occurs at [ ]^{a,b} in the test and 50 seconds in the simulation. NOTRUMP predicts that the upper head drains completely while the test indicates some water remains in the head until approximately 800 seconds.

The next series of plots show the comparisons between the flows in the safety-related systems during the test and simulation.

Figure 8.3.7-21 shows the CMT-1 injection line mass flow rate for the test and the NOTRUMP simulation. Figure 8.3.7-22 shows the CMT-2 injection line mass flow rates. These figures show reasonable agreement between the test and the simulation.

Figure 8.3.7-23 shows the accumulator 1 injection line mass flow rates for the test and the NOTRUMP simulation. Figure 8.3.7-24 shows the accumulator 2 injection line mass flow rates. The prediction and the data are in reasonable agreement, demonstrating that this highly ranked PIRT item is reasonably predicted by NOTRUMP.

Figure 8.3.7-25 shows the IRWST-1 injection line mass flow rates for the test and the NOTRUMP simulation. Figure 8.3.7-26 shows the IRWST-2 injection line flow rates. Subsequent to the initial delay in IRWST injection, which results from the ADS-4 actuation delay for the NOTRUMP simulation, the trends observed between the test and NOTRUMP are in reasonable agreement. The test and the simulation results are similar with the test reaching full flow at a slower rate due to slightly higher DVI line pressures in the test compared to the simulation. It should be noted that the NOTRUMP model does not reflect the existence of the IRWST overflow path to the sump. As such, the static head of water in the IRWST is over-predicted in the NOTRUMP simulation resulting in IRWST flow being predicted to occur at approximately the same time as observed in the test even though the ADS-4 actuation was delayed. This also results in the higher predicted IRWST flow when compared to the observed test data.

Figure 8.3.7-27 shows the integrated mass flow through ADS stages 1 through 3 for the test and the NOTRUMP simulation. The differences between the test and the simulation occur near the accumulator injection phase of the transient. The test data indicate that more RCS inventory is maintained in the pressurizer prior to accumulator injection. As a result, the test indicates higher liquid discharge rates through the ADS 1-3 valves than predicted by NOTRUMP until the simulation eventually re-establishes pressurizer level during accumulator injection. In addition, the delay in receiving the ADS-4 signal in the NOTRUMP code, due to the predicted CMT refill period, results in a delay in the termination of liquid discharge through the ADS 1-3 valves. However, the observed trends are reasonable and demonstrate that the PIRT highly ranked items related to ADS 1-3 (critical flow, two-phase pressure drop, and valve loss coefficients) are reasonably well represented by the NOTRUMP code. Figure 8.3.7-28 shows the integrated mass flow through ADS stage 4 for the test and the simulation. These curves also demonstrate reasonable agreement for the ADS flows once the delay in ADS-4 actuation is accounted for. The agreement of these curves supports the conclusion that the PIRT highly ranked items related to ADS stage 4 (critical flow, two-phase pressure drop, and valve loss coefficients) are predicted well by NOTRUMP.

Figure 8.3.7-30 shows the PRHR return line mass flow rate for the test and the corresponding NOTRUMP analysis. These are in reasonable agreement up to 300 seconds (see below). Figure 8.3.7-31 shows the PRHR inlet and outlet temperatures for the test and the NOTRUMP simulation. These show that while the same general trends are followed, the NOTRUMP simulation underpredicts the PRHR heat removal as evidenced by the significantly higher predicted PRHR outlet temperature when

compared to the test simulation. For code execution efficiency, the PRHR node calculations are turned off and removed from the NOTRUMP simulation 193 seconds after ADS-3 is actuated (300 seconds into the transient). This differs from the PRHR removal method used for all other transient simulations in that the removal is delayed beyond ADS-3 actuation. For this simulation, the PRHR remains an effective heat removal source for a period of time following ADS-3 activation as observed in the test data. The removal of the PRHR system from the simulation at ADS-3 time would be overly conservative and significantly skew the transient comparisons. For this reason, the removal of the PRHR is delayed by 193 seconds when the observed and predicted PRHR heat transfer rates are smaller. Removal of these fluid nodes, at this time, enhances code execution without significantly impacting the transient results. Once the calculations for these nodes are eliminated, the plotted values remain at the last calculated value, even though the actual heat transfer is zero. Figure 8.3.7-32 shows the NOTRUMP PRHR heat removal rate versus time for this simulation. There is no directly comparable data available from the test, so the plot only contains the simulation information.

Figure 8.3.7-33 shows the CMT-1 test temperatures at various elevations. Figure 8.3.7-34 shows temperatures for the four NOTRUMP fluid nodes representing CMT-1. A direct comparison between Figures 8.3.7-33 and 8.3.7-34 cannot easily be performed because the NOTRUMP temperatures are averages over a region while the test data represents distinct elevations. The trends of the data can be compared however. The agreement is reasonable between the test and the simulation with the differences in the heatup and saturation of the top node resulting in different CMT drain performance. The temperature profiles for CMT-2 are contained in Figures 8.3.7-35 and 8.3.7-36. Relating this information to the CMT related PIRT items, the temperature agreement at the top of the tank indicates reasonable NOTRUMP code prediction for the natural circulation between the CMT and the cold leg balance line. As observed in other tests, the NOTRUMP code underpredicts the time at which the temperature at the bottom of the CMT increases resulting in warmer conditions in the DVI line and subsequently the lower plenum and core. This indicates that thermal stratification is not well represented by NOTRUMP. Due to the nature of this test simulation, the prediction of thermal stratification in the CMT is not as important as for smaller breaks since it does not affect ADS actuation times significantly.

SG-related information is provided in Figures 8.3.7-37 through 8.3.7-39. Figure 8.3.7-37 shows the SG secondary pressures for the test and the NOTRUMP simulation. The NOTRUMP simulation secondary pressures are higher than the test for the entire transient. This is primarily due to not modeling the ambient heat losses; however, the effect of the higher pressures is insignificant on the primary to secondary heat transfer. The temperatures of the secondary side of the SGs are provided in Figure 8.3.7-38. As can be seen, the NOTRUMP secondary temperatures exhibit sharp drops in temperature. These drops in temperatures correspond to periods of liquid flow into the primary side steam generator tubes for the NOTRUMP simulations which are not observed in the test data. This liquid subsequently flashes, due to secondary to primary heat transfer, and results in the secondary temperature drop. As a result, additional secondary energy is transferred to the primary in the simulation compared to the test. This additional energy must be removed by the passive safety systems in the simulation.

Figure 8.3.7-39 shows the collapsed SG levels for the test and the NOTRUMP simulation. The levels are initialized lower in the simulation than the test. The NOTRUMP simulation represents the secondary side as a single node, whereas the test represents a full recirculating SG design. This low level for the simulation is not important since the tubes remain covered with water at all times, and therefore, the heat transfer characteristics are not significantly affected.

Figures 8.3.7-40 and 8.3.7-41 show the total DVI line flow rate for each of the DVI lines. The agreement between the test and the NOTRUMP simulation is reasonable for these parameters with the greatest differences resulting following ADS-4 actuation and subsequent IRWST injection.

Additional comparisons between the test and the NOTRUMP simulation that are provided include core inlet temperature (see Figure 8.3.7-42) and core outlet temperature (see Figure 8.3.7-43). The core inlet temperature is higher for the simulation compared to the test, while the outlet temperature indicates saturation conditions during most of the transient.

The final two plots (see Figures 8.3.7-44 and 8.3.7-45), the integrated core inlet flow and the upper head bypass flow, only include the results of the simulation. There is no test data available for these items. They are included for completeness.

TABLE 8.3.7-1
SB14 SEQUENCE OF EVENTS

Event	Definition	OSU (seconds)	NOTRUMP (seconds)
Break Opens		0	0
R Signal		0	0
S Signal		0.5	0
MFW Isolation Valve Closes		3.6	3.1
CMT Isolation Valves Open		6.1	5.6
RCPs Trip		9	6
CMT-1 Starts Draindown Phase	CMT level dropping and top of tank saturated	74	211
CMT-2 Starts Draindown Phase	CMT level dropping and top of tank saturated	74	176
ADS-1	CMT level 41 in. + 15 sec	0	0
Accumulators Start		116	121
ADS-2	ADS-1 + 47 sec.	49	47
ADS-3	ADS-1 + 107 sec.	108	107
Accumulators Empty		332	332
ADS-4		784	952
IRWST Injection		992	1040

TABLE 8.3.7-2 FIGURES FOR OSU INADVERTENT ADS ACTUATION (SB14)	
Figure No.	**Title**
8.3.7-1	Facility Response Summary
8.3.7-2	Pressurizer Pressure
8.3.7-3	Pressurizer Level (Relative to Bottom Tap)
8.3.7-4	CMT-1 Level (Relative to Bottom Tap)
8.3.7-5	CMT-2 Level (Relative to Bottom Tap)
8.3.7-6	Steam Generator 2 Hot Side Collapsed Level (Relative to Bottom Tap)
8.3.7-7	Steam Generator 2 Cold Side Collapsed Level (Relative to Bottom Tap)
8.3.7-8	Steam Generator 1 Hot Side Collapsed Level (Relative to Bottom Tap)
8.3.7-9	Steam Generator 1 Cold Side Collapsed Level (Relative to Bottom Tap)
8.3.7-10	Cold Leg Balance Line 1 Levels (Relative to Bottom Tap)
8.3.7-11	Cold Leg Balance Line 2 Levels (Relative to Bottom Tap)
8.3.7-12	ACC-1 Level (Relative to Bottom Tap)
8.3.7-13	ACC-2 Level (Relative to Bottom Tap)
8.3.7-14	Core Collapsed Liquid Levels (Relative to Bottom of Lower Plenum)
8.3.7-15	Upper Plenum Collapsed Levels (Relative to Bottom of Lower Plenum)
8.3.7-16	NOTRUMP Upper Plenum 2-phase Level (Relative to Bottom of Lower Plenum)
8.3.7-17	Average Core Void Fraction
8.3.7-18	Collapsed Downcomer Levels (Relative to Bottom of Lower Plenum)
8.3.7-19	Not Applicable
8.3.7-20	Upper Head Collapsed Liquid Level (Relative to Bottom of Lower Plenum)
8.3.7-21	CMT-1 Injection Line Mass Flow
8.3.7-22	CMT-2 Injection Line Mass Flow
8.3.7-23	ACC-1 Injection Line Mass Flow
8.3.7-24	ACC-2 Injection Line Mass Flow
8.3.7-25	IRWST-1 Injection Line Mass Flow
8.3.7-26	IRWST-2 Injection Line Mass Flow
8.3.7-27	ADS Stage 1-3 Integrated Flows
8.3.7-28	ADS Stage 4 Integrated Total Flow
8.3.7-29	Not Applicable
8.3.7-30	PRHR Return Line Mass Flow
8.3.7-31	PRHR Inlet and Exit Temperatures
8.3.7-32	NOTRUMP PRHR Heat Transfer Rate
8.3.7-33	Test CMT-1 Temperature Profile
8.3.7-34	NOTRUMP CMT-1 Temperature Profile
8.3.7-35	Test CMT-2 Temperature Profile
8.3.7-36	NOTRUMP CMT-2 Temperature Profile

TABLE 8.3.7-2 (Cont.) FIGURES FOR OSU INADVERTENT ADS ACTUATION (SB14)	
Figure No.	**Title**
8.3.7-37	Steam Generator Pressures
8.3.7-38	Steam Generator Secondary Fluid Temperatures
8.3.7-39	Steam Generator Secondary Liquid Levels (Relative to Top of Tube Sheet)
8.3.7-40	Total DVI Line 1 Flow
8.3.7-41	Total DVI Line 2 Flow
8.3.7-42	Core Inlet Temperatures
8.3.7-43	Core Outlet Temperatures
8.3.7-44	Integrated Core Inlet Flow
8.3.7-45	Upper Head Bypass Flow

Figures 8.3.7-1 through 8.3.7-45 are not included in the non-proprietary version of this report.

8.4 Assessment of NOTRUMP Comparison to Oregon State University Integral Systems Tests

8.4.1 Introduction

The overall performance of NOTRUMP with respect to the OSU tests is discussed in this section. The approach used is similar to that used for SPES in Section 7.4, with assessments of event timing, safety systems flows, and overall system mass. In the SPES analysis, it is found that with the exception of test S00401, the time of CMT draining, ADS actuation, and IRWST initiation are overpredicted. Once the events listed above were predicted, the break flow, ADS flow, CMT flow, and IRWST flow were found to compare well with the data. It was also found that NOTRUMP underpredicts the total system mass for all tests at the time of IRWST injection.

8.4.2 Comparison of NOTRUMP-Predicted Event Times and Flows for Oregon State University

Figures 8.4-1 to 8.4-6 compare ADS-1 initiation time, time of CMT draining, ADS-4 initiation time, and time of IRWST initiation. Note that these comparisons do not include test SB23 (0.5-in. cold leg break). In that test, ADS initiation is predicted to occur much later using the base model. In addition, the break area is adjusted to match the initial measured break flow. Since the break, PRHR, and CMT NOTRUMP models were deliberately modified to force agreement with the initial break flow and actual ADS initiation time in this test, a comparison with the data is not appropriate. For these reasons this test is discussed separately. For the remaining tests, Figures 8.4-1 to 8.4-6 show that NOTRUMP predicts generally late ADS-1 and CMT initiation times for OSU, consistent with SPES predictions, while other event times are predicted well.

Figures 8.4-7 to 8.4-13 compare average flow rates through the break, CMT, ADS valves, and IRWST for all the tests except test SB23. These averages are obtained in the same fashion as for SPES by calculating the approximate slope of the integral. In all the OSU tests, NOTRUMP underpredicts the total mass ejected from the ADS 1 to 3 valves, and overpredicts the total mass ejected from the break by about the same or a greater amount. This difference is believed to be due to one or both of the following factors:

a) Overprediction of the break flow rate and delayed ADS actuation. This results in additional loss of system mass prior to ADS actuation (this is seen more clearly when system mass plots are presented in the next section). When ADS is actuated, the lower mass inventory results in only a partial refilling of the pressurizer, leading to high-quality or all steam ADS flow in the prediction. In the test, the pressurizer refills nearly completely and leads to low-quality and higher-density ADS flow. Some evidence that this is an important contributing factor may be seen in the inadvertent ADS test (SB14, Subsection 8.3.7). In this test, agreement between predicted and measured pressurizer levels, and ADS flows up to accumulator injection is better than in other tests because there is no break to drain the system beforehand.

b) Underprediction of the entrainment rate above the mixture level following ADS actuation. During the early stages of ADS flow, the steam flow rate in the pressurizer is significant. While this leads to level swell, which is correctly predicted by the NOTRUMP model, it may also lead to significant levels of entrainment from the mixture to the steam space, which would not be predicted by the NOTRUMP models (this is consistent with observations from the GE level swell tests, where some entrainment was inferred from the vessel mass data). This results in less liquid being entrained back into the pressurizer and out the ADS.

Figures 8.4-12 and 8.4-13 indicate that NOTRUMP overpredicts the rate of injection of IRWST flow into the system for some tests. This higher rate is likely due to a higher predicted water level in the IRWST. In the simulations, overflow of water from the IRWST to the sump is not modeled.

8.4.3 Comparison of NOTRUMP-Predicted System Mass for Oregon State University

Figures 8.4-14 to 8.4-19 compare measured and predicted primary system mass for all the tests except test SB23, which is discussed later. The measured mass is a summation of the mass in the primary system components, excluding the accumulators, CMT tanks and lines, and a few minor components for which dP data is not available. These plots therefore represent primarily the total mass in the vessel, pressurizer, and main coolant loops. The NOTRUMP-predicted mass is obtained by summing the fluid node masses in the corresponding components. It is observed that prior to the test, a difference of about 220 lb (10 percent of the initial system mass) exist between the measurement and NOTRUMP, with NOTRUMP higher in all cases. About 80 lb can be attributed to small differences between the assumed and actual component volumes. The remaining discrepancy of about 140 lb, or 6 percent of the total mass, is attributed to biases in level measurements or regions in the system not covered by dP cell spans and not accounted for in the measurement. The figures show the NOTRUMP masses adjusted downward by 80 lb, compared with the data.

It can be seen that in all the tests except test SB23, the predicted system mass is underpredicted late in the transient. This is consistent with what is observed in the SPES test predictions and indicates that at the time of IRWST, NOTRUMP predicts a conservatively low system mass inventory. In addition, the system mass at the time of ADS-1 actuation is also underpredicted by NOTRUMP, which explains the previously noted differences in predicted and measured ADS flows.

8.4.4 Assessment of Oregon State University Test SB23 (0.5-in. Cold Leg Break)

Test SB23 is a test with the smallest break simulation, 0.5-in. The NOTRUMP prediction of this test is not good. The prediction of ADS initiation is several hundred seconds late. When the base NOTRUMP model is used (i.e., the same model as used in the other simulations), the CMTs begin to refill, significantly delaying ADS. This is due to the following factors:

a) Underprediction of the PRHR heat transfer rate to the IRWST.
b) Overprediction of the temperature of the fluid exiting the CMT and entering the vessel.

Both these factors result in excess core steam generation and system repressurization. In a transient in which a substantial fraction of the energy removed from the system is through the PRHR, the code's tendency to underpredict the PRHR heat transfer becomes a significant deficiency. In addition, for cases in which CMT recirculation occurs for an extended period of time prior to CMT draining, the lack of a thermal stratification model also becomes a significant deficiency.

Figures 8.4-20 and 8.4-21 show the predicted and measured system mass for both the base model and the modified model. In both cases, the system mass is overpredicted prior to ADS actuation. This trend is opposite to the observed trends in all the other tests. Once ADS is actuated, however, the mass is once again underpredicted.

The system mass is overpredicted prior to ADS because the predicted system pressure is lower. This causes the accumulators to inject excess mass into the system in the simulation.

The system pressure is too low because the break flow is overpredicted (see Figure 8.3.5-29) during the natural circulation period. Although the difference is small, the prolonged time period removes sufficient mass and energy to reduce the predicted pressure. In the modified case, the additional heat removal from the modified PRHR increases the depressurization, so the overprediction of system mass is more severe in this case.

It should be noted that once the ADS has actuated (at 3800 seconds for the base case and 2200 seconds for the modified case), the predicted system mass falls below the measured data. This indicates that the drift flux and level swell models in NOTRUMP compensate during the depressurization phase by ejecting more mass from the ADS and the break. In addition, a comparison of the measured system mass for this test with the other tests indicates that the smaller breaks are the least challenging relative to the amount of mass that must be replenished by the passive safety-related systems.

8.4.5 Conclusion

The predictions of the OSU tests are in general consistent with the predictions of the SPES-2 tests. For breaks larger than 2-in., the NOTRUMP models predict event times and safety system flows reasonably well, with a conservative bias in the predicted system mass that must be replenished by the safety-related systems.

In the Appendix K application of NOTRUMP to the AP600, the following additional conservatisms are applied:

- Use of the 1971 ANS standard for decay heat, plus 20 percent.
- Increased resistance in the ADS, CMT, accumulator, and IRWST lines to reduce the replacement flow from the safety-related systems.

- Identification of the limiting break size and location. It should be noted that Appendix K requires use of the Moody critical flow model, which is known to overpredict the critical flow rate. However, ranging the discharge coefficient is equivalent to ranging the break area. That is, the limiting area using Moody is smaller than the limiting area using a best-estimate model, but the transient with least mass inventory is identified.

TABLE 8.4-1 FIGURES FOR SECTION 8.4	
8.4-1	Comparison of ADS-1 Actuation Time
8.4-2	Comparison of CMT-1 Draindown Time
8.4-3	Comparison of CMT-2 Draindown Time
8.4-4	Comparison of ADS-4 Actuation Time
8.4-5	Comparison of IRWST-1 Injection Time
8.4-6	Comparison of IRWST-2 Injection Time
8.4-7	Comparison of Average Break Flow
8.4-8	Comparison of Average CMT-1 Recirculation Flow
8.4-9	Comparison of Average CMT-2 Recirculation Flow
8.4-10	Comparison of Average ADS 1-3 Flow
8.4-11	Comparison of Average ADS-4 Flow
8.4-12	Comparison of Average IRWST-1 Flow
8.4-13	Comparison of Average IRWST-2 Flow
8.4-14	Comparison of System Mass for Test SB09
8.4-15	Comparison of System Mass for Test SB10
8.4-16	Comparison of System Mass for Test SB12
8.4-17	Comparison of System Mass for Test SB13
8.4-18	Comparison of System Mass for Test SB14
8.4-19	Comparison of System Mass for Test SB18
8.4-20	Comparison of System Mass for Test SB23-Base Model
8.4-21	Comparison of System Mass for Test SB23-Modified Model

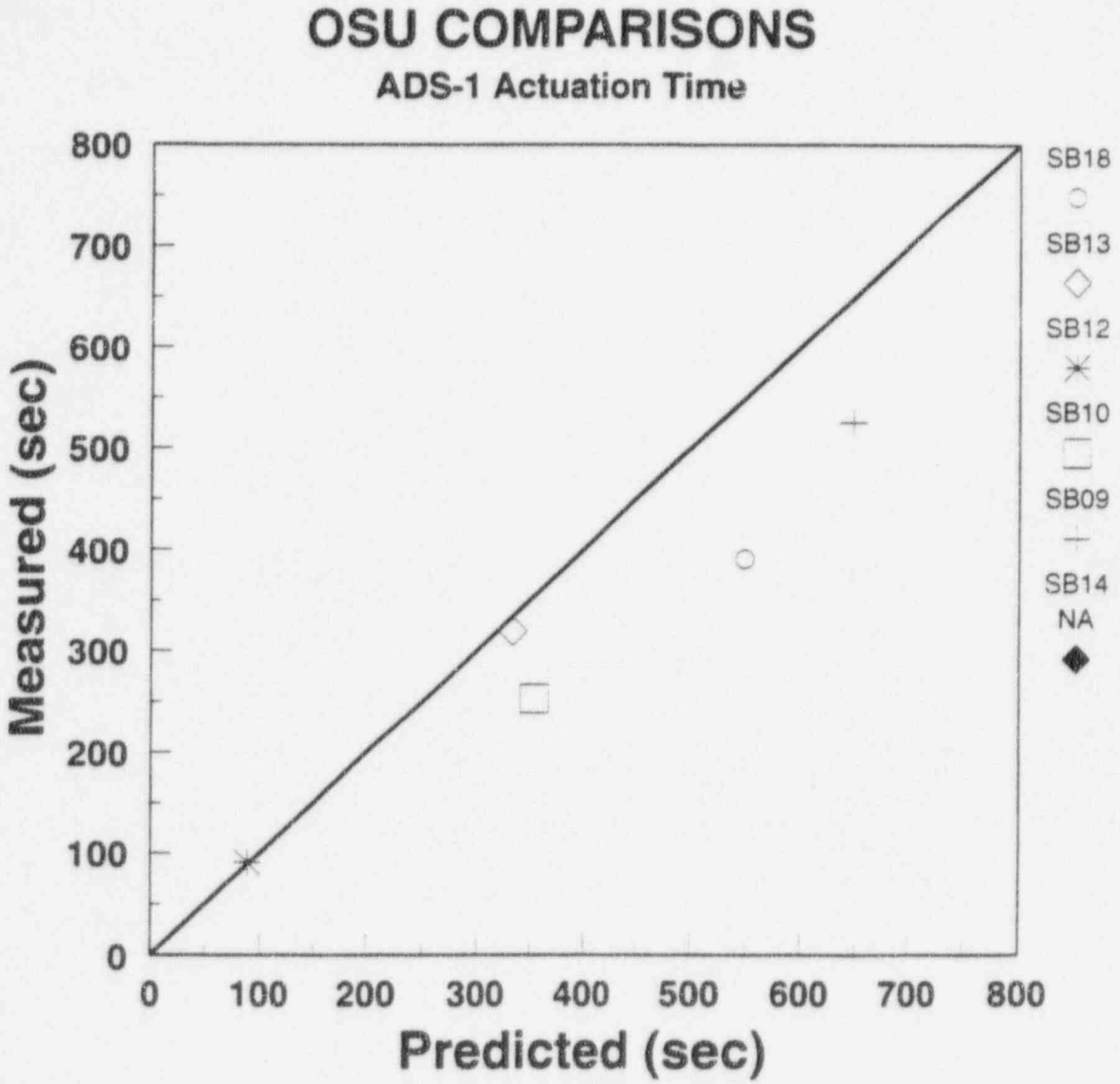

Figure 8.4-1 Comparison of ADS-1 Actuation Time

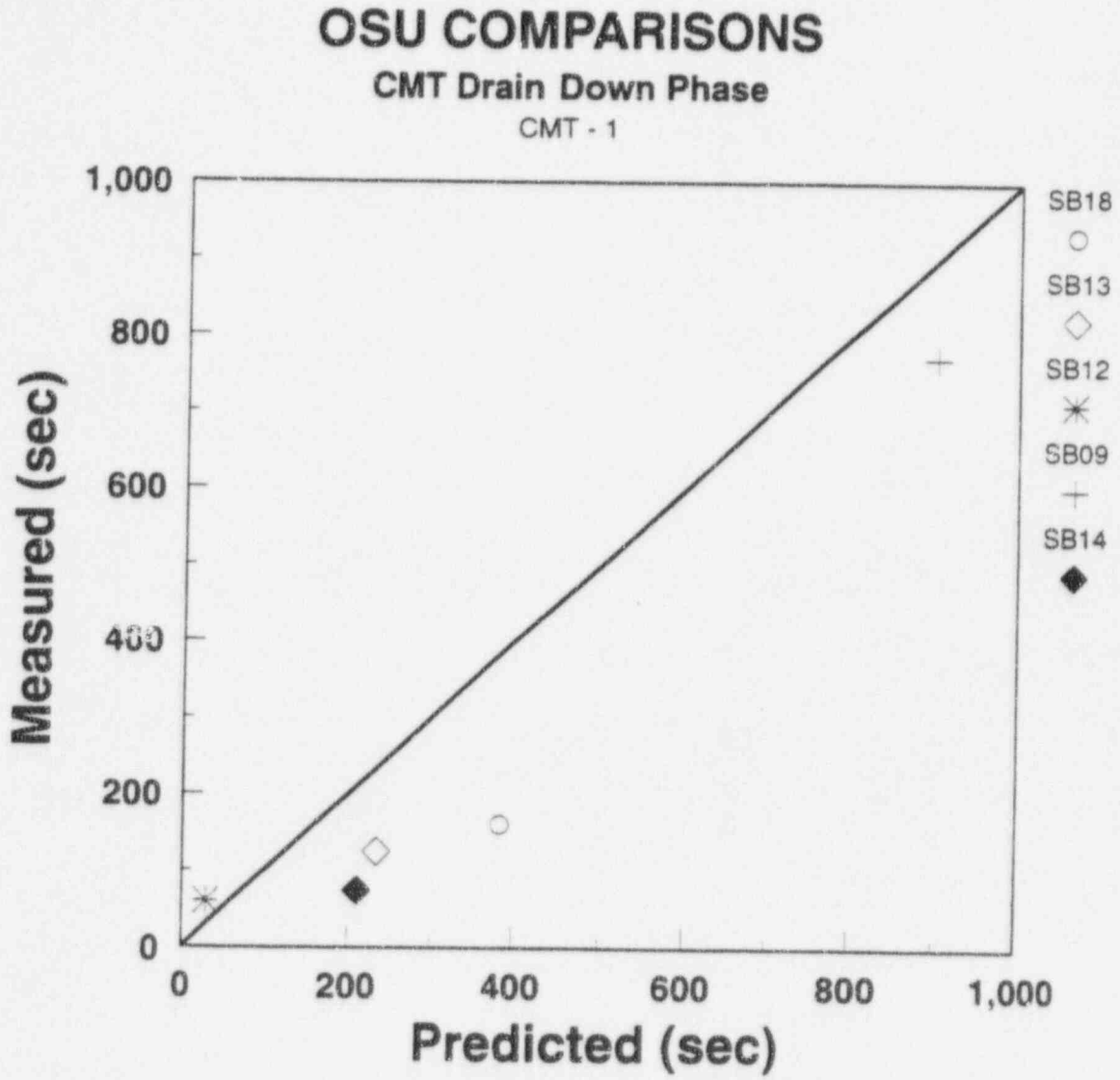

Figure 8.4-2 Comparison of CMT-1 Draindown Time

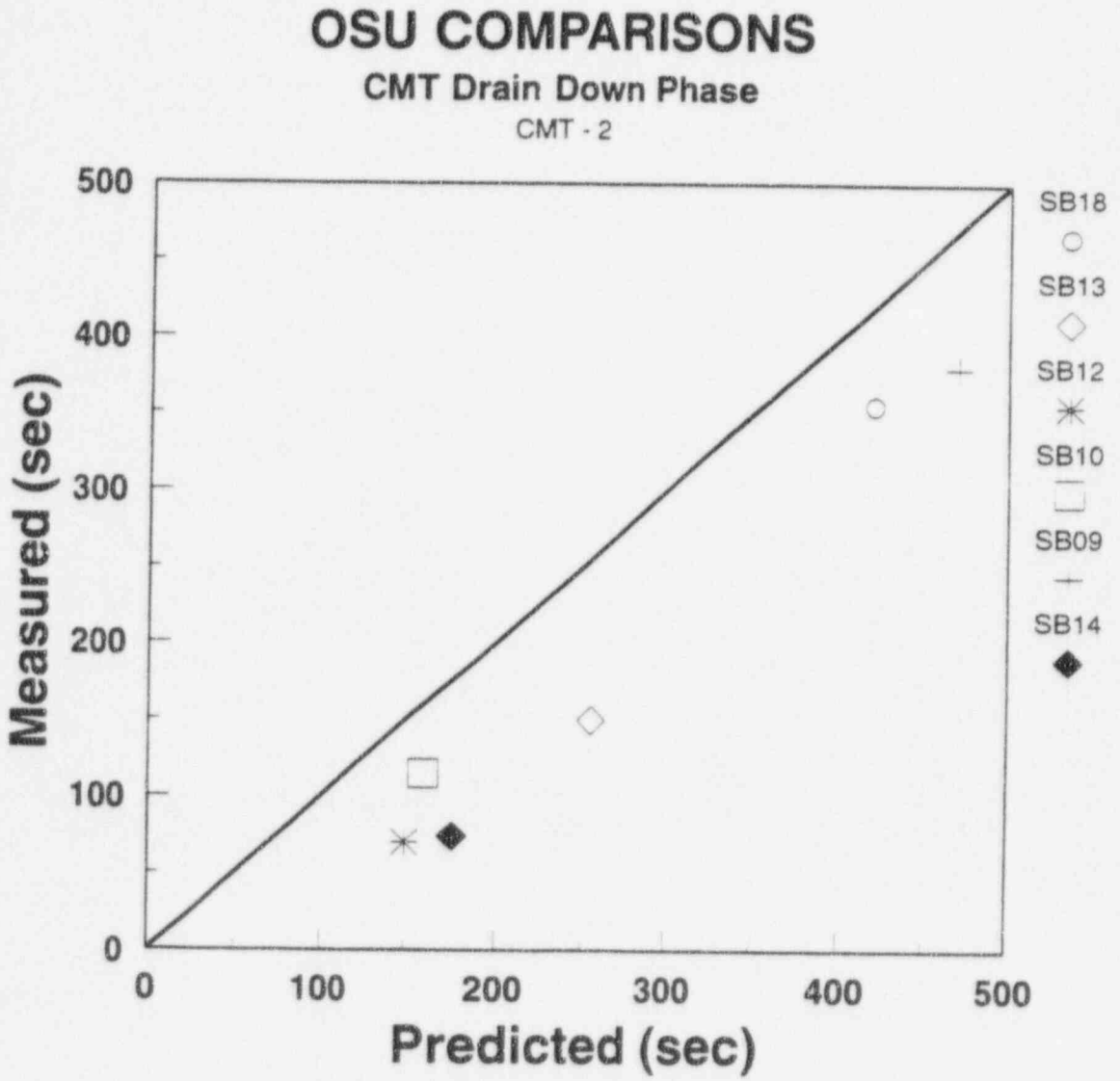

Figure 8.4-3 Comparison of CMT-2 Draindown Time

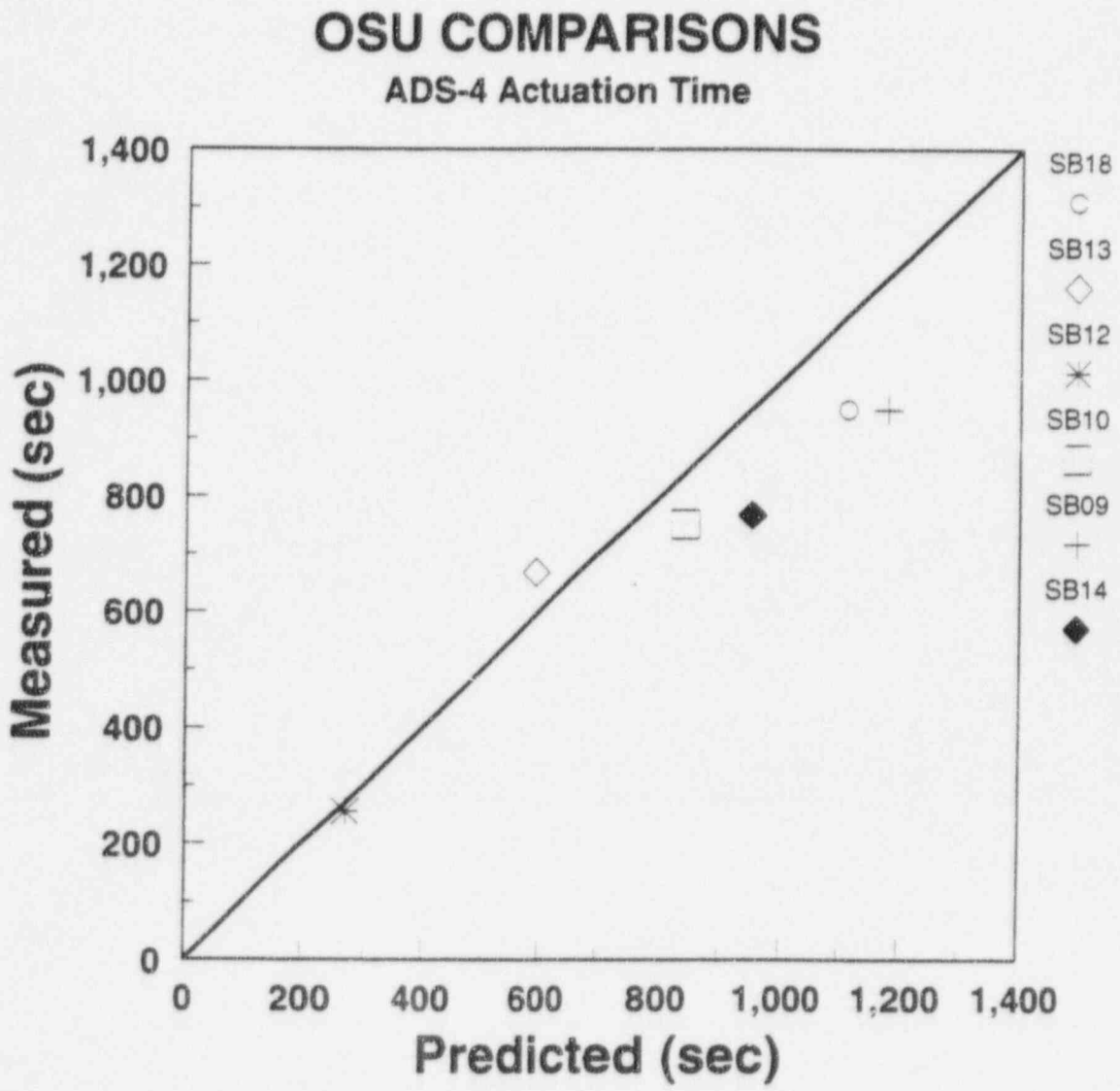

Figure 8.4-4 Comparison of ADS-4 Actuation Time

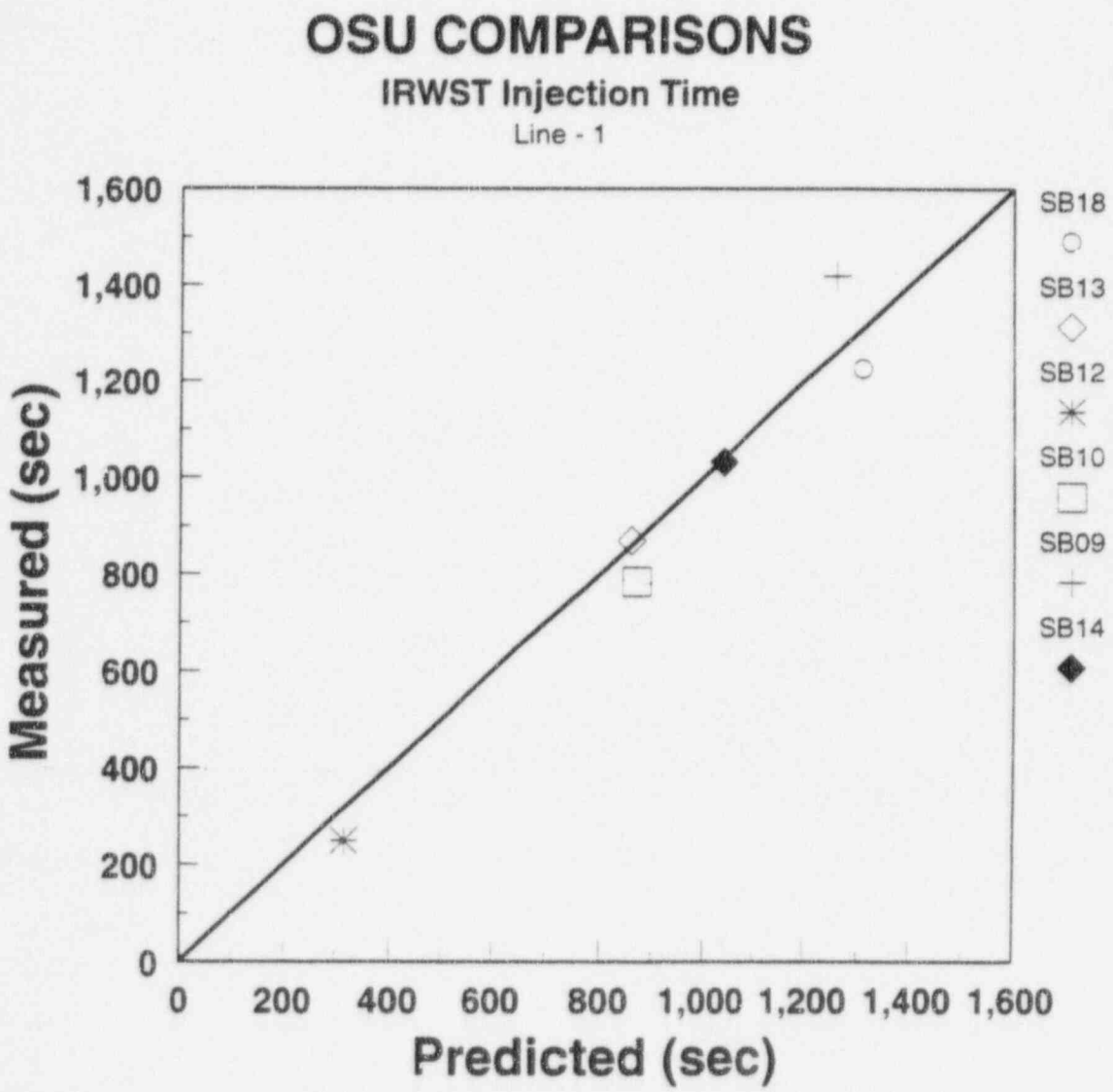

Figure 8.4-5 Comparison of IRWST-1 Injection Time

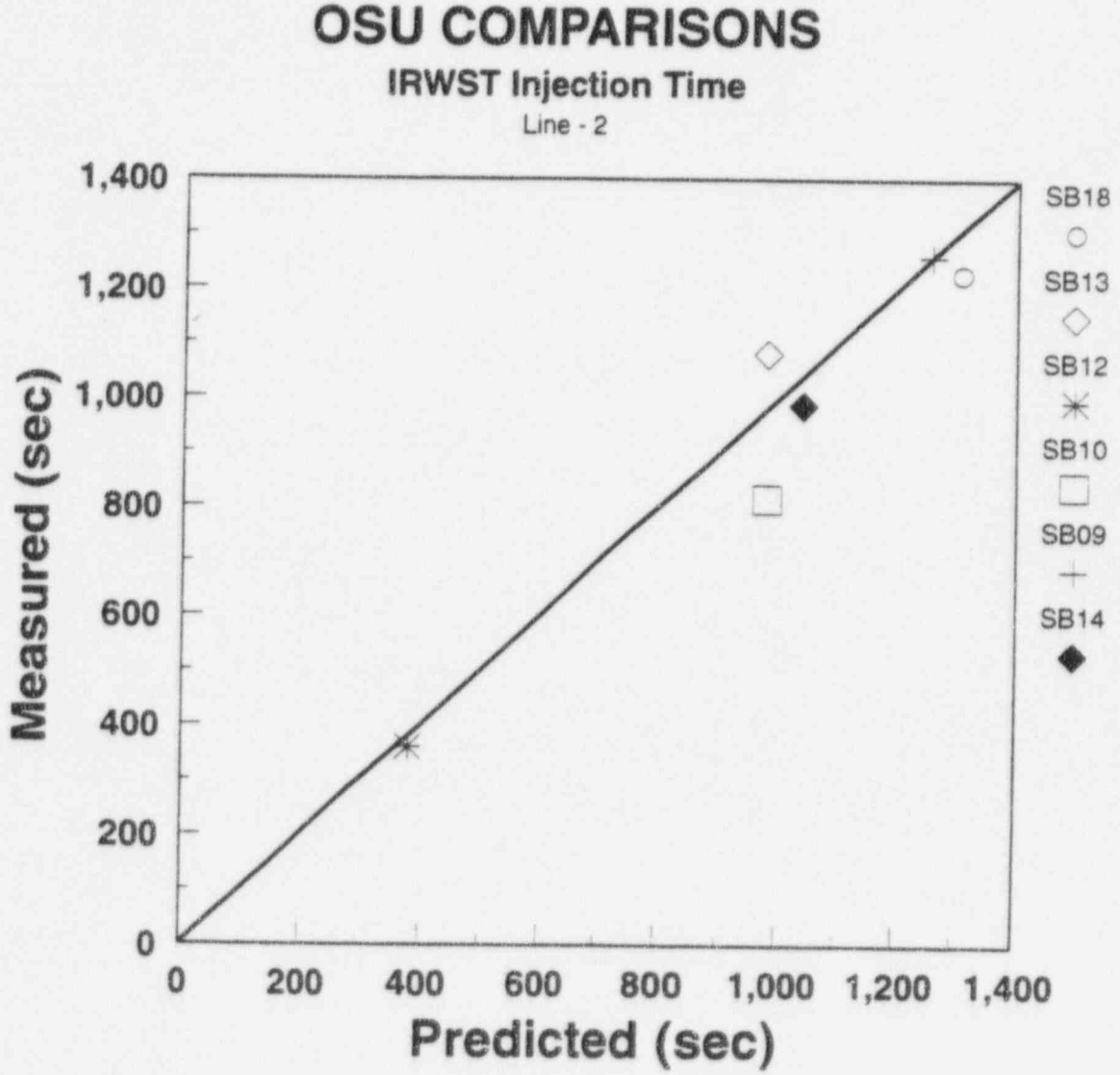

Figure 8.4-6 Comparison of IRWST-2 Injection Time

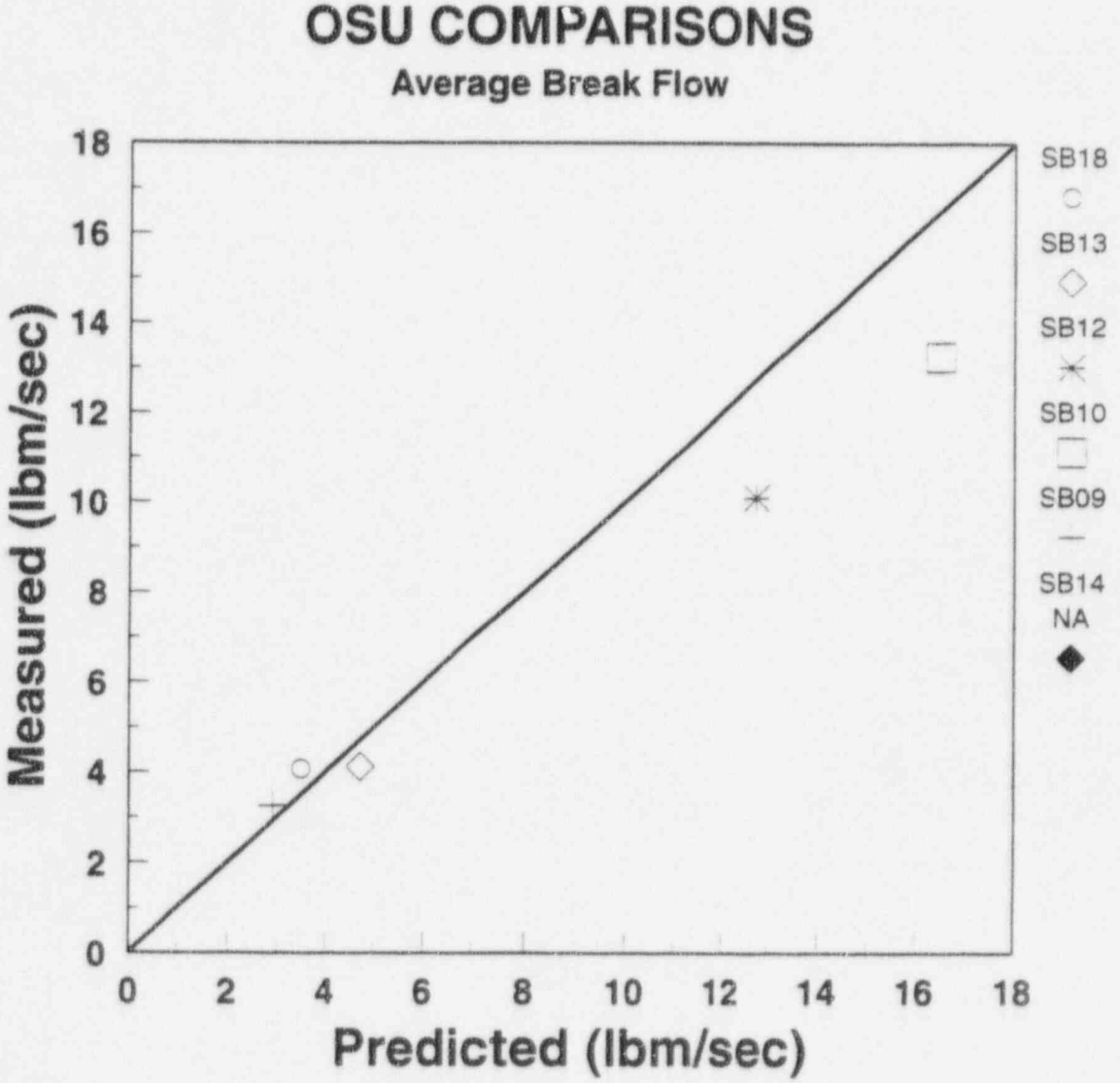

Figure 8.4-7 Comparison of Average Break Flow

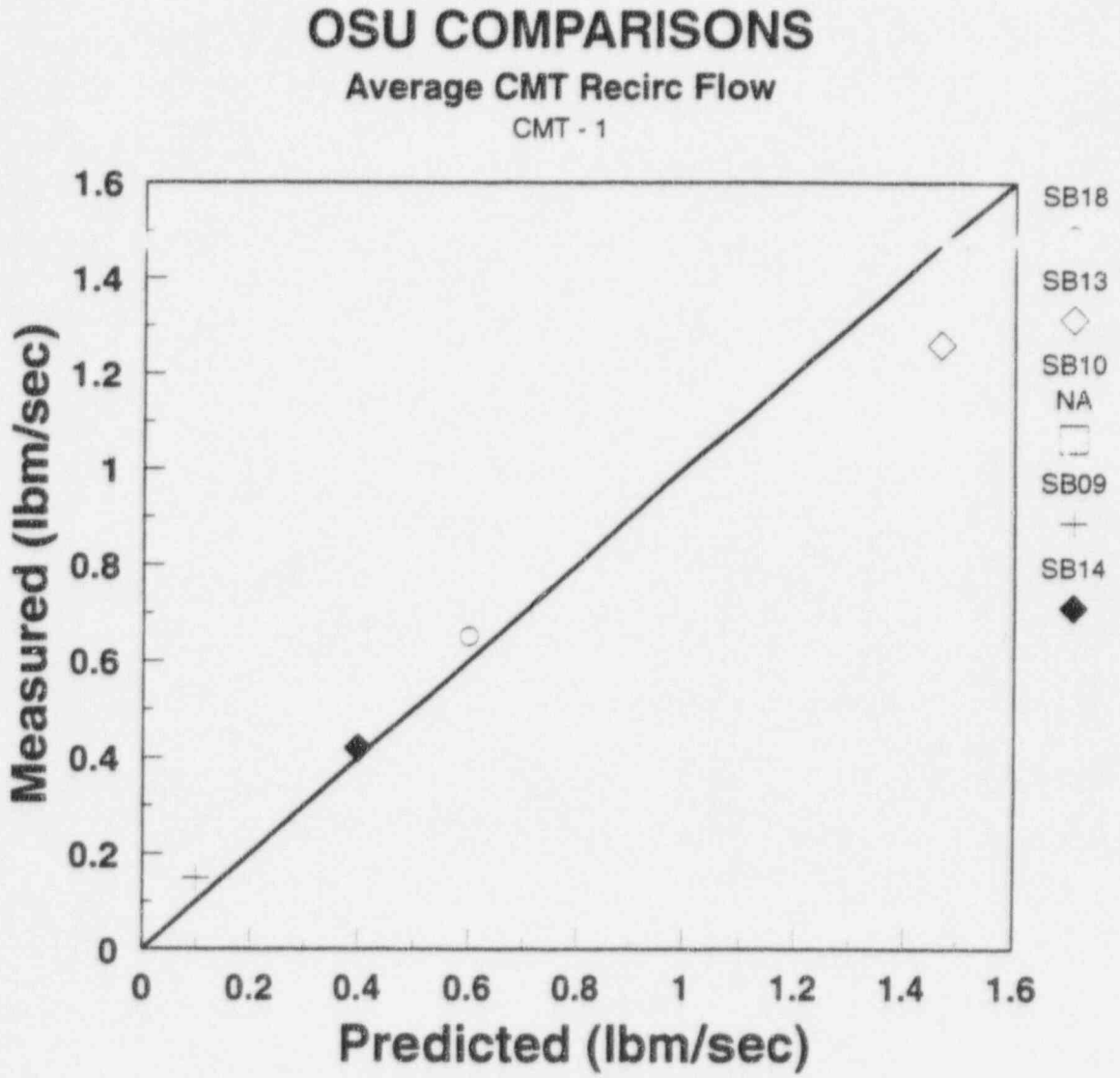

SB12 - Not included (flows exceeded test measurement range)

Figure 8.4-8 Comparison of Average CMT-1 Recirculation Flow

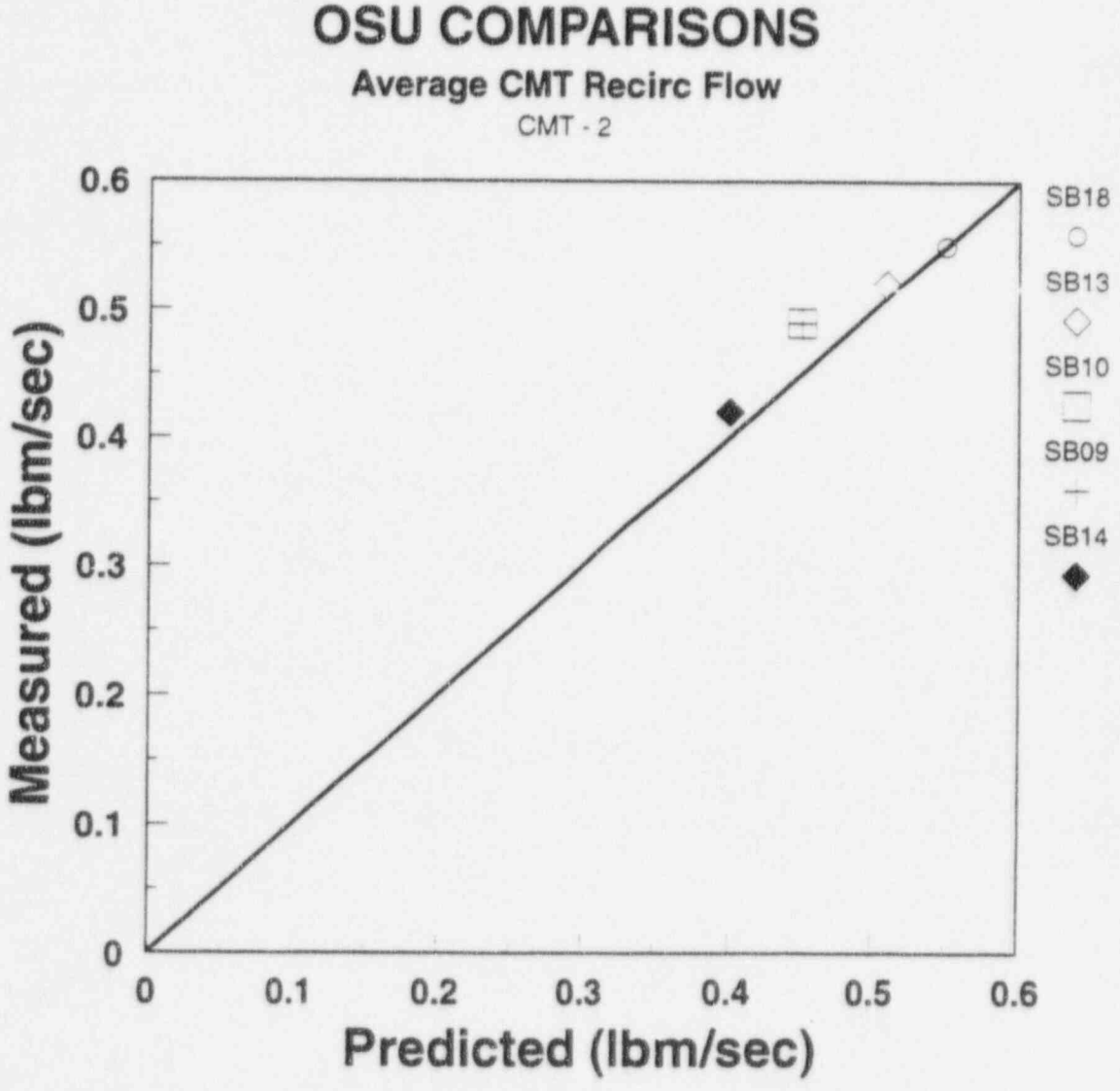

SB12 - Not included (flows exceeded test measurement range)

Figure 8.4-9 Comparison of Average CMT-2 Recirculation Flow

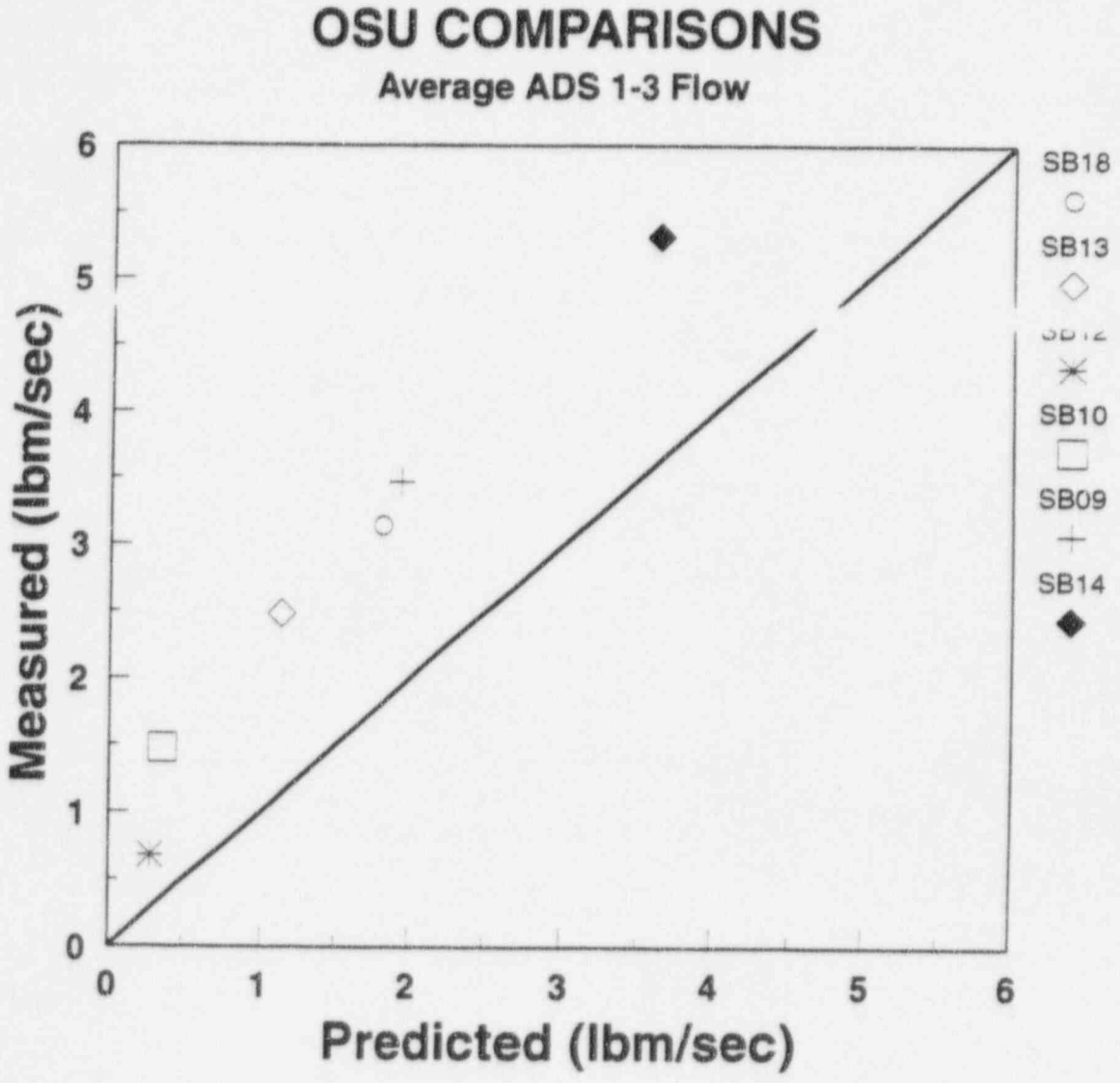

Figure 8.4-10 Comparison of Average ADS 1-3 Flow

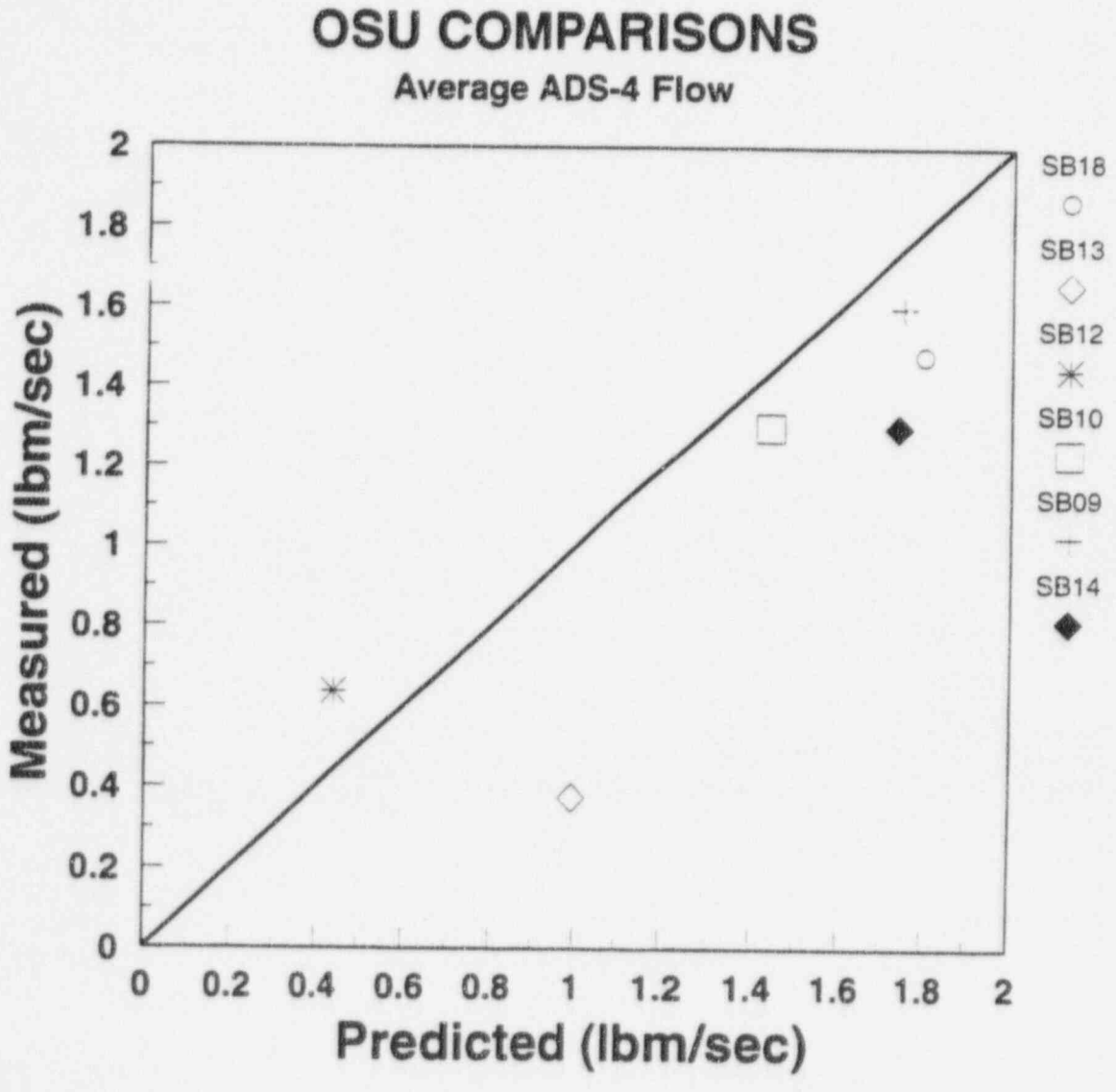

Figure 8.4-11 Comparison of Average ADS-4 Flow

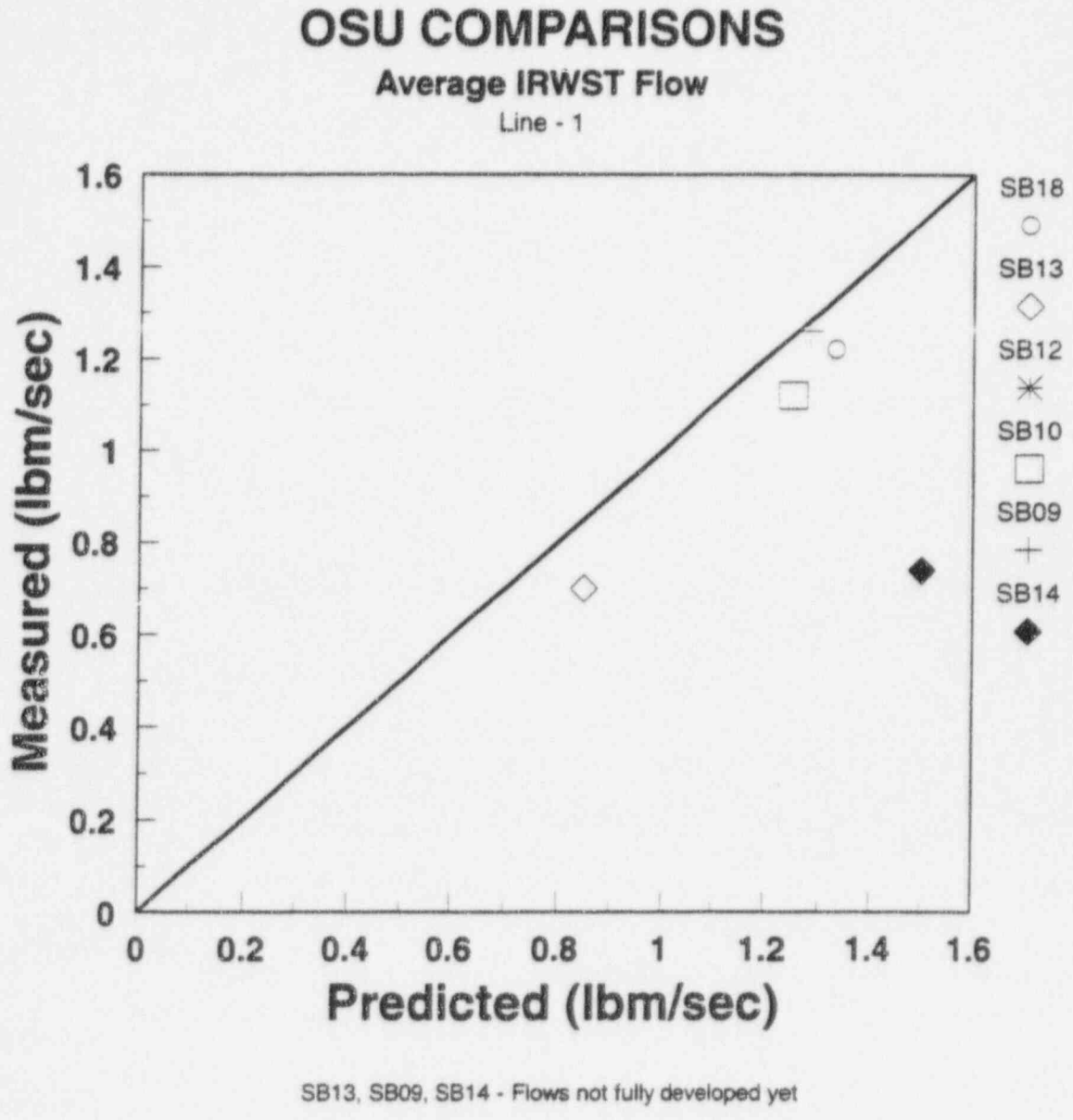

Figure 8.4-12 Comparison of Average IRWST-1 Flow

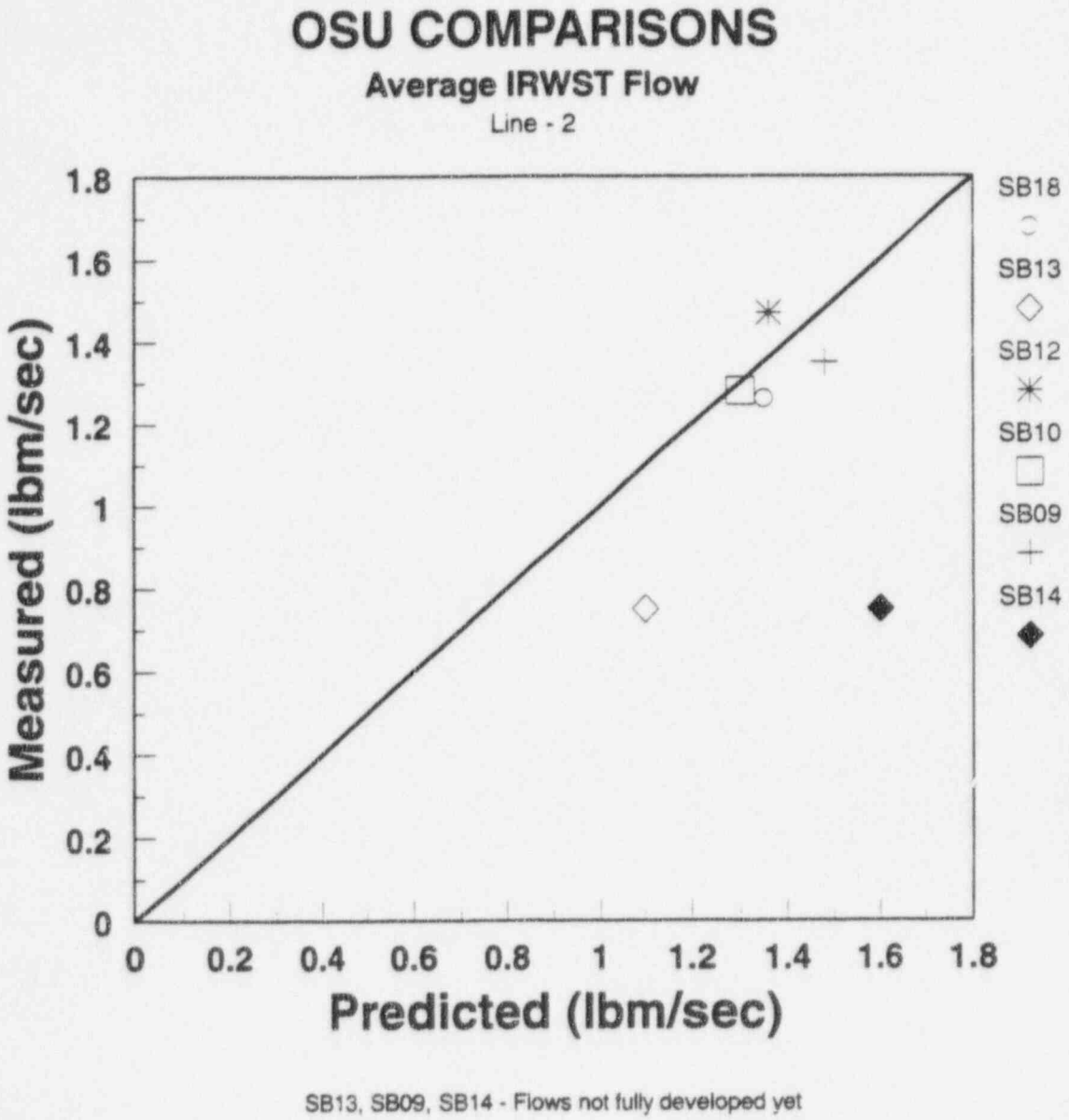

Figure 8.4-13 Comparison of Average IRWST-2 Flow

Figures 8.4-14 through 8.4-21 are not included in the non-proprietary version of this report.

8.5 References

8-1 Dumsday, C. L., et al., *AP600 Low-Pressure Integral Systems Test at Oregon State University Final Data Report*, WCAP-14252, Revision 0 (May 1995)

8-2 Andreycheck, T. S., et al., *AP600 Low-Pressure Integral Systems Test at Oregon State University Test Analysis Report*, WCAP-14292, Revision 0 (September 1995)

8-3 Reyes, J. N., et al., *AP600 Low-Pressure Integral Systems at Oregon State University Facility Scaling Report*, WCAP-14270, Revision 0 (January 1995)

9 CONCLUSIONS

The process used to develop the ranking of the phenomena of importance for the AP600 small-break loss-of-coolant accident (LOCA) identifies the important thermal-hydraulic behavior to be predicted by the analysis tool used to assess the accident mitigation performance of the AP600 passive core cooling system (PXS). The phenomena of interest and their relative importance are contained in a phenomena identification and ranking table (PIRT), Table 1.3-1. Using the PIRT as a guide, the NOTRUMP code was improved so that it could reasonably predict the PIRT phenomena at the low pressures typical of the AP600. The PIRT was also used to develop the code validation effort so that the highly ranked PIRT phenomena that most significantly affect the system response to the small-break transient are validated against appropriate test data.

The PIRT process was used in the selection of tests to be analyzed. The PIRT was the basis for selecting the benchmark cases used to evaluate the adequacy of selected code models and modeling approaches. The separate effects and integral systems tests were analyzed from a PIRT perspective with the emphasis on closing on the highly ranked PIRT phenomena.

Several models and code improvements were incorporated into the NRC-approved version of the NOTRUMP code to enhance its capability to properly analyze the low-pressure aspects of the AP600 small-break transient. As part of the verification of the models, a series of "benchmark" problems were analyzed to demonstrate the specific features of the refined models using simple examples or thought problems. Successful analysis of the benchmark problems confirms that the models, as coded into NOTRUMP, perform as the analysts intended.

A series of separate effects tests were analyzed to validate the NOTRUMP code for specific highly ranked PIRT phenomena. Validation of the separate effects tests is described in the following four paragraphs.

The small-break LOCA PIRT identifies that the two-phase mixture level is a highly ranked phenomenon for the reactor vessel, core, upper head, and upper plenum. The mixture level in the core is important because it represents the interface between "good" cooling when the fuel rods are in nucleate boiling, and "poor" cooling when the fuel rods are in steam cooling above the mixture level. Therefore, the prediction of the mixture level determines the calculated peak cladding temperature for the small-break transient. In the AP600 small-break LOCA analysis, core uncovery is not calculated and the predicted mixture level is above the core. Therefore, the NOTRUMP prediction of the two-phase mixture level must be accurate so that there is confidence that the conclusion of no core uncovery for AP600 is correct.

The comparisons of NOTRUMP to the three series of two-phase level swell tests indicate that NOTRUMP underpredicts the mixture level over a wide range of thermal-hydraulic conditions typical of the AP600 small-break LOCA transient. The assessment of the NOTRUMP two-phase level swell models confirms that they are applicable for the AP600 small-break LOCA transient. NOTRUMP predicts a conservatively low core mixture level for a set of thermal-hydraulic conditions, therefore the conclusion of no core uncovery for AP600 is valid.

A number of highly ranked PIRT phenomena are associated with core makeup tank (CMT) performance for the AP600 small-break LOCA transient. NOTRUMP has been compared to the 300-series and 500-series CMT separate effects tests, which simulate the highly ranked phenomena for CMT circulation and draindown behavior. The calculated flow rates from the NOTRUMP calculations agree well for most of the tests and are within the data uncertainty. The calculated time-averaged flow rates over the duration of the test also agree well with the measured data. The average fluid temperatures predicted for the CMT are usually lower for the NOTRUMP calculation, even with the numerical smearing effects caused by the code numerics and coarse noding. The overall response of the code and the tests are similar. Agreement with the majority of the data for these tests indicates that NOTRUMP captures the key thermal-hydraulic behavior observed in the CMT tests and identified in the AP600 small-break LOCA PIRT.

The AP600 small-break LOCA PIRT identifies a number of highly ranked phenomena for the automatic depressurization system (ADS). NOTRUMP has been compared to six of the 200-series tests and two of the 300-series tests from the ADS Phase B full-scale separate effects test matrix. The critical flow model used in NOTRUMP accurately predicts the critical flow at the locations where the flow is observed (within the data uncertainty) to be choked. The total overall pressure drops are not as accurately predicted by NOTRUMP. Prediction of the overall pressure drop is consistent with the excellent predictions of the ADS flows, which addresses the highly ranked PIRT phenomenon for this component.

In addition to the separate effects tests, the SPES-2 AP600 small-break integral systems LOCA tests were analyzed over a range of break sizes and break locations. NOTRUMP predicts all the phenomena observed in the tests, including all the highly ranked phenomena given in the AP600 small-break LOCA PIRT. For all but one of the tests, NOTRUMP predicts a delay in the timing for ADS stage 1 actuation. However, the reasons for the timing delay are explained. When the code results are shifted in time to account for the timing delay, the agreement with the test data is significantly improved. The impact of the delay in the actuation of ADS stage 1 has been assessed by comparing the predicted SPES-2 system inventory at the initiation of in-containment refueling water storage tank (IRWST) injection with the measured mass in the system at the time of IRWST injection. This comparison shows that NOTRUMP is either predicting less mass or the same mass as the test for all of the transients. Therefore, the delay in the ADS stage 1 timing results in a conservative calculation for the mass inventory in the test at the beginning of IRWST injection.

Additional integral system LOCA tests were analyzed for the OSU AP600 facility. This facility also examined a range of break sizes and break locations, as was done for the SPES-2 facility. A similar observation for the OSU facility simulations can be made to that observed in the SPES-2 facility results. That is, for all but one of the tests, NOTRUMP predicts a delay in the time for ADS-1 actuation and CMT draindown. An additional observation was made for OSU that indicates that the ADS stages 1 through 3 relief is underpredicted while the break flows are overpredicted. These two items compensate for each other in terms of inventory depletion but affect the predicted mass distributions. However, as observed in the SPES-2 facility, the NOTRUMP code conservatively predicts a lower system mass inventory at the ADS-1 and IRWST injection times, relative to that observed in the tests.

The NOTRUMP code is used to determine the accident mitigation performance of the AP600 PXS for small-break LOCA transients. The NOTRUMP models have been enhanced to improve predictions at low system pressures typical of the AP600 small-break LOCA. The NOTRUMP code has also been compared to a wide range of benchmark problems for model verification and to separate effects and integral systems effects tests that capture the highly ranked PIRT phenomena for the AP600 small-break LOCA. The results of the NOTRUMP verification and validation effort support the application of the NOTRUMP code using Appendix K requirements for small-break LOCA analysis for the AP600.

WCAP-14808
Revision 1

NOTRUMP Final Validation Report for AP600

Westinghouse Energy Systems

Westinghouse
Non-Proprietary Class 3

WCAP-14808
Revision 1

NOTRUMP Final Validation Report For AP600

February 1997